Preparation and Applications of Fluoroalkyl End-capped Oligomers/Polyaniline Nanocomposites

Doctoral Course
Graduate School of Science and Technology
Hirosaki University

Doctor Thesis

September 2015

Taiki Tsuzuki-ishi

Contents

General Introduction

1. Properties of fluorine and fluorinated compounds

The unique characteristics which fluorinated compounds possess are derived from the fact as follows:

(1) Fluorine is the most electronegative of all the elements. The high electronegativity is conducive to high oxidation potential, high ionization energy and high electron affinity.[1)]

(2) It has the second smallest atomic radius following hydrogen.[2)]

(3) It can form very strong and relatively short bonds with other atoms. For example, the strength of the carbon - fluorine bond (484 $kJ \cdot mol^{-1}$) exceeds that of the carbon–hydrogen bond (412 $kJ \cdot mol^{-1}$) and the carbon - oxygen bond (360 $kJ \cdot mol^{-1}$) as shown in Table 1.[1, 3)] Such strength of bonds formed by fluorine gives extraordinary thermal and oxidative stability to fluorinated compounds.[1, 3)]

(4) The dispersion force interaction acting between perfluorochemicals is weak due to the lower polarizability of fluorine.[1, 4)] The volatile characteristic of fluorinated compounds becomes considerably higher than that of their chlorine analogues as

shown in Table 2. However, partially fluorinated compounds such as hydrofluoric acid and hydrofluorocarbon are well known to exhibit a high boiling point compared with those of perfluorinated and nonfluorinated compounds due to the formation of hydrogen bonds.

(5) Perfluorochemicals also have the low reflective indices and surface tension as shown in Table 3.[3-6] For example, the surface tension of poly(tetrafluoroethylene) [PTFE : $-(CF_2-CF_2)_n-$; 18.5 mN/m] becomes lower than that of polyethylene [$-(CH_2-CH_2)_n-$; 31 mN/m].

Thus, it is of particular interest to develop a wide variety of fluorinated and fluoroalkylated compounds, from the developmental viewpoints of new fluorinated functional materials.

Table 1 Physical properties of some atoms[1–4]

Physical property	Element				
	H	C	O	F	Cl
Ionization energy [eV]	13.60	11.26	13.62	17.42	12.97
Electron affinity [eV]	0.75	1.26	1.46	3.40	3.62
Electronegativity (Pauling)	2.20	2.55	3.44	3.98	3.16
Van der Waals radius [Å]	1.20	1.70	1.52	1.47	1.75
Polarizability [$Å^3$]	0.67	1.63	0.90	0.56	2.18
Bond energy of C-X [$kJ•mol^{-1}$]	412	348	360	484	338
Bond length of C-X [Å]	1.1	1.5	1.4	1.3	1.8

Table 2 Boiling point of fluorine compounds and their analogue[1,4)]

	Boiling point [ºC]		Boiling point [ºC]		Boiling point [ºC]
F_2	–188.2	H_2	–252.8	Cl_2	–34.0
CF_4	–127.9	CH_4	–161.5	CCl_4	76.7
PF_3	–101.5	PH_3	–87.7	PCl_3	75.7
HF	19.5				
CH_2F_2	–52				

Table 3 Refractive indices and surface tensions of fluorocarbons, hydrocarbons, and water[3–6)]

Compound	Refractive index (n_D^{20})	Surface tension [mN/m]
n-C_6F_{14}	1.252	11.4
n-C_6H_{14}	1.372	17.9
–$(CF_2CF_2)_n$–	1.380	18.5
–$(CH_2CH_2)_n$–	1.510	31.0
H_2O	1.333	72.8

2. Applications of fluorinated compounds

There have been hitherto numerous reports on the application of inorganic fluorinated compounds in a variety of fields such as medicinal chemistry, electronics, catalysts and energy industry as shown in Table 4 due to their exhibiting various unique properties such as high acidity, high oxidizing ability, low boiling point and good chemical stability.[7-13)]

Table 4 Typical inorganic fluorinated compounds and their applications[7-13)]

Compound	Application
NaF	Additive for dentifrice
Na_3AlF_6	Flux
$LiPF_6$	Electrolytes for lithium-based rechargeable battery
SbF_5	Storong Lewis acid
PtF_6	Storong oxidant (generation of $XePtF_6$ by reaction with Xe)
UF_6	Uranium enrichment on nuclear industry
SF_6	Ultrasonographic contrast agent for characterization of focal liver lesions

Similarly, there have been great interests in numerous organofluorine compounds in a variety of fields such as pharmaceuticals, dyes, organic semiconductors and surfactants as shown in Fig. 1.[14-19)]

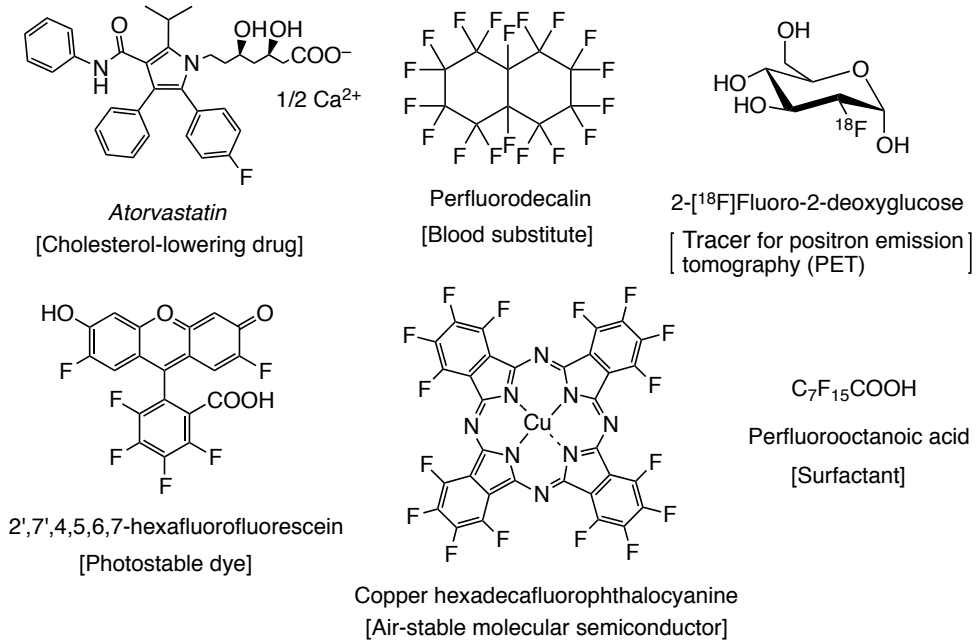

Fig. 1 Several organofluorine compounds[14-19)]

F-substitutents on fluorinated pharmaceuticals such as *Atorvastain* prefer to orient toward electropositive regions of receptor sites through C–F···X interactions.[14] Perfluorochemicals such as perfluorodecalin can dissolve large volumes of O_2 and other respiratory gases.[15] Glucose containing ^{18}F of fluorine radioisotope (Fluorodeoxyglucose) is known as a radiopharmaceutical for real-time prognosis for petastatic thyroid carcinoma by positron emission tomography (PET).[16]

3. Fluoropolymers

There have been attracted significant attention in fluoropolymers over the past few decades to their unique properties such as high thermal stability, improved chemical resistance and lower surface tension.[20, 21] Some typical fluoropolymers are listed in Fig. 2.[20–28] Poly(tetrafluoroetylene) (PTFE) is one of the most widely used polymers owing to its high melting, high thermal stability, good chemical resistance, low coefficient of friction and a low dielectric constant.[20] Not only PTFE but also main-chain fluorinated polymers such as poly(vinyldene fluoride), perfluoropolyether, perfluorinated polyimide have been applied to the membranes, lubricants and optics materials.[21-23] In addition, organosilicone and

phosphazene polymers containing fluoroalkyl side-chains have also attracted considerable attention in numerous fields such as water repellents and gas permeable materials. [24-28)]

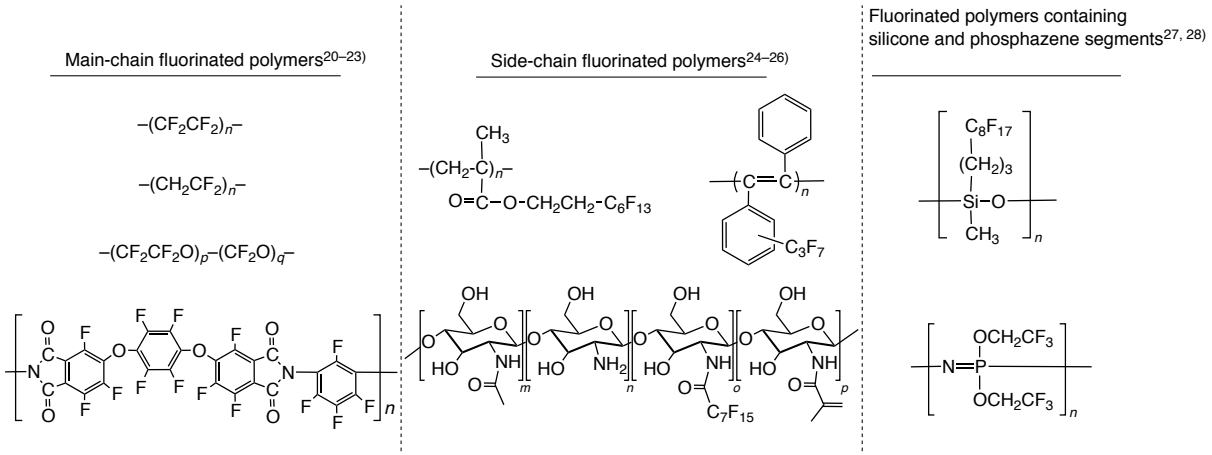

Fig. 2 Several fluoropolymers

Longer fluoroalkylated polymers are in general solvophobic.[29)] Thus, in order to improve their solubilities toward traditional organic media including water, fluorinated multiblock copolymers containing hydrophilic blocks and hydrophobic blocks are prepared by a polycondensation reaction between disulfonated poly(arylene ether sulfone)s and fluorinated poly(arylene ether)s as shown in Scheme 1 and can exhibit a well-defined phase separation and higher proton conductivities compared to the random copolymers such as Nafion®.[30)]

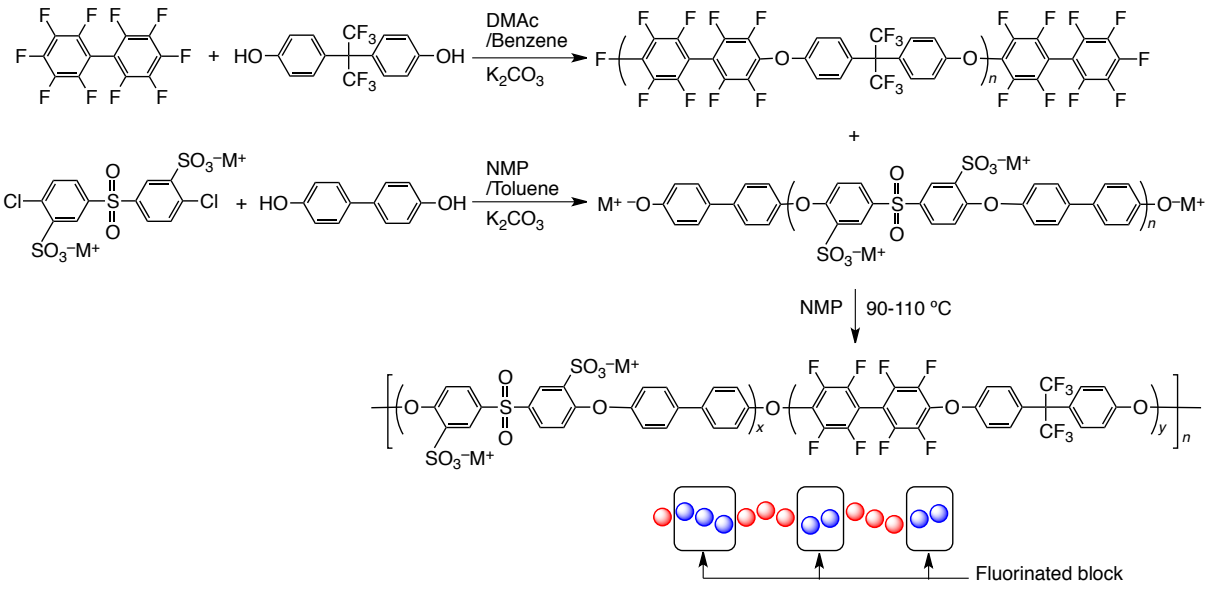

Scheme 1 [30]

There have been a variety of reports on the preparation of fluoroalkylated diblock copolymers.[29, 31-34] For example, diblock copolymers with perfluoroalkyl side chains (PMMA-*b*-PFMA) have been prepared by living anion copolymerization of methyl methacrylate (MMA) and 2-perfluorooctylethyl methacrylate (FMA) as shown in Scheme 2.[31-33] Interestingly, these copolymers have a good solubility in organic solvents such as chloroform and can form the self-assembled molecular aggregates; although the corresponding fluorinated homopolymer cannot exhibit such solubility in chloroform.[33] In addition, their obtained films by these copolymers afford lower surface free energy than that of the corresponding random copolymer due to the higher arrangement ability of perfluoroalkyl side chains on the film surface.[32]

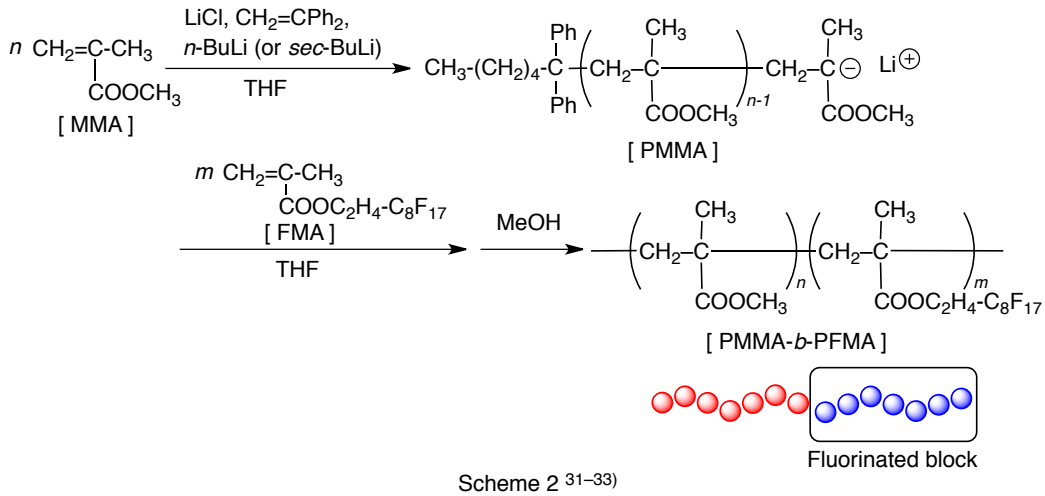

Scheme 2 [31–33]

Poly(methyl methacrylate)-*block*-perfluoroalkylated methacrylate copolymer (PMMA-*block*-PFMA) has been synthesized by atom transfer radical polymerization (ATRP) as shown in Scheme 3.[34] These fluorinated polymer cast films can give a good hydrophobic characteristic.

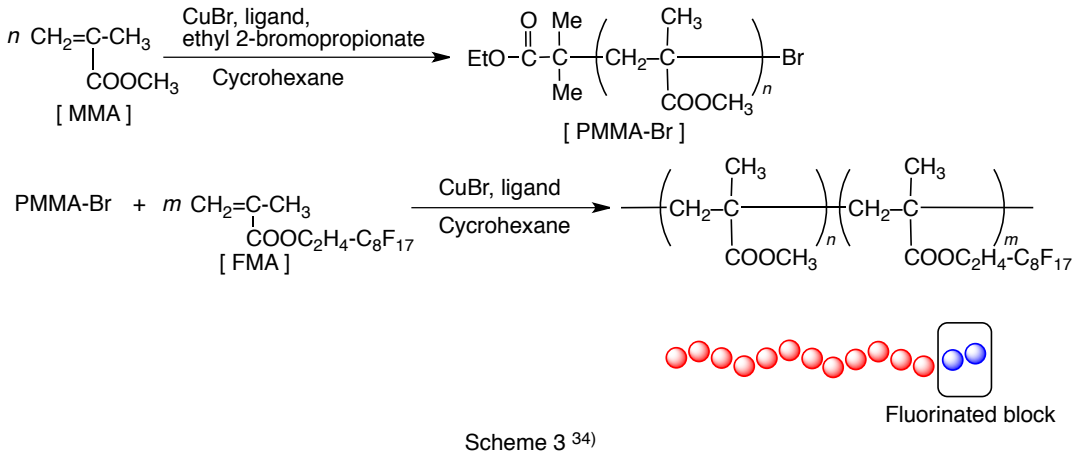

Scheme 3 [34]

A-B-C triblock-type hydrophilic-hydrophobic-fluorophilic copolymers (PVBM-*b*-PS-*b*-PVBFP) are prepared by a three-step reversible addition fragmentation transfer (RAFT) polymerization and can form polymeric micelles with a diameter of 20 ~ 30 nm (see Scheme 4). [35)]

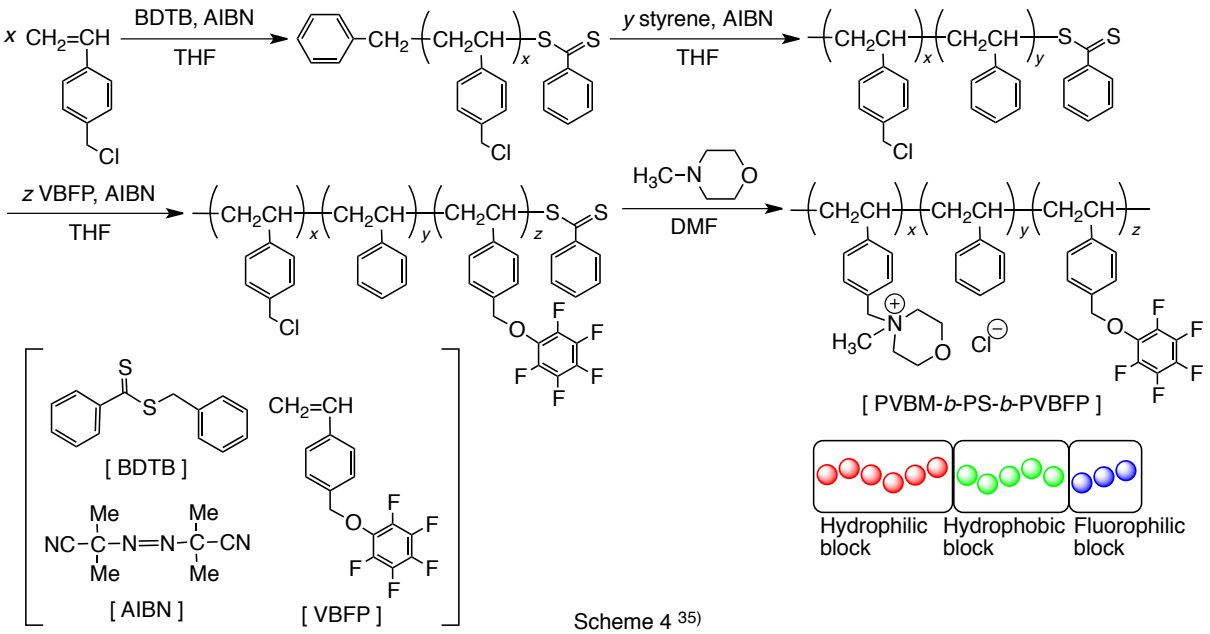

Scheme 4 [35)]

In a variety of fluorinated polymers, A-B-A triblock-type fluoroalkyl end-capped oligomers are one of the most remarkable materials because they can exhibit many unique properties such as high solubility, surface-active properties, biological activities and nanometer size-controlled self-assembled molecular aggregates through the aggregations of end-capped fluoroalkyl groups, which cannot be achieved by the corresponding nonfluorinated and randomly fluoroalkylated ones.[36-46)] Fluoroalkyl end-capped oligomers

can be easily prepared by using fluoroalkanoyl peroxide as a key intermediate. A-B-A triblock-type fluoroalkyl end-capped acrylic acid oligomers have been already prepared by primary radical termination or radical chain transfer to the fluoroalkanoyl peroxide under the oligomeric conditions, in which the concentration of the peroxide was almost the same as that of acrylic acid as shown in Scheme 5.[38)]

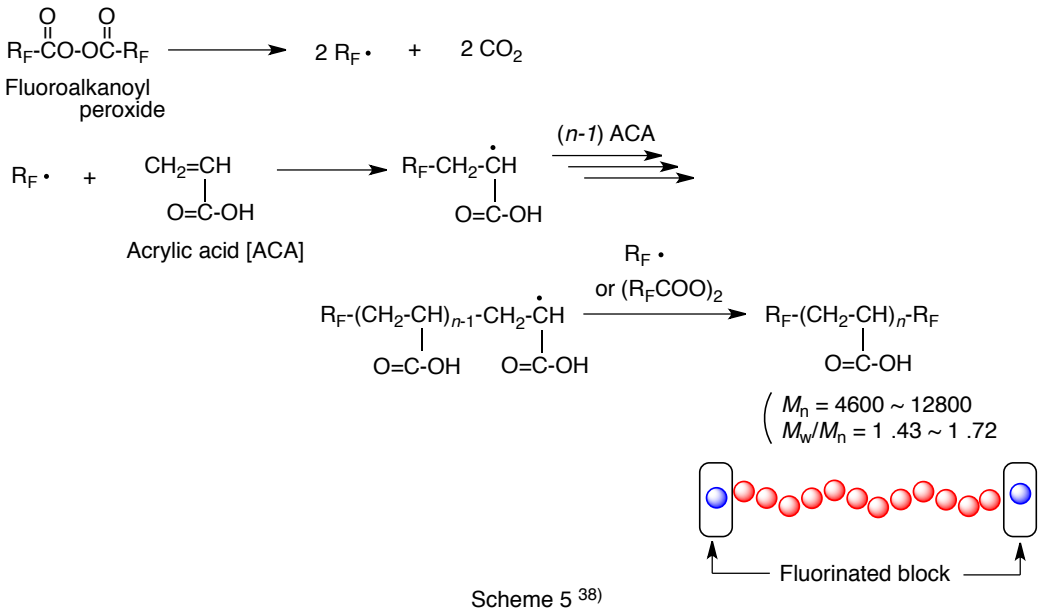

Scheme 5 [38)]

A-B block-type fluorinated acrylic acid oligomers were effective for reducing the surface tension of water compared to that of randomly fluoroalkylated polysoaps.[47)] A-B-A triblock-type fluoroalkyl end-capped oligomers are more effective for reducing the surface tension of water compared to that of A-B block-type fluoroalkylated polysoaps.[38)] Fluoroalkyl groups in fluoroalkyl end-capped oligomers are likely to be arranged regularly above the

water surface, where all the fluoroalkyl groups are parallel to each other similar to the general low-molecular fluorinated surfactants as shown in Fig. 3-(b).

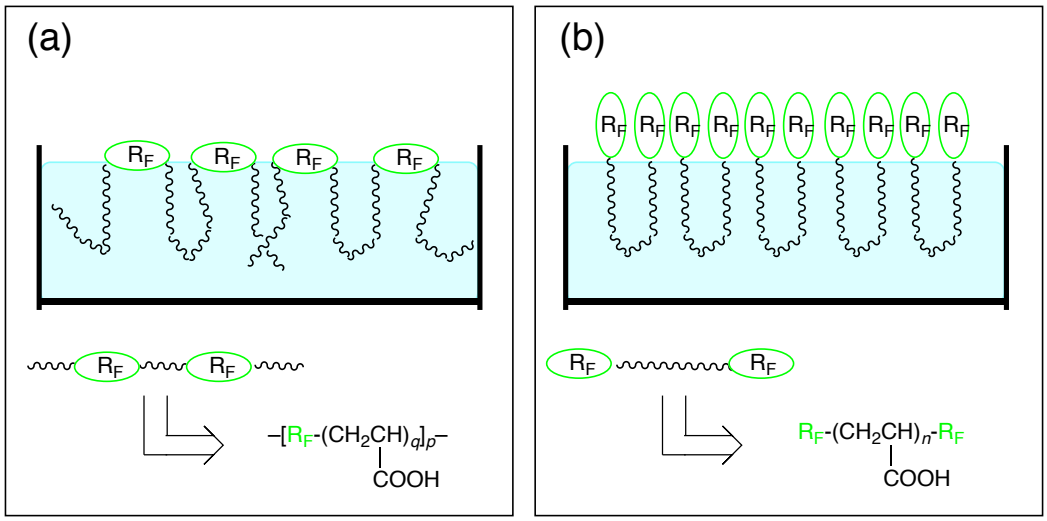

Fig. 3 Suface arrangement of A-B block-type fluoroalkylated polysoaps (a) and A-B-A triblock-type fluoroalkyl end-capped acrylic acid oligomers (b) in aqueous solutions.[38, 47)]

In contrast, blocked fluoroalkyl groups are not likely to be arranged regularly above the water surface compared to those of fluoroalkyl end-capped oligomers as shown in Fig. 3-(a). In addition, these fluoroalkyl end-capped oligomers have been applied to the surface modification of traditional organic polymers such as PMMA to exhibit a good oleophobic characteristic imparted by fluorine.[48)]

As shown in Fig. 4-[A], fluoroalkyl end-capped oligomers can form the nanometer size-controlled self-assembled oligomeric aggregates with the aggregations of end-capped

fluoroalkyl groups in aqueous and organic media, which cannot be achieved by the corresponding non-fluorinated and randomly fluoroalkylated ones (see Fig. 4-[B]).[49, 50)]

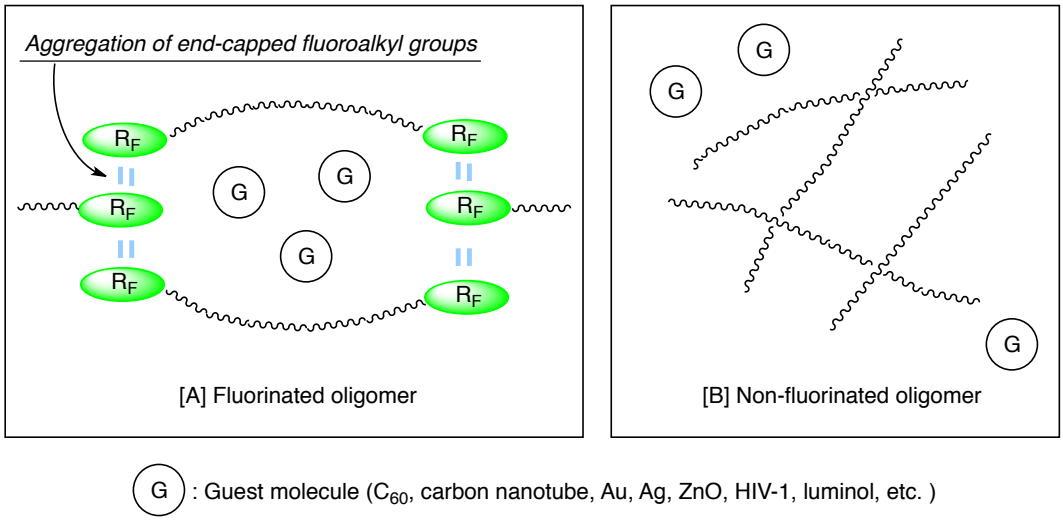

Fig. 4 Schematic illustration for the interaction of self-assembled fluoroalkyl end-capped oligomers with guest molecules[39, 40, 42,43, 45, 49–57)]

These fluorinated oligomeric aggregates formed by fluoroalkyl end-capped oligomers can interact with a variety of guest molecules such as fullerene and gold nanoparticles to afford the fluorinated oligomeric aggregates/guest molecule nanocomposites.[39, 40, 42, 43, 45, 51-57)] These fluorinated oligomeric nanocomposites have been also applied to the surface modification of traditional organic polymers such as PMMA to exhibit not only a good surface-active property imparted by fluorine but also unique characteristics related to the presence of guest molecules on the modified PMMA film surface.[53-57)]

4. Conducting polymers; polyaniline

Intrinsically conducting polymers (ICP) are conducting in nature due to the presence of a conjugated π electron system in their structures (see Fig. 5).[58, 59)]

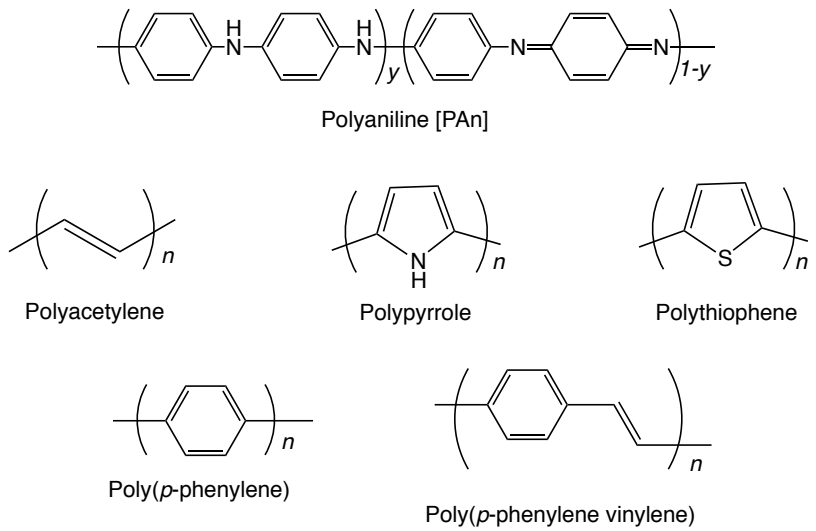

Fig. 5 A series of intrinsically conducting polymers [58, 59)]

These polymers have numerous different characteristics such as a low energy optical transition, low ionization potential and a high electron affinity from those of the traditional non-conjugated ones.[58–62)] A high level of conductivity (near metallic) can be achieved in ICPs through oxidation–reduction as well as doping with a suitable dopant such as AsF_3 and I_2.[58, 59)]

Among a variety of electrically conducting polymers, polyaniline (**PAn**) is one of the most

remarkable materials owing to its ease of synthesis, low cost, good environmental stability and high electrical conductivity.[59, 62–70] The oxidation of aniline is the most widely employed synthetic route to **PAn**, and **PAn** can be prepared through electrochemical or chemical reaction process as shown in Scheme 6.[63, 68]

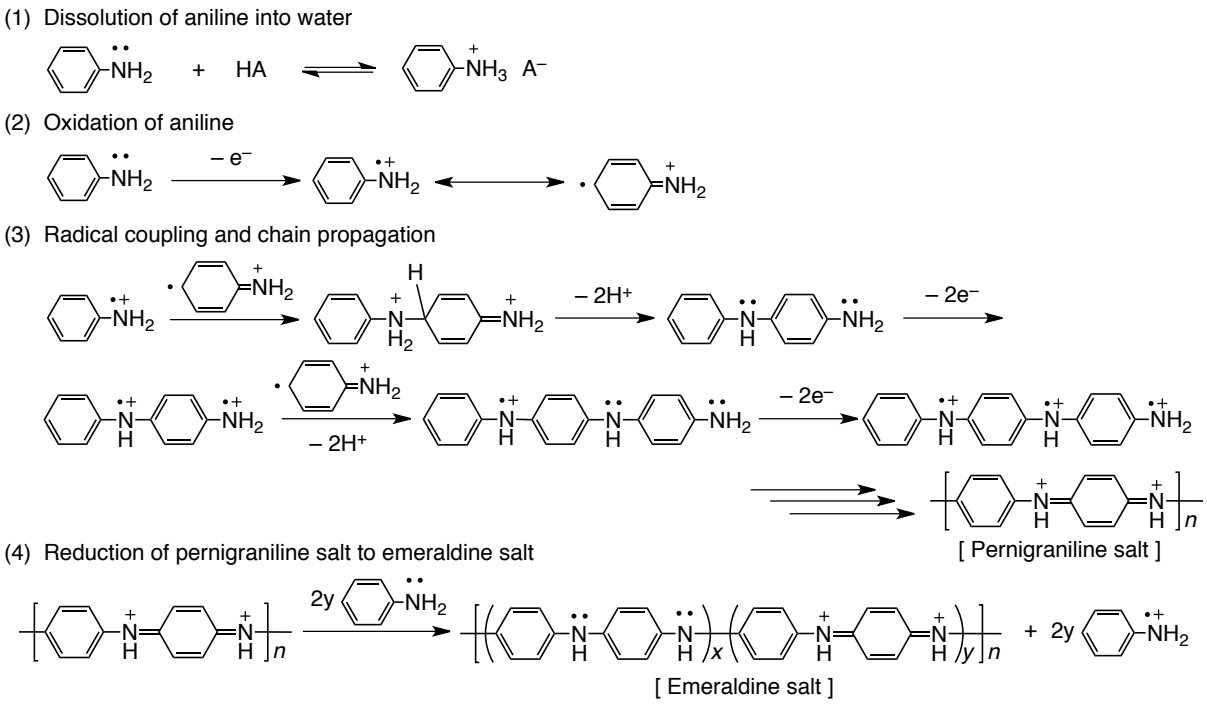

Scheme 6 [63, 68]

The reaction is usually carried out in acidic media such as aqueous solutions containing HCl and $HClO_4$.[59, 63–66]

As shown in Scheme 7, **PAn** exhibits reversible redox behavior controlled by simple doing/dedoping approach, and **PAn** can change its characteristics such as optical property and

conductivity.[63-65, 68)]

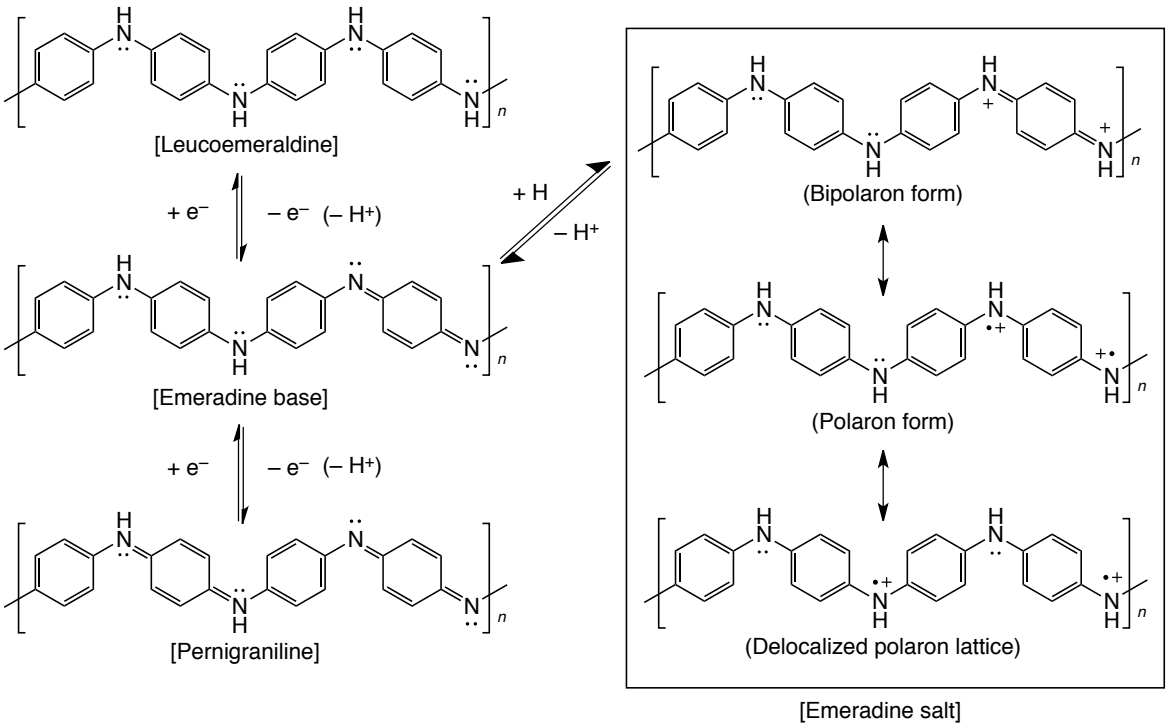

Scheme 7 [59, 63-65, 68)]

The oxidation states of **PAn** correspond to leucoemeraldine (fully reduced state), emeraldine (half oxidized state) and pernigraniline (fully oxidized state), respectively.[59, 63-65, 68)] The protonated **PAn** changes its structure from emeraldine base to emeraldine salt to afford a high conducting through the generation of charge carriers.[59, 63-65, 68)] Such electrical properties enable **PAn** to apply into the sensing, electro/chemochromic, catalytic and other fields.[71-73)]

5. Non-fluorinated polymer/polyaniline composites

It is well known that the conjugated polymers such as **PAn** are infusible in nature and generally insoluble in common solvent. Therefore, it is of particular interest to develop **PAn** composites with improved processability and mechanical properties while maintaining the inherent properties of the conducting polymer. From the developmental viewpoints of new functional **PAn** composite materials, the incorporation of **PAn** into the traditional polymer matrices has attracted considerable attention in numerous fields such as flexible super capacitors, actuators, light-emitting diodes and sensors. [74-82)]

As shown in Fig. 6, there are some reports on the preparation of organic polymer/**PAn** composites by using not only the in-situ polymerization of aniline monomer in the presence of the corresponding polymers: (I) but also the doping technique with the protonic acids: (II) and the blend technique of the parent **PAn** with the traditional organic polymers through the dispersion into the polar solvents such as *N*-methyl-2-pyrrolidinone: (III). [74-82)] However, we have some difficulties to increase the dispersibility and stability of the parent **PAn** by using these traditional organic polymers. From this point of view, it is deeply desirable to explore the **PAn** composites possessing the higher dispersibilty and stability by the use of the surface-active polysoaps such as fluorinated polysoaps

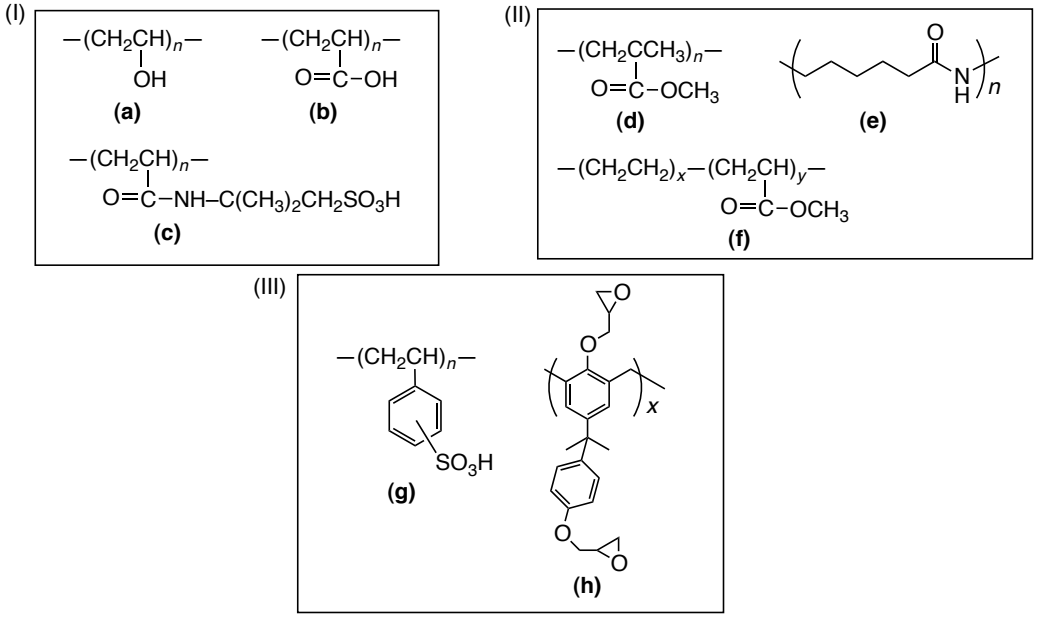

Fig. 6 Preparation of **PAn** composites possessing good dispersibility by using a variety of the traditional organic polymers[74-82)]

(I) The in-situ polymerization of aniline monomer in the presence of the traditional organic polymers: **(a) ~ (c)**
(II) The traditional organic polymers: **(d) ~ (f)** used in the doping methods with the protonic acids
(III) The blend method of **PAn** with the traditional organic polymers: **(g)** and **(f)** in the polar solvents

6. Fluorinated polymer/polyaniline composites

Fluorinated **PAn** derivatives can exhibit not only unique characteristics imparted by fluorine but also **PAn** as shown in Fig. 7.[83-88)] These **PAn** derivatives can give good oxidative resistance stability and with the increase of the solubility; however the electrical conductivity of these derivatives should became lower than that of the original **PAn** due to the steric hindrance and the electron-withdrawing effect of fluorine.[83-88)]

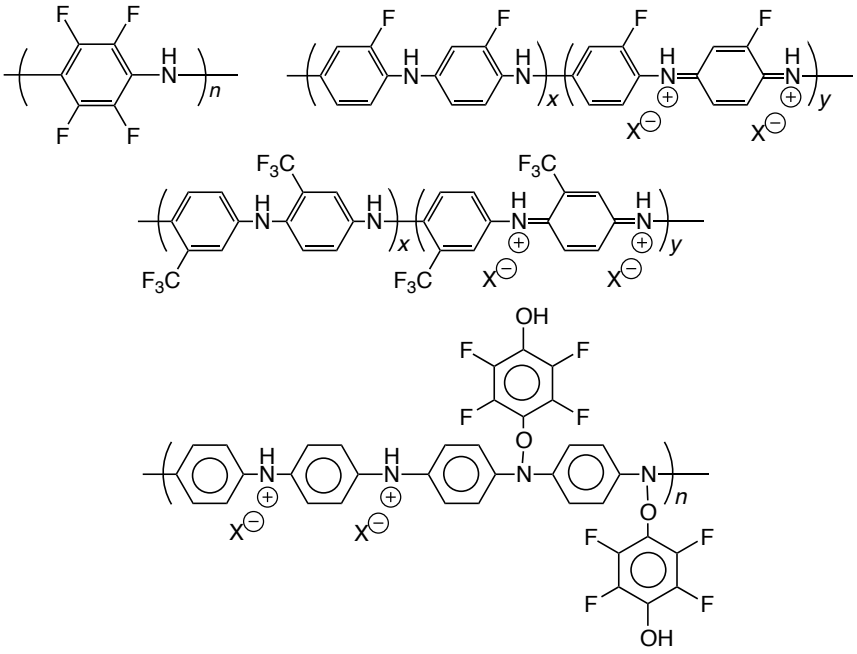

Fig. 7 Fluorinated polyaniline derivartives [83–88)]

On the other hand, **PAn** doped by the acid containing fluorine such as fluorinated carboxylic acid can give high specific capacitance, reversible wettability switching, solid-phase microextraction property, high proton conductivity and adsorbing heavy metal-ion from water together with a variety of applications in fields such as electronics, coating, sensor and biotechnology as shown in Fig. 8.[89-97)] For example, **PAn** which was prepared by chemical polymerization of aniline monomer in the presence of lithium triflate can form hierarchical micro/nanostructures such as star-shape and leaf-shape to exhibit the superhydrophobicity.[90)] Thus, fluorinated polymer/**PAn** composites can be considered as a new class of materials due to their improved properties, compared with those of the parent fluorinated polymers and **PAn**.

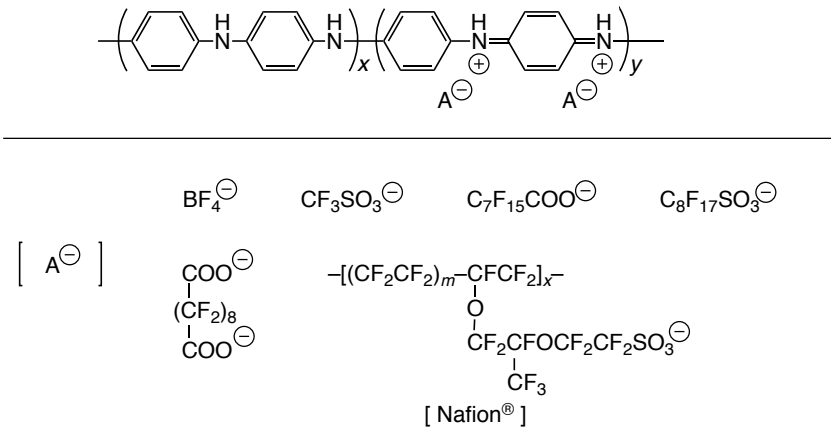

Fig. 8 Polyaniline doped by fluorinated organic and inorganic acids[89–97)]

However, studies on the preparation of fluorinated polymers/**PAn** composites have been hitherto very limited, although their fluorinated compounds are attractive functional polymeric materials. Therefore, it is of particular interest to develop novel fluorinated polymer/**PAn** nanocomposites possessing unique characteristics imparted by both fluorine and **PAn**, from the developmental viewpoints of new fluorinated functional materials.

7. Thesis outline

As mentioned before, fluoroalkyl end-capped oligomers are attractive functional materials due to their various unique properties such as high solubility, surface-active properties and the ability to form nanometer size-controlled self-assembled molecular aggregates.[36-57)] Especially, these fluorinated oligomeric aggregates formed by the aggregation of terminal fluoroalkyl

groups in oligomer can interact with a variety of guest molecules such as fullerene and gold nanoparticles to afford the fluorinated oligomeric aggregates/guest molecule nanocomposites. On the other hand, polyaniline (**PAn**) is one of the most remarkable conducting polymers owing to its ease of synthesis, low cost, good environmental stability, high electrical conductivity and reversible redox behavior.[59, 62-70)] From the developmental viewpoint of new fluorinated nanocomposite materials, it is of particular interest to develop fluorinated oligomer/**PAn** nanocomposites.

In this study, firstly, the preparation and properties of fluoroalkyl end-capped oligomer/**PAn** nanocomposites are described. Secondly, the preparation and properties of fluorinated **PAn** nanocomposites-encapsulated guest molecules by the interaction of these fluorinated **PAn** nanocomposites with a variety of guest molecules are also described.

In chapter 1, colloidal stable fluoroalkyl end-capped 2-(methacryloyloxy)ethanesulfonic acid oligomer [R_F-(MES)$_n$-R_F]/**PAn** nanocomposites were prepared by the polymerization of aniline catalyzed by ammonium persulfate (APS) in the presence of the corresponding oligomer as shown in Scheme 8.

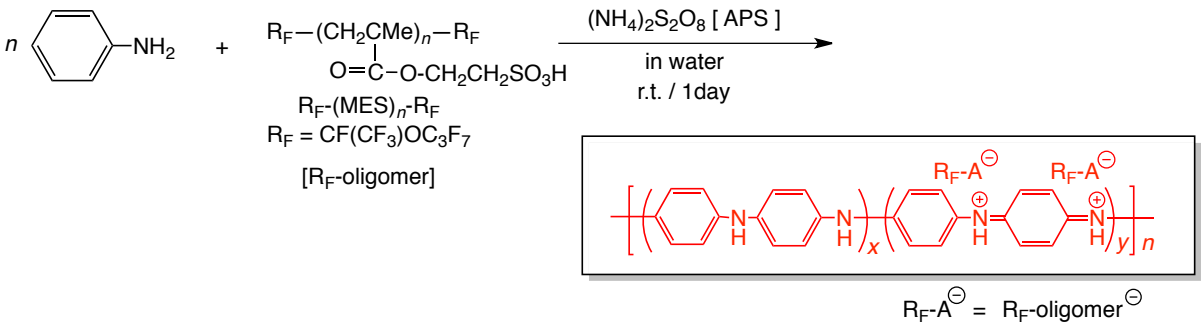

Scheme 8

In order to verify the interaction of **PAn** with fluoroalkyl end-capped oligomers, the interaction of the fluorinated oligomer with phenyl-capped aniline dimer: *N,N'*-diphenyl-1,4-phenylenediamine (**An-dimer**), which is considered to be an excellent model of **PAn** is also discussed.

In chapter 2, the interaction of R_F-$(MES)_n$-R_F/**PAn** nanocomposites with a variety of basic compounds such as ammonia, sodium hydroxide and silica particles bearing 3-aminopropyl groups (*Amino*-SiO_2) is described (see Scheme 9). Especially, the reversible color-changing behavior of **PAn** under air and ammonia vapor on the composite film is also discussed.

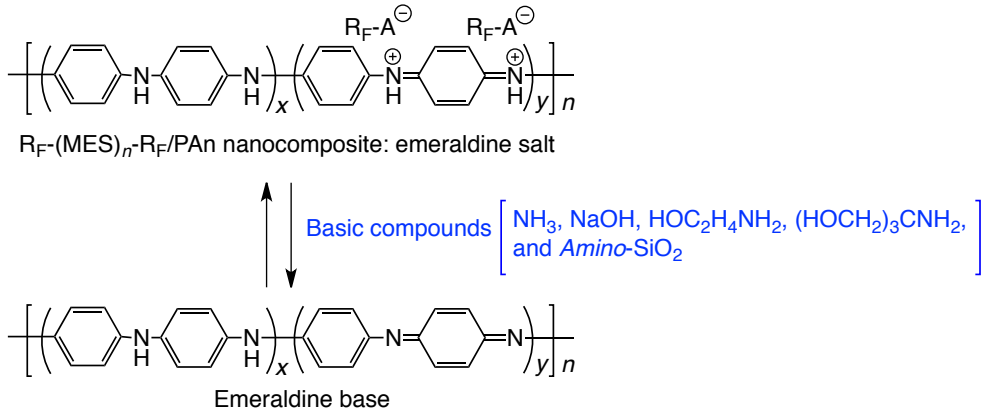

Scheme 9

In chapter 3, the interaction of these fluorinated oligomer/**PAn** nanocomposites with gold ions to afford the corresponding fluorinated oligomers/**PAn**/Au nanocomposites is described (see Scheme 10).

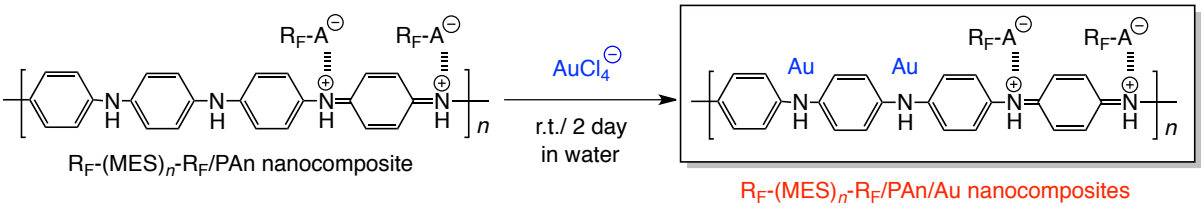

Scheme 10

In chapter 4, the preparation of R_F-(MES)$_n$-R_F/**PAn**/TiO_2 nanocomposites by the interaction of these R_F-(MES)$_n$-R_F/**PAn** nanocomposites with anatase-type titanium oxide nanoparticles are described (see Scheme 11).

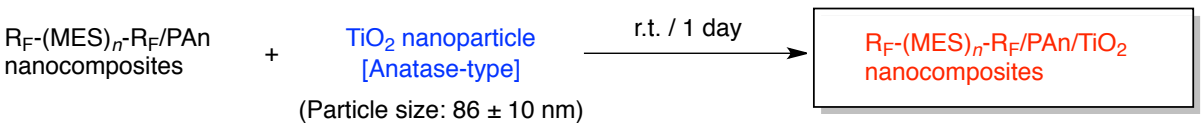

Scheme 11

Reference

1) D. F. Shriver and P. W. Atkins, "*Inorganic Chemistry, 3rd Ed.*", Oxford University press, Oxford, (1999).

2) A. Bondi, *J. Phys. Chem.*, **68**, 441 (1964).

3) D. R. Lide, ed., "*CRC Handbook of Chemistry and Physics*", CRC press, London (2005).

4) B. E. Smart, *J. Fluorine Chem.*, **109**, 3 (2001).

5) (a) C. J. Drummond, G. Georgaklis, and D. Y. C. Chan, *Langmuir*, **12,** 2617 (1996); (b) A. V. Sorokin, M. Bai, S. Ducharme, and M. Poulsen, *J. Appl. Phys.*, **92**, 5977 (2002).

6) M. P. Krafft, and J. G. Riess, *Chem. Rev.*, **109**, 1714 (2009).

7) V. C. Marinho, J. P. Higgins, A. Sheiham, and S. Logan, *Cochrane Database Syst. Rev.*, **1** (2003).

8) T. A. Utigard, K. Friesen, R. R. Roy, J. Lim, A. Silny, and C. Dupuis, *JOM*, **50**, 38 (1998).

9) K. Xu, *Chem. Rev.*, **104**, 4303 (2004).

10) G. A. Olah, G. S. Prakash, J. Sommer, and A. Molnar, "*Superacid chemistry*",

John Wiley & Sons, New York, (2009).

11) L. Graham, O. Graudejus, N. K. Jha, and N. Bartlett, *Coord. Chem. Rev.*, **197**, 321 (2000).

12) L. Gagliardi, A. Willetts, C. K. Skylaris, N. C. Handy, S. Spencer, A. G. Ioannou, and A.M. Simper, *J. Am. Chem. Soc.*, **120**, 11727 (1998).

13) E. Quaia, F. Calliada, M. Bertolotto, S. Rossi, L. Garioni, L. Rosa, and R. Pozzi-Mucelli, *Radiology*, **232**, 420 (2004).

14) K. Müller, C. Faeh, and F. Diederich, *Science*, **317**, 1881 (2007).

15) K. C. Lowe, *J. Fluorine Chem.*, **109**, 59 (2001).

16) R. J. Robbins, Q. Wan, R. K. Grewal, R. Reibke, M. Gonen, H. W. Strauss, R. M. Tuttle, W. Drucker, and S. M. Larson, *J. Clin. Endocrinol. Metab.*, **91**, 498 (2006).

17) C. C. Spagnuolo, W. Massad, S. Miskoski, G. O. Menendez, N. A. García, and E. A. Jares-Erijman, *Photochem. Photobiol.*, **85**, 1082 (2009).

18) J. L. Yang, S. Schumann, R. A. Hatton, and T. S. Jones, *Org. Electron.*, **11**, 1399 (2010).

19) H. Hoffmann and J. Würtz, *J. Mol. Liq.*, **72**, 191 (1997).

20) Z. Cui, E. Drioli, and Y. M. Lee, *Prog. Polym. Sci.*, **39**, 164 (2014).

21) B. Ameduri, *Chem. Rev.*, **109**, 6632 (2009).

22) S. K. Sinha, M. Kawaguchi, T. Kato, and F. E. Kennedy, *Tribology Int.*, **36**, 217 (2003).

23) S. Ando, T. Matsuura, and S. Sasaki, *Macromolecules*, **25**, 5858 (1992).

24) I. J. Park, S. B. Lee, C. K. Choi, and K. J. Kim, *J. Colloid Interface Sci.*, **181**, 284 (1996).

25) Y. Hayakawa, M. Nishida, H. Kimoto, S. Fujii, and H. Sawada, *Polym. Bulletin*, **32**, 661 (1994).

26) H. Li, A. Wijekoon, and N. D. Leipzig, *Annals Biomedical Eng.*, **42**, 1456 (2013).

27) Y Furukawa and T Yoneda, *J. Polym. Sci. Part A: Polym. Chem.*, **41**, 2704 (2003).

28) H. R. Allcock, *Curr. Opinion Solid State Mater. Sci.*, **10**, 231 (2006).

29) T. Imae, *Curr. Opinion Colloid Interface Sci.*, **8**, 307 (2003).

30) H. Ghassemi, J. E. McGrath, and T. A. Zawodzinski Jr, *Polymer*, **47**, 4132 (2006).

31) T. Imae, H. Tabuchi, K. Funayama, A. Sato, T. Nakamura, and N. Amaya, *Colloids Surf., A*, **167**, 73 (2000).

32) T. Nishino, Y. Urushihara, M. Meguro, and K. Nakamae, *J. Colloid Interface Sci.*, **279**, 364 (2004).

33) T. Nishino, Y. Urushihara, M. Meguro, and K. Nakamae, *J. Colloid Interface Sci.*, **283**,

533 (2005).

34) H. Ni, X. Wang, W. Zhang, X. Wang, and Z. Shen, *Surf. Sci.*, **601**, 3632 (2007).

35) S. Kubowicz, J. F. Baussard, J. F. Lutz, A. F. Thünemann, H. von Berlepsch, and A. Laschewsky, *Angew. Chem. Int. Ed.*, **44**, 5262 (2005).

36) H. Sawada and T. Kawase, *Kobunshi Ronbunshu*, **58**, 147 (2001).

37) H. Sawada and T. Kawase, *Kobunshi Ronbunshu*, **58**, 255 (2001).

38) H. Sawada, Y.-F. Gong, Y. Minoshima, T. Matsumoto, M. Nakayama, M. Kosugi, and T. Migita, *J. Chem. Soc., Chem. Commun*., 537 (1992).

39) H. Sawada, K. Tanba, N. Itoh, C. Hosoi, M. Baba, T. Kawase, M. Mitanid, and H. Nakajima, *J. Fluorine Chem.*, **77**, 51 (1996).

40) H. Sawada, N. Itoh, T. Kawase, M. Mitani, H. Nakajima, M. Nishida, and Y. Moriya, *Langmuir*, **10**, 994 (1994).

41) H. Sawada, T. Kawase, Y. Ikematsu, Y. Ishii, M. Oue, and Y. Hayakawa, *Chem. Commun.*, 179 (1996).

42) H. Sawada, A. Ohashi, M. Baba, T. Kawase, and Y. Hayakawa, *J. Fluorine Chem.*, **79**, 149 (1996).

43) H. Sawada, S. Katayama, Y. Ariyoshi, T. Kawase, Y. Hayakawa, T. Tomita, and M. Baba, *J. Mater. Chem.*, **8**, 1517 (1998).

44) H. Sawada, Y. Yoshino, Y. Ikematsu, and T. Kawase, *Eur. Polym. J.*, **36**, 231 (2000).

45) H. Sawada, Y. Yoshino, T. Kawase, and K. Fujimori, *Eur. Polym. J.*, **36**, 1533 (2000).

46) H. Sawada, K. Ikeno, and T. Kawase, *Macromolecules*, **35**, 4306 (2002).

47) H. Sawada, E. Sumino, M. Oue, M. Baba, T. Kira, S. Shigeta, M.Mitani, H. Nakajima, M. Nishida, and Y. Moriya, *J. Fluorine Chem*., **21**, 74 (1995).

48) H. Sawada, K. Yanagida, Y. Inaba, M. Sugiya, T. Kawase, and T. Tomita, *Eur. Polym. J.*, **37**, 1433 (2001).

49) J. Nakagawa, K. Kamogawa, H. Sakai, T. Kawase, H. Sawada, J. Manosroi, A. Manosroi, and M. Abe, *Langmuir*, **14**, 2055 (1998).

50) J. Nakagawa, K. Kamogawa, H. Sakai, T. Kawase, H. Sawada, J. Manosroi, A. Manosroi, and M. Abe, *Langmuir*, **14**, 2061 (1998).

51) H. Sawada, J. Iidzuka, T. Maekawa, R. Takahashi, T. Kawase, K. Oharu, H. Nakagawa, and K. Ohira, *J. Colloid Interface Sci.*, **263**, 1 (2003).

52) M. Mugisawa and H. Sawada, *Langmuir*, **24**, 9215 (2008).

53) H. Sawada, J. Iidzuka, T. Kawase, K. Oharu, and H. Nakagawa, *Eur. Polym. J.*, **39**, 1991 (2003).

54) H. Sawada, K. Shindo, J. Iidzuka, K. Ueno, and K. Hamazaki, *Eur. Polym. J.*, **41**, 2232 (2005).

55) H. Sawada, A. Sasaki, K. Sasazawa, T. Kawase, K. Ueno, and K. Hamazaki, *Colloid Polym. Sci.*, **283**, 583 (2005).

56) H. Sawada, A. Sasaki, K. Sasazawa, K. Toriba, H. Kakehi, M. Miura, and N. Isu, *Polym. Adv. Technol.*, **19**, 419 (2008).

57) K. Sasazawa, Y. Hirayama, and H. Sawada, *Polym. Int.*, **58**, 177 (2009).

58) H. Shirakawa, E. J. Louis, A. G. MacDiarmid, C. K. Chiang, and A. J. Heeger, *J. Chem. Soc., Chem. Commun.*, 578 (1977).

59) S. Bhadra, D. Khastgir, N. K. Singha, and J. H. Lee, *Prog. Polym. Sci.*, **34**, 783 (2009).

60) C. L. Chochos and S. A. Choulis, *Prog. Polym. Sci.*, **36**, 1326 (2011).

61) Y. Z. Long, M. M. Li, C. Gu, M. Wan, J. L. Duvail, Z. Liu, and Z. Fan, *Prog. Polym. Sci.*, **36**, 1415 (2011).

62) A. A. Syed and M. K. Dinesan, *Talanta*, **38,** 815 (1991).

63) E. T. Kang, K. G. Neoh, and K. L.Tan, *Prog. Polym. Sci.*, **23**, 277 (1998).

64) J. C. Chaing and A. G. MacDiarmid, *Synth. Met.*, **1**, 193 (1986).

65) W. J. Feast, J. Tsibouklis, K. L. Pouwer, L. Groenendaal, and E. W. Meijer, *Polymer*, **37**, 5017 (1996).

66) L.-M. Hung, C.-H. Chen, and T.-C. Wen, *Electrochimica Acta*, **51**, 5858 (2006).

67) B. Wessling, *Polymer*, **2**, 786 (2010).

68) K. M. Molapo, P. M. Ndangili, R. F. Ajayi, G. Mbambisa, S. M. Mailu, N. Njomo, M. Masikini, P. Baker, and E. I. Iwuoha, *Int. J. Electrochem. Sci.*, **7**, 11859 (2012).

69) Y. Wang, *Int. J. Mater. Res.*, **105**, 3 (2014).

70) H. S Kolla, S. P. Surwade, X. Zhang, A. G. MacDiamid, and S. K. Manohar, *J. Am. Chem. Soc.*, **127**, 16770 (2005).

71) S. Virji, J. Huang, R. B. Kaner, and B. H. Weiller, *Nano Lett.*, **4**, 491 (2004).

72) J. Huang, S. Virji, B. H. Weiller, and R. B. Kaner, *J. Am. Chem. Soc.*, **125**, 314 (2003).

73) E. Song and J.-W. Choi, *Nanomaterials*, **3**, 498 (2013).

74) M. E. Nicho, M. Trejo, A. Garcuía-Valenzuela, J. M. Saniger, J. Palacios, and H. Hu, *Sens. Actuators B Chem.*, **76**, 18 (2001).

75) H. Zengin, W. Zhou, J. Jin, R. Czerw, D. W. Smith, L. Echegoyen, D. L. Carroll, S. H. Foulger, and J. Ballato, *Adv. Mater.*, **14**, 1480 (2002).

76) G. M. O. Barra, M. E. Leyva, B. G. Soares, and M. Sens, *Synth. Met.*, **130**, 239 (2002).

77) A. Pud, N. Ogurtsov, A. Korzhenko, and G. Shapoval, *Prog. Polym. Sci.*, **28**, 1701 (2003).

78) A. Mirmohseni and G.G. Wallace, *Polymer*, **44**, 3523 (2003).

79) S. K. Siddhanta and R. Gangopadhyay, *Polymer*, **46**, 2993 (2005).

80) T. Hino, T. Namiki, and N. Kuramoto, *Synth. Met.*, **156**, 1327 (2006).

81) A. Airoudj, D. Debarnot, B. Bêche, and F. Poncin-Epaillard, *Talanta*, **77**, 1590 (2009).

82) D.-W. Wang, F. Li, J. Zhao, W. Ren, Z.-G. Chen, J. Tan, Z.-S. Wu, I. Gentle, G. Q. Lu, and H.-M. Cheng, *ACS Nano*, **3**, 1745 (2009).

83) J. Niessen, U. Schröder, M. Rosenbaum, and F. Scholz, *Electrochem. Commun.*, **6**, 571 (2004).

84) M. Sahin, L. Özcan, A. Özcan, B. Usta, Y. Sahin, and K. Pekmez, *J. Appl. Polym. Sci.*, **115**, 3024 (2010).

85) W. E. Rudzinski, L. Thrower, R. Sutcliffe, and M. Bahrami, *Synth. Met.*, **94**, 193 (1998).

86) M. Ranger and M. Leclerc, *Synth. Met.*, **84**, 85 (1997).

87) E. S. Matveeva, R. C. Patil, and M. J. Gonzalez Tejera, *Synth. Met.*, **123**, 343 (2001).

88) N. A. Zaidi, J. P. Foreman, G. Tzamalis, S. C. Monkman, and A. P. Monkman, *Adv. Funct. Mater.*, **14**, 479 (2004).

89) S. Palaniappan and S. L. Devi, *J. Appl. Polym. Sci.*, **107**, 1887 (2008).

90) H. Fan, H. Wang, J. Guo, N. Zhao, and J. Xu, *J. Colloid Interface Sci.*, **409**, 255 (2013).

91) X. Zhou, Z. Zhang, X. Xu, X. Men, and X. Zhu, *Appl. Surf. Sci.*, **276**, 571 (2013).

92) Y. Zhu, L. Feng, F. Xia, J. Zhai, M. Wan, and L. Jiang, *Macromol. Rapid Commun.*, **28**, 1135 (2007).

93) L. Xu, Z. Chen, W. Chen, A. Mulchandani, and Y. Yan, *Macromol. Rapid Commun.*, **29**, 832 (2008).

94) Y. Wang, J. Zhang, D. Sheng, and C. Sun, *J. Chromatogr. A*, **1217**, 4523 (2010).

95) Y. Zhu, J. Li, H. He, M. Wan, and L. Jiang, *Macromol. Rapid Commun.*, **28**, 2230 (2007).

96) J. Yang, P. K. Shen, J. Varcoe, and Z. Wei, *J. Power Sources*, **189**, 1016 (2009).

97) Z. Shi, H. Zhou, T. Dai, and Y. Lu, *J. Colloid Interface Sci.*, **385**, 211 (2012).

CHAPTER 1

Preparation of Novel Fluoroalkyl End-capped Oligomers/Polyaniline and /*N,N'*-Diphenyl-1,4-phenylenediamine Nanocomposites

1.1. Introduction

Among a variety of electrically conducting polymeric materials, polyaniline (**PAn**) has attracted considerable attention in recent years due to its high environmental stability, ease of preparation, low cost, high electrical conductivity and potential applications in electronic devises, batteries and sensors.[1–3] However, **PAn** is infusible thermally and insoluble in traditional organic solvents due to its rigid conjugated backbone. Thus, there have been hitherto numerous attempts for the preparation of colloidal stable **PAn** by using a variety of surfactants such as sodium dodecylsulfate and dodecylbenzenesulfonic acid, because this is a practical way to alleviate the poor processability associated with this material.[4, 5] Another method is the preparation of **PAn** derivatives through the incorporation of some substituted groups such as sulfo and boronic acid units into aniline monomer.[6–13] Partially fluoroalkylated polymers, especially fluoroalkyl end-capped oligomers are attractive polymeric surfactants, because they exhibit various unique properties such as high solubility, surface-active properties, biological activities and nanometer size-controlled molecular aggregates, which cannot be achieved by the corresponding non-fluorinated and randomly fluoroalkylated ones.[14–18] For example, self-assembled fluorinated oligomeric aggregates formed by fluoroalkyl end-capped oligomers could interact with a variety of guest molecules

such as fullerene and single-walled carbon nanotube to afford the fluorinated oligomeric aggregates/guest molecule nanocomposites.[19–23] Therefore, it is in particular interest to develop novel fluoroalkyl end-capped oligomers/**PAn** nanocomposites possessing unique characteristics imparted by both fluorine and **PAn**, from the developmental viewpoints of new fluorinated functional materials. This chapter shows that **PAn** and phenylcapped aniline dimer (**An-dimer**: *N,N'*-diphenyl-1,4-diphenyldiamine), which is considered to be an excellent model of **PAn**, are applied to the preparation of the novel fluorinated oligomeric nanocomposites possessing a good dispersibility and stability under mild conditions by the use of fluoroalkyl end-capped oligomers such as fluoroalkyl end-capped acrylic acid oligomer, 2-(methacryloyloxy)ethanesulfonic acid oligomer and 2-acrylamido-2-methylpropane-sulfonic acid oligomer.

1.2. Experimental

1.2.1. Measurements

Molecular weight of R_F-$(ACA)_n$-R_F oligomer [Mn = 3,520] was measured using a Shodex DS-4 (pump) and Shodex RI-71 (detector) gel permeation chromatography (Tokyo, Japan) calibrated with polystyrene standard using tetrahydrofuran (THF) as the eluent. Molecular weights of R_F-$(MES)_n$-R_F oligomer (Mn = 13,700) and R_F-$(AMPS)_n$-R_F [Mn = 20,500] were determined by using the same gel permeation chromatography calibrated pullulan (molecular weights: 2,000 ~ 50,000) and poly(ethylene glycol) (molecular weight, 1,000 ~ 40,000) standards, respectively, by using 0.5 mol dm^{-3} Na_2HPO_4 aqueous solution as the eluent. Thermal analyses were recorded by raising the temperature around 800 °C (the heating rate, 10 °C/min) under atmospheric conditions by the use of Bruker axs TG-DTA2000SA differential thermobalance (Kanagawa, Japan). Dynamic light-scattering (DLS) measurements were performed using Otsuka Electronics DLS-7000 HL (Tokyo, Japan). FE-SEM images were measured by using a JEOL JSM-5300 (Tokyo, Japan). UV-vis spectra were measured by using Shimadzu UV-1600 UV–vis spectrophotometer (Kyoto, Japan).

1.2.2. Materials

Acrylic acid was used as received from Toagosei Co., Ltd. (Tokyo, Japan). 2-(Methacrylolyoxy)ethanesulfonic acid and 2-acrylamido-2-methylpropanesulfonic acid were purchased from Polyscience, Inc. (PA, USA) and Wako Pure Chemical Industries, Ltd. (Osaka, Japan), respectively. Aniline and **An-dimer** were purchased from Tokyo Kasei Kogyo Co., Ltd. **PAn** (emeraldine base) was purchased from Alfa Aesar, A Johnson Matthey Company Inc. (MA, USA). R_F-$(ACA)_n$-R_F oligomer, R_F-$(MES)_n$-R_F oligomer and R_F-$(AMPS)_n$-R_F oligomer were prepared by reaction of fluoroalkanoyl peroxide with the corresponding monomers according to the previously reported methods.[24-26)]

1.2.3. Preparation of fluoroalkyl end-capped acrylic acid oligomer/PAn nanocomposites

To an aqueous solution (12 ml) of fluoroalkyl end-capped acrylic acid oligomer {R_F-$[CH_2CHC(=O)OH]_n$-R_F [R_F-$(ACA)_n$-R_F]; R_F=$CF(CF_3)OC_3F_7$ (6 mg)}, was added aniline (24 mg). The mixture was stirred with a magnetic stirring bar at room temperature for 30 min. A 5.5 ml APS (58 mg) aqueous solution was added dropwise to the solution containing aniline and fluorinated oligomer with continuously stirring at room temperature for 1 day.

After the removal of solvent, the crude product was dialyzed in water to give the expected R_F-(ACA)$_n$-R_F/**PAn** nanocomposites. The nanocomposites thus obtained were dried in vacuo at 50 °C for 2 days to afford brown-colored powders (11.3 mg). R_F-(MES)$_n$-R_F/**PAn** and R_F-(AMPS)$_n$-R_F/**PAn** nanocomposites were also prepared under similar conditions to afford dark green-colored powders, respectively.

1.2.4 Preparation of R_F-(MES)$_n$-R_F/An-dimer nanocomposites

R_F-(MES)$_n$-R_F oligomer [R_F=CF(CF_3)OC_3F_7: 60 mg] was added to a methanol solution (10 ml) of **An-dimer** (10 mg). The mixture was stirred with a magnetic stirring bar at room temperature for 1 day. After the removal of solvent, the nanocomposites thus obtained were dried in vacuo at 50 °C for 2 days to afford light-blue colored powders. R_F-(AMPS)$_n$-R_F/**An-dimer** nanocomposites and R_F-(ACA)$_n$-R_F/**An-dimer** nanocomposites were also prepared under similar conditions to give light blue-colored powders.

1.3. Results and discussion

The polymerization of aniline catalyzed by ammonium persulfate (APS) was conducted in the presence of fluoroalkyl end-capped acrylic acid oligomer [R_F-$(ACA)_n$-R_F] in aqueous solutions at room temperature.

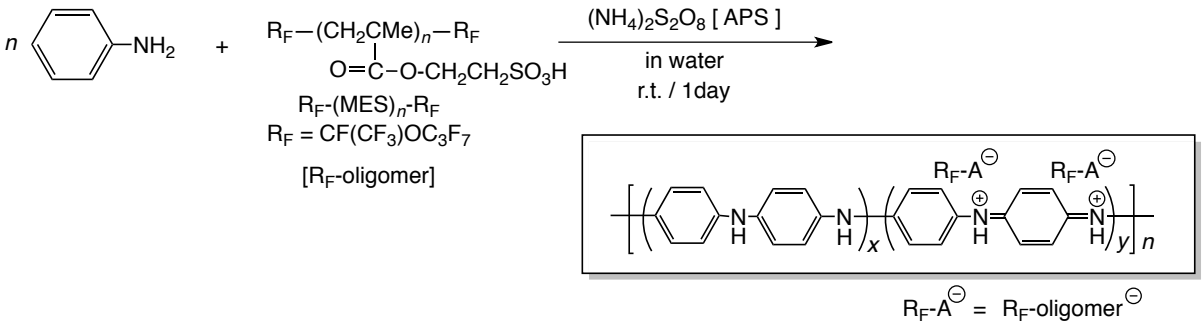

Scheme 1-1

The color change from colorless to brown is observed in this polymerization system. However, fluoroalkyl endcapped 2-(methacryloyloxy)ethanesulfonic acid oligomer [R_F-$(MES)_n$-R_F] (see Scheme 1-1) and 2-acrylamido-2-methylpropanesulfonic acid oligomer [R_F-$(AMPS)_n$-R_F] were found to afford the clear color change from colorless to dark green in the polymerizations of aniline. Such differences in the color changes would be due to the lower acidic R_F-$(ACA)_n$-R_F oligomer, compared with that of R_F-$(MES)_n$-R_F oligomer or R_F-$(AMPS)_n$-R_F oligomer. It is suggested that the polymerizations of aniline catalyzed by APS in the presence of R_F-$(MES)_n$-R_F oligomer and R_F-$(AMPS)_n$-R_F oligomer can proceed

smoothly to give the expected corresponding oligomers/**PAn** nanocomposites. In fact, Ultraviolet-visible (UV-vis) spectra showed that an absorption peak around 289 nm related to the residual aniline monomer has been completely consumed through each polymerization process; however, small amounts (Run 1, 0.7%; Run 2, 0.01% based on the products) of unreacted aniline monomer have been detected after polymerization with R_F-$(ACA)_n$-R_F oligomer (see Table 1-1 and Figs. 1-1 ~ 1-3).

Table 1-1 Preparation of fluoroalkyl end-capped oligomers(R_F-oligomers)/PAn nanocomposites

Run	Aniline (mg)	R_F-oligomer (mg)	APS (mg)	Product yield (%) [a]	Size of nanocomposites (nm) [b]
R_F-$(ACA)_n$-R_F (size of this oligomeric aggregates, 36 ± 6 nm) [b]					
1	24	6	58	38 [c, e]	136 ± 24
2	24	140	58	77 [d, e]	281 ± 23.6
R_F-$(MES)_n$-R_F (size of this oligomeric aggregates, 58 ± 8 nm) [b]					
3	47	48	115	89 [e] (77) [f]	128 ± 15 [e] (98 ± 12) [f]
4	47	94	115	96 [e] (85) [f]	105 ± 14 [e] (103 ± 13) [f]
5	47	189	115	97 [e] (87) [f]	124 ± 12 [e] (33 ± 6) [f]
6	47	280	115	94 [e] (80) [f]	54 ± 5 [e] (33 ± 5) [f]
R_F-$(AMPS)_n$-R_F (size of this oligomeric aggregates, 27 ± 7 nm) [b]					
7	47	47	115	74 [f]	118 ± 13
8	47	94	115	61 [f]	131 ± 17
9	47	188	115	99 [f]	79 ± 9
10	47	282	115	95 [f]	75 ± 7

[a] Yields were based on the used aniline and R_F-oligomer
[b] Determined by dynamic light scattering(DLS) measurements
[c] Residual amount of aniline in the product, 0.7% (determined by UV-vis spectra)
[d] Residual amount of aniline in the product, 0.01% (determined by UV-vis spectra)
[e] Purified by dialysis
[f] Purified by the reprecipitation method (H_2O/tetrahydrofuran)

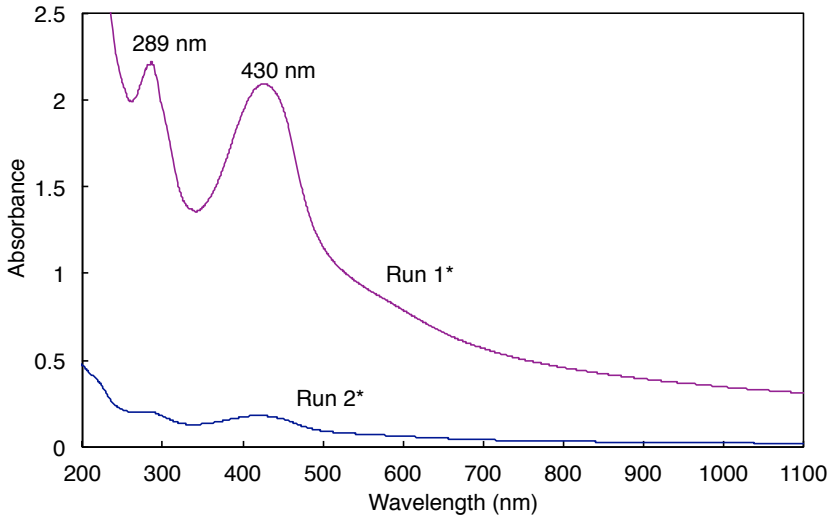

Fig. 1-1 UV-vis spectra of aqueous solutions of R_F-$(ACA)_n$-R_F/PAn nanocomposites; Run 1*: concentration of composites, 200 mg/dm^3 and Run 2*: concentration of composites, 100 mg/dm^3
*Each different from that of Table 1-1

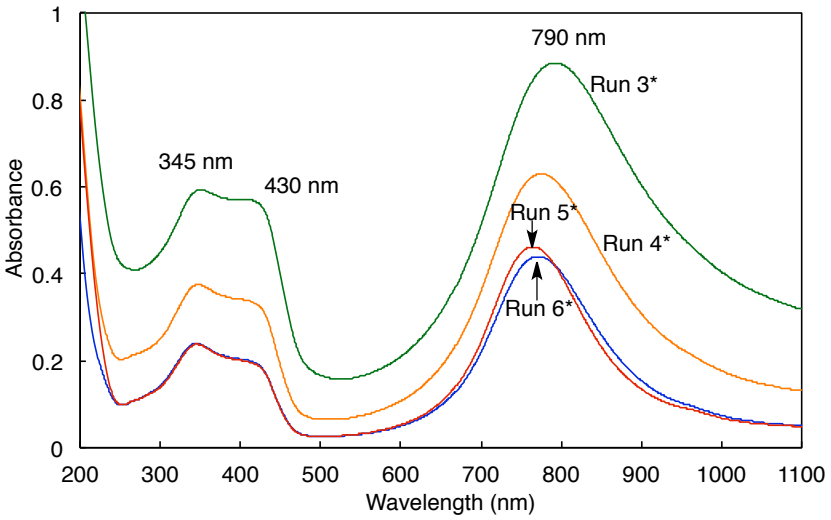

Fig. 1-2 UV-vis spectra of aqueous solutions of R_F-$(MES)_n$-R_F/PAn nanocomposites**; concentration of composites, 33 mg/dm^3.
*Each different from that of Table 1.
**These composites were purified by the reprecipitation method.

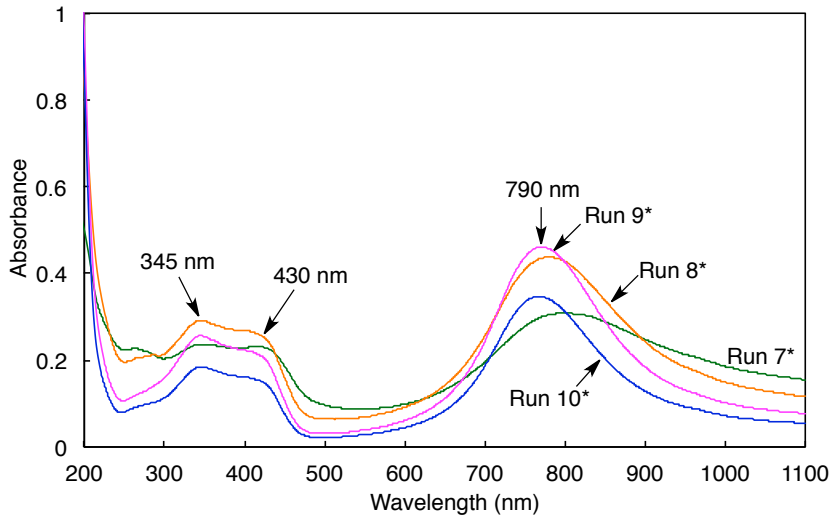

Fig. 1-3 UV-vis spectra of aqueous solutions of R_F-$(AMPS)_n$-R_F/PAn nanocomposites**; concentration of composites, 33 mg/dm^3.
*Each different from that of Table 1.
**These composites were purified by the reprecipitation method.

In this way, R_F-$(MES)_n$-R_F oligomer and R_F-$(AMPS)_n$-R_F oligomer can interact with aniline to cause a completely disappearance of an absorption band around 289 nm related to aniline monomer; however, R_F-$(ACA)_n$-R_F oligomer cannot afford such an effective acid–base interaction under similar conditions due to its lower acidity. Especially, lower acidic R_F-$(ACA)_n$-R_F oligomer is not likely to protonate the imine nitrogens on the polymer backbone in the self-assembled R_F-$(ACA)_n$-R_F oligomeric aggregate cores. The outline of these polymerization processes and the product yields were summarized in Scheme 1-1 and Table 1-1. The isolated yields of R_F-$(ACA)_n$-R_F/**PAn** nanocomposites increased from 38% to 77%, with increasing the feed amounts of R_F-$(ACA)_n$-R_F oligomer, and the similar increase from 89% to 97% or 61% to 99% was observed in R_F-$(MES)_n$-R_F/**PAn** nanocomposites or R_F-$(AMPS)_n$-R_F/**PAn** composites. A higher feed amount of fluorinated MES oligomer or

AMPS oligomer based on the aniline monomer would afford the effective formation of anilinium cations to proceed the smooth redox polymerizations as shown in Scheme 1-1.

Fluorinated oligomers/**PAn** composites thus obtained were shown to exhibit a good dispersibility and stability not only in water but also in traditional organic media such as methanol, ethyl acetate, acetic acid, acetonitrile, 1,2-dichloroethane and *N,N*-dimethylformaide. Of particular interest, R_F-(ACA)$_n$-R_F/**PAn** composites and R_F-(MES)$_n$-R_F/**PAn** composites were also found to exhibit a dispersibility in fluorinated aliphatic solvents such as AK-225: 1:1 mixed solvents of 1,1-dichloro-2,2,3,3,3-pentafluoropropane and 1,3-dichloro-1,2,2,3,3-pentafluoropropane. This finding would be due to the presence of fluorinated oligomers in the composites. Thus, the present fluorinated **PAn** composites were found to exhibit a good dispersibility in methanol. The size of these fluorinated composites in methanol has been measured by dynamic light-scattering (DLS) measurements at 25 °C, and the results were also shown in Table 1-1. Each fluorinated composite in Table 1-1 was nanometer size-controlled very fine nanoparticles from 33 to 281 nm. In order to clarify the formation of fluorinated nanocomposite particles, the field emission scanning electron micrograph (FE-SEM) of methanol solutions of R_F-(ACA)$_n$-R_F/**PAn** nanocomposites, R_F-(MES)$_n$-R_F/**PAn**

nanocomposites and R_F-$(AMPS)_n$-R_F/**PAn** nanocomposites has been measured, and the results were shown in Fig. 1-4.

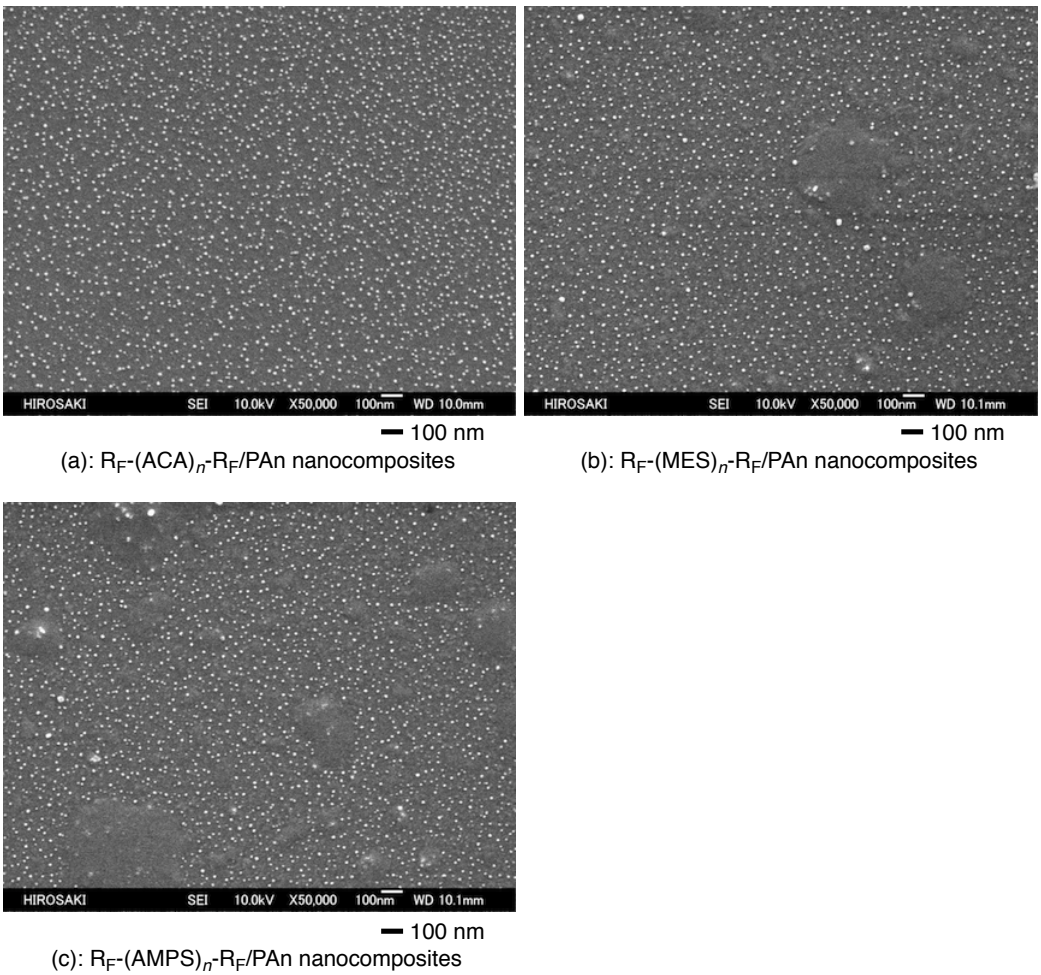

(a): R_F-$(ACA)_n$-R_F/PAn nanocomposites

(b): R_F-$(MES)_n$-R_F/PAn nanocomposites

(c): R_F-$(AMPS)_n$-R_F/PAn nanocomposites

Fig. 1-4 Field emission scanning electron microscopy images of (a): R_F-$(ACA)_n$-R_F/PAn nanocomposites (Run 1 in Table 1), (b): R_F-$(MES)_n$-R_F/PAn nanocomposites (Run 3 in Table 1), and (c): R_F-$(AMPS)_n$-R_F/PAn nanocomposites (Run 7 in Table 1)

Electron micrograph of these composites also showed the formation of fluorinated composite fine particles with mean diameters of 15 nm [(**a**) in Fig. 1-4], 17 nm [(**b**) in Fig. 1-4] and 16 nm [(**c**) in Fig. 1-4], and the smaller size values than those (118 ~ 136 nm) of

DLS were obtained in FE-SEM measurements. The difference in the average sizes determined by DLS and SEM would be due to the strong aggregate characteristic between the end-capped fluoroalkyl segments in fluorinated oligomers/**PAn** nanocomposites in methanol during DLS measurements.

UV-vis spectra of aqueous solutions of R_F-(ACA)$_n$-R_F/**PAn** nanocomposites, R_F-(MES)$_n$-R_F/**PAn** nanocomposites, and R_F-(AMPS)$_n$-R_F/**PAn** nanocomposites have been measured in order to clarify the presence of **PAn** in the composites, and the results were shown in Figs. 1-1 ~ 1-3.

The absorption spectra for R_F-(MES)$_n$-R_F/**PAn** nanocomposites and R_F-(AMPS)$_n$-R_F/**PAn** nanocomposites are similar to those of the pure acid-doped **PAn** system.[27, 28] The characteristic peaks of acid-doped **PAn** appears around 350, 430 and 780 nm, which can be attributed to π–π* transition in the benzenoid structure, polaron–π* and π–polaron transition, respectively, suggesting that the present prepared **PAn**s in the nanocomposites are in the doped state as shown in Scheme 1-1. R_F-(ACA)$_n$-R_F/**PAn** nanocomposites can exhibit polaron–π* transition around 430 nm. However, the UV-vis spectra of R_F-(ACA)$_n$-R_F/**PAn** nanocomposites are quite different from those in R_F-(MES)$_n$-R_F/**PAn** nanocomposites and R_F-(AMPS)$_n$-R_F/**PAn** nanocomposites. R_F-(ACA)$_n$-R_F/**PAn** nanocomposites exhibited only a sharp polaron absorption around 430 nm with a small amounts of unreacted aniline

monomer's absorption around 289 nm. It is well known that UV-vis spectra of **PAn**/poly(2-methoxyaniline-5-sulfonic acid) nanocomposites in water exhibit some bands which are attributed to π-π* transition at 330 nm and the lower wavelength polaron band at 474 nm with the broad delocalized polaron transition.[12] Poly(acrylic acid)-doped **PAn**, which was prepared by the addition of acrylic acid to the reaction mixture containing aniline and HCl catalyzed by ammonium persulfate, exhibits the π-π* transition of the benzenoid rings around 320 nm and the localized polarons around 400 ~ 420 nm, together with increasing absorbance around 850 ~ 1100 nm in *m*-cresol.[29] Yang et al. reported that poly(acrylic acid)-doped **PAn** also showed the similar UV-vis absorptions as those of acrylic acid-doped **PAn**.[30] Similar UV-vis absorptions to those of acrylic acid and poly(acrylic acid)-doped **PAn**s were observed in dodecybenzenesulfonic acid- and pentadecybenzensulfonic acid-doped **PAn** in *m*-cresol.[31] Kuramoto et al. reported that absorption peaks of HCl-doped **PAn**s, which were prepared in the presence of sodium dodecylsulfate, are very sensitive to the pH changes.[4] The lower pH region from 3.3 to 7.8 gives the absorption peaks around 788 ~ 860 nm, and the higher pH region (8.6 ~ 11.0) can give the blue-shifted absorption peaks (616 ~ 554 nm), respectively.[4] These spectra changes from lower to higher pH regions are based on the changes from the protonated quinoid diimine structure to the corresponding unprotonated structure.[32, 33] On the other hand, the present R_F-$(ACA)_n$-R_F/**PAn**

nanocomposites can exhibit only a sharp polaron transition around 430 nm as shown in Fig. 1-1. This finding would be dependent upon it that the polaron structures, which are characteristic of the protonated **PAn** cation radicals, can form the more stable delocalized polaron structures in the fluoroalkyl end-capped acrylic acid oligomeric aggregates as shown in Scheme 1-2.

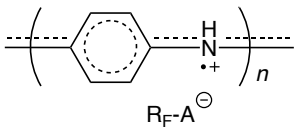

$R_F\text{-}A^{\ominus}$: $R_F\text{-}(CH_2CH)_n\text{-}R_F$ with $O{=}C{-}O^{\ominus}$

Scheme 1-2

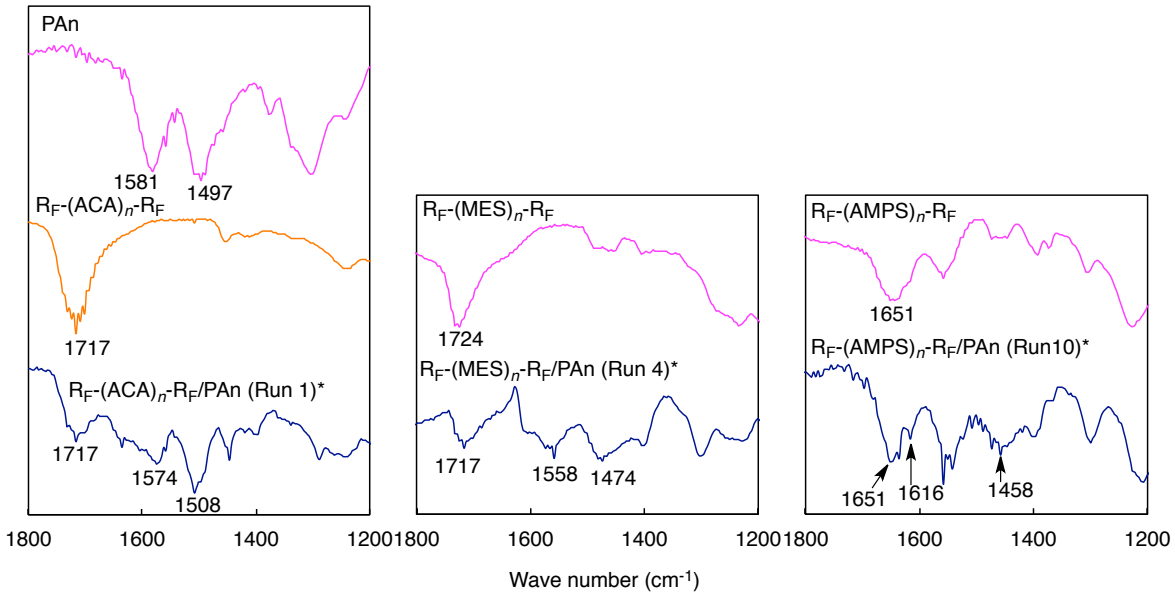

Fig. 1-5 FT-IR spectra of fluoroalkyl end-capped oligomers/PAn nanocomposites, PAn (commercial grade), and parent fluoroalkyl end-capped oligomers.
* Each different from those of Table 1

Fig. 1-5 shows the FT-IR spectra of R_F-$(ACA)_n$-R_F/**PAn** nanocomposites, R_F-$(MES)_n$-R_F/**PAn** nanocomposites and R_F-$(AMPS)_n$-R_F/**PAn** nanocomposites, respectively. Each FT-IR spectrum of the nanocomposites shows the presence of the corresponding fluorinated oligomer, due to exhibiting typical absorption bands related to carboxyl, ester, or amide groups in oligomers around 1,651 ~ 1,724 cm^{-1}. The characteristic peaks of **PAn** in the composites were also assigned as follows: the peaks at 1,574 ~ 1,616 cm^{-1} and 1,458 ~ 1,508 cm^{-1} were attributable to C=N and C=C stretching mode for quinoid and benzenoid rings.[34] The ratio of the relative intensities of benzenoid to quinoid ring modes ($I_{benzenoid}/I_{quinoid}$) shows the percentage of benzenoid units in **PAn**, and a higher $I_{benzenoid}/I_{quinoid}$ value: 1.7 was obtained in R_F-$(ACA)_n$-R_F/**PAn** nanocomposites, compared with 1.1 of R_F-$(MES)_n$-R_F/**PAn** nanocomposites, or 0.6 of R_F-$(AMPS)_n$-R_F/**PAn** nanocomposites. These findings suggest that R_F-$(ACA)_n$-R_F/**PAn** nanocomposites are likely to form the more stable delocalized polaron structure[1] to exhibit only a polaron–π^* transition around 430 nm as shown in Scheme 1-2.

In order to clarify the presence of fluoroalkyl end-capped oligomers in the nanocomposites, these nanocomposites have been analyzed by the use of TGA (thermogravimetric analyses) measurements, in which the weight loss of these composites was measured by raising the temperature to around 800 °C, and the results were shown in Fig. 1-6.

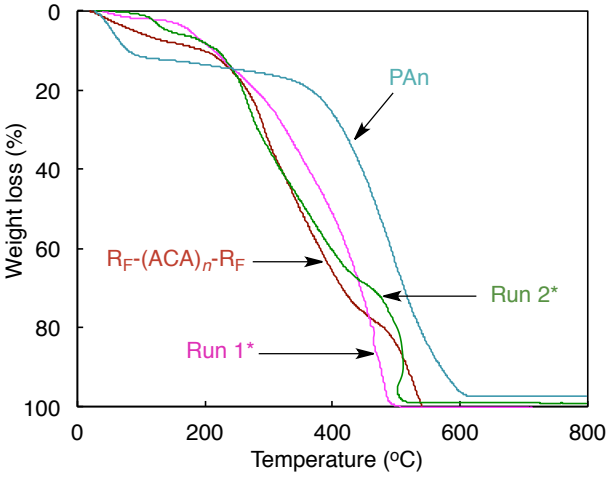

(a): R_F-(ACA)$_n$-R_F/PAn nanocomposites

Feed amounts of R_F-(ACA)$_n$-R_F oligomer (mg)		T_{dec} (°C)
Run 1*	6	279
Run 2*	140	260
Parent R_F-(ACA)$_n$-R_F oligomer		267
PAn (commerical grade)		367

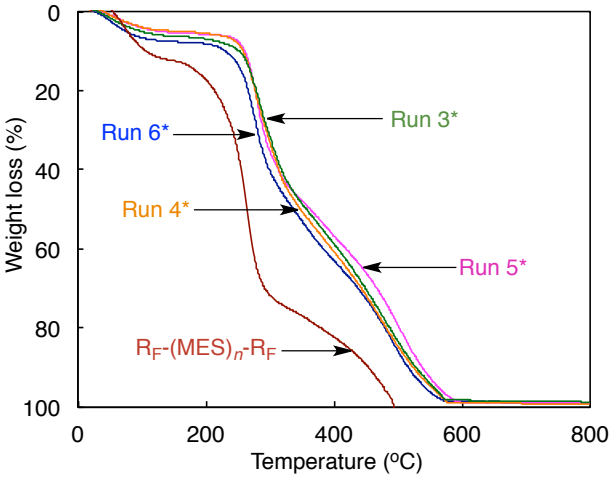

(b): R_F-(MES)$_n$-R_F/PAn nanocomposites

Feed amounts of R_F-(MES)$_n$-R_F oligomer (mg)		T_{dec} (°C)
Run 3*	48	278
Run 4*	94	277
Run 5*	189	277
Run 6*	280	266
Parent R_F-(MES)$_n$-R_F oligomer		213

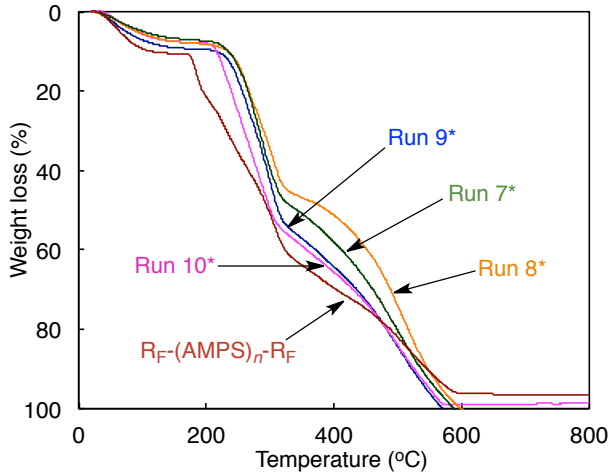

(c): R_F-(AMPS)$_n$-R_F/PAn nanocomposites

Feed amounts of R_F-(AMPS)$_n$-R_F oligomer (mg)		T_{dec} (°C)
Run 7*	47	265
Run 8*	94	267
Run 9*	188	239
Run 10*	282	256
Parent R_F-(AMPS)$_n$-R_F oligomer		195

Fig. 1-6 Thermogravimetric analyses of (a): R_F-(ACA)$_n$-R_F/PAn nanocomposites, (b): R_F-(MES)$_n$-R_F/PAn nanocomposites, and (c): R_F-(AMPS)$_n$-R_F/PAn nanocomposites
*Each different from those in Table 1

The TGA curve of these composites showed a variety of fluoroalkyl end-capped oligomers/**PAn** nanocomposites in Table 1-1 lost 20% of their weights around 239 ~ 279 °C. The thermal stability: T_{dec} (defined by a 20% mass loss 10 °C/min heating rate under air atmosphere conditions) of fluorinated nanocomposites decreased with an increase of fluorinated oligomers in the absolute amounts of the corresponding oligomers based on aniline monomer in nanocomposite preparations in Table 1-1 from 6 to 282 mg. The thermal stability of R_F-(ACA)$_n$-R_F/**PAn** nanocomposites, R_F-(MES)$_n$-R_F/**PAn** nanocomposites and R_F-(AMPS)$_n$-R_F/**PAn** nanocomposites were in general superior to that of the corresponding parent fluorinated oligomers, indicating that these nanocomposites contain fluorinated oligomers and **PAn**.

In order to verify the interaction of **PAn** with fluoroalkyl end-capped oligomers illustrated

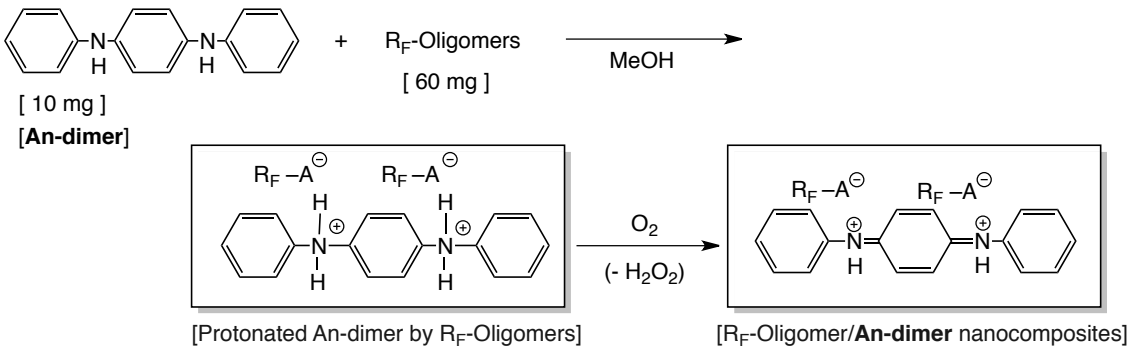

Size of nanocomposites:
R_F-(ACA)$_n$-R_F/**An-dimer** nanocomposites: 37 ± 4 nm [36 ± 6 nm]*
R_F-(MES)$_n$-R_F/**An-dimer** nanocomposites: 11 ± 2 nm [58 ± 8 nm]*
R_F-(AMPS)$_n$-R_F/**An-dimer** nanocomposites: 10 ± 1 nm [27 ± 7 nm]*
*Size of parent R_F-Oligomeric aggregates

Scheme 1-3

in Scheme 1-1, the interaction of these fluorinated oligomers with phenyl-capped aniline dimer: *N,N'*-diphenyl-1,4-diphenyldiamine (**An-dimer**), which is considered to be an excellent model of **PAn**, is tried to study. The results are shown in Scheme 1-3 and Fig. 1-7.

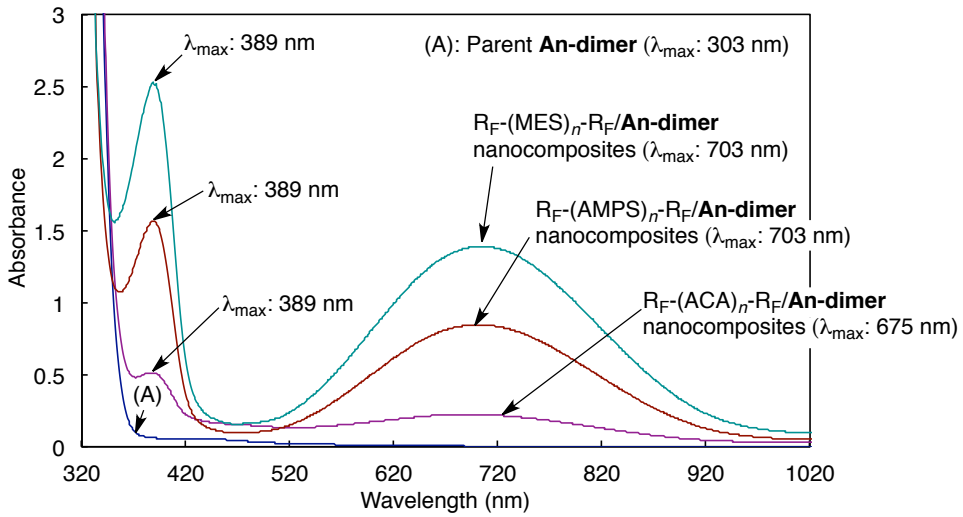

Fig. 1-7 UV-vis spectra of methanol containing R_F-Oligomers/An-dimer nanocomposites and parent An-dimer in methanol; concentration of R_F-Oligomers, 6.0 g/dm^3 and concentration of An-dimer, 1.0 g/dm^3

As shown in Scheme 1-3 and Fig. 1-7, fluoroalkyl end-capped oligomers were found to react with **An-dimer** to afford fluorinated oligomers/**An-dimer** composites through the formation of protonated **An-dimer** salt by fluorinated oligomers at room temperature. A distinct color change from yellow to deep blue was observed in each composite reaction. In fact, UV-vis spectra show that these fluorinated **An-dimer** composites have two absorption peaks around 389 nm and 675 ~ 703 nm, respectively, corresponding to the protonated **An-dimer** and the polaron transition in the doped forms. Previously, Wudl and Heeger et al.

reported the preparation of phenyl-capped octaaniline [C_6H_5-NH-(C_6H_4-NH)$_7$-C_6H_5], and UV-vis spectra of this aniline derivative shows an absorption peak around 320 nm in *N,N*-dimethylformaide (DMF).[32] Hydrochloric acid doped phenyl-capped octaaniline in DMF can exhibit similar absorption peaks around 380 and 700 nm to those of the present fluorinated **An-dimer** composites, indicating that the Brønsted acid doping behavior of the present nanocomposites is consistent with that of octaaniline derivative.[32] Interestingly, the absorbance around 700 nm was found to become higher with the increase of the acidity of fluorinated oligomers, and the higher absorbance was obtained in R_F-(MES)$_n$-R_F oligomer or R_F-(AMPS)$_n$-R_F oligomer. This finding is quite similar to that of the formation of fluorinated oligomers/**PAn** nanocomposites, and R_F-(MES)$_n$-R_F oligomer or R_F-(AMPS)$_n$-R_F oligomer are effective for the preparation of the expected **PAn** nanocomposites. The size of these fluorinated oligomers/**An-dimer** composites in methanol has been measured by the use of DLS measurements. The size of these composites is nanometer size-controlled: 10 ~ 37 nm, and the size of these composites was different from that of the parent fluorinated oligomeric aggregates (27 ~ 58 nm) as shown in Scheme 1-3. This suggests that the nanocomposite reactions should proceed smoothly to afford the fluorinated oligomers/**An-dimer** nanocomposites under very mild conditions.

1.4. Conclusion

In conclusions, novel fluoroalkyl end-capped oligomers/**PAn** composites were prepared by the polymerization of aniline catalyzed by ammonium persulfate in the presence of the corresponding oligomers. These obtained fluorinated oligomers/**PAn** composites exhibited a good dispersibility and stability in water and traditional organic media such as methanol, *t*-butyl alcohol, acetic acid, dimethyl sulfoxide, DMF, acetonitrile, ethyl acetate, 1,2-dichloroethane and fluorinated aliphatic solvents such as AK-225. DLS and FE-SEM measurements showed that these composites can form the nanometer size-controlled fine particles in methanol. UV-vis spectra of R_F-$(MES)_n$-R_F/**PAn** nanocomposites and R_F-$(AMPS)_n$-R_F/**PAn** nanocomposites in aqueous solutions showed three characteristic absorption bands of acid-doped **PAn** around 350, 430 and 780 nm, which were attributed to π-π*, polaron–π* and π-polaron transitions, respectively. On the other hand, R_F-$(ACA)_n$-R_F/**PAn** nanocomposites were found to exhibit only a sharp polaron absorption peak around 430 nm. This is due to the lower acidity of R_F-$(ACA)_n$-R_F oligomer, compared with that of R_F-$(MES)_n$-R_F oligomer or R_F-$(AMPS)_n$-R_F oligomer. Especially, the polaron structures in R_F-$(ACA)_n$-R_F/**PAn** nanocomposites, which are characteristic of the protonated **PAn** cation radicals, can form the more stable delocalized polaron structures in the

fluoroalkyl end-capped acrylic acid oligomeric aggregate cores. R_F-$(ACA)_n$-R_F oligomer, R_F-$(MES)_n$-R_F oligomer and R_F-$(AMPS)_n$-R_F oligomer can react with **An-dimer** to afford the protonated **An-dimer** cations and the protonated quinoid-type **An-dimer**, respectively. The formation of protonated quinoid-type **An-dimer** is quite similar to that of the corresponding oligomers/**PAn** nanocomposites.

References

1) S. Bhadra, D. Khastgir, N. K. Singha, and J. H. Lee, *Prog. Polym. Sci.*, **34**, 783 (2009).

2) J. Huang, S. Virji, B. H. Weiller, and R. B. Kaner, *Chem. Eur. J.*, **10**, 1314 (2004).

3) E. T. Kang, K. G. Neoh, and K. L. Tan, *Prog. Polym. Sci.*, **23**, 277 (1998).

4) N. Kuramoto and E. M. Geniès, *Synth. Met.*, **68**, 191 (1995).

5) L. Yu, J.-I. Lee, K.-W. Shin, C.-E. Park, and R. Holze, *J. Appl. Polym. Sci.*, **88**, 1550 (2003).

6) Y. Haba, E. Segal, M. Narkis, G.I. Titelman, and A. Siegmann, *Synth. Met.*, **106**, 59 (1999).

7) E. V. Strounina, R. Shepherd, L. A. P. Kane-Maguire, and G. G. Wallace, *Synth. Met.,* **135–136**, 289 (2003).

8) B. A. Deore and M. S. Freund, *Macromolecules*, **42**, 164 (2009).

9) J. Yue and A. J. Epstein, *J. Am. Chem. Soc.*, **112**, 2800 (1990).

10) B. A. Deore, I. Yu, and M. S. Freund, *J. Am. Chem. Soc.*, **126**, 52 (2004).

11) F. Masdarolomoor, P. C. Innis, S. Ashraf, R. B. Kaner, and G. G. Wallance, *Macromol. Rapid Commun.*, **27**, 1995 (2006).

12) B. C. Roy, M. D. Gupta, L. Bhoumik, and J. K. Ray, *Synth. Met.*, **130**, 27 (2002).

13) Y.-P. Zhang, S.-H. Lee, K. R. Reddy, A. I. Gopalan, and K.-P. Lee, *J. Appl. Polym. Sci.*, **104**, 2743 (2007).

14) H. Sawada, *Chem. Rev.*, **96**, 1779 (1996).

15) H. Sawada, *J. Fluorine Chem.*, **105**, 219 (2000).

16) H. Sawada, *Prog. Polym. Sci.*, **32**, 509 (2007).

17) H. Sawada, *Polym. J.*, **39**, 637 (2007).

18) H. Sawada, *J. Fluorine Chem.*, **121**, 111 (2003).

19) H. Sawada, J. Iidzuka, T. Maekawa, R. Takahashi, T. Kawase, K. Oharu, H. Nakagawa, and K. Ohira, *J. Colloid Interface Sci.*, **263**, 1 (2003).

20) H. Sawada, J. Iidzuka, T. Kawase, K. Oharu, and H. Nakagawa, *Eur. Polym. J.*, **39**, 1991 (2003).

21) H. Sawada, N. Naitoh, R. Kasai, and M. Suzuki, *J. Mater. Sci.*, **43**, 1080 (2008).

22) H. Sawada, K. Shindo, K. Ueno, and K. Hamazaki, *Polym. Adv. Technol.*, **16**, 764 (2005).

23) H. Sawada, K. Shindo, J. Iidzuka, K. Ueno, and K. Hamazaki, *Eur. Polym. J.*, **41**, 2232 (2005).

24) H. Sawada, Y.-F. Gong, Y. Minoshima, T. Matsumoto, M. Nakayama, M. Kosugi, and T. Migita, *J. Chem. Soc., Chem. Commun.*, 537 (1992).

25) H. Sawada, A. Ohashi, M. Baba, T. Kawase, and Y. Hayakawa, *J. Fluorine Chem*, **79**,

149 (1996).

26) H. Sawada, S. Katayama, Y. Ariyoshi, T. Kawase, Y. Hayakawa, T. Tomita, and M. Baba, *J. Mater. Chem.*, **8**, 1517 (1998).

27) H. Xia, Q. Wang, *Chem. Mater.*, **14**, 2158 (2002).

28) S. Stafström, J. L. Brédas, A. J. Epstein, H. S. Woo, D. B. Tanner, W. S. Huang, and A. G. MacDiarmid, *Phys. Rev. Lett.*, **59**, 1464 (1987).

29) A. A. Athawale, M. V. Kulkarni, and V. V. Chabukswar, *Mater. Chem. Phys.*, **73**, 106 (2002).

30) Y. Yang and W. Yang, *Polym. Adv. Technol.*, **16**, 24 (2005).

31) S.-J. Su and N. Kuramoto, *Synth. Met.*, **114**, 147 (2000).

32) E. M. Genies, A. Boyle, M. Lapkowski, and C. Tsintavis, *Synth. Met.*, **36**, 139 (1990).

33) E. M. Genies and P. Noel, *Synth. Met.*, **46**, 285 (1992).

34) C. Bian, Y. Yu, and G. Xue, *J. Appl. Polym. Sci.*, **104**, 21 (2007).

35) F.-L. Lu , F. Wudl, M. Nowak, and A. J. Heeger, *J. Am. Chem. Soc.*, **108**, 8311 (1986).

CHAPTER 2

Color-changing Behavior of Fluoroalkyl End-capped 2-Methacryloyloxyethanesulfonic acid Oligomer/Polyaniline Nanocomposites, Triggered by a Variety of Basic Compounds

2.1. Introduction

Among a wide variety of conducting polymers, polyaniline (**PAn**) is one of the most remarkable materials owing to its ease of synthesis, good environmental stability, high electrical conductivity, and reversible redox behavior controlled by simple doping/dedoping approach.[1-9] Such electrical property of **PAn** has attracted a considerable attention to using **PAn** in sensing, electro/chemochromic, catalytic and other applications.[10-12] Especially, the well-known **PAn** property to participate in acid-base interactions leading to changes in its spectral and electrical characteristics is applicable as a sensing element in the measurements of **PAn** electrochemical responses and conductivity.[13-15] **PAn** is also a suitable organic material for sensing the basic substrates in doped state, and the undoped state can afford the effective sensing of the acidic substrates.[16-18] In fact, there have been hitherto numerous reports on the electrical and optical sensors for ammonia sensors based on doped **PAn**.[19-27] However, apart from a variety of attractive properties of **PAn** based on gas sensors, some fundamental problems related to the poor solubility and long-term mechanical and chemical properties of **PAn** imply difficulties in its practical use.[28, 29] From this point of view, much attention has been focused on the **PAn**/organic polymer composites because these composites should increase the mechanical properties and chemical stability, and in fact, numerous

organic polymers such as poly(methyl methacrylate), poly(vinyl chloride), polystyrene and epoxy resin can be used.[30, 31] These gas sensor composite films in general show slow recovery time and regeneration difficulty.[32] Therefore, it is deeply desirable to explore new fluorinated polymers/**PAn** nanocomposites possessing an excellent surface active characteristic derived from the fluorinated polymers. Hitherto, the preparation and applications of fluoroalkylated polymers, especially, ABA triblock-type fluoroalkyl end-capped oligomers [R_F-(M)$_n$-R_F: R_F = fluoroalkyl groups, M = radical polymerizable monomer] have been comprehensively studied, and these fluorinated oligomers can exhibit a wide variety of unique properties such as high solubility, surface-active property and nanometer size-controlled molecular aggregates, which cannot be achieved by the corresponding non-fluorinated and randomly fluoroalkylated ones.[33-37] The self-assembled fluorinated oligomeric aggregates formed by these fluoroalkyl end-capped oligomers can provide suitable host moieties to interact with numerous guest molecules such as fullerene, carbon nanotubes, gold, silver and copper nanoparticles, and organic dyes, affording the corresponding fluorinated aggregates/guest molecules nanocomposites.[38-47] In addition, preparation of poly(vinylidene fluoride) copolymers/silica nanocomposites has been reported including their unique properties.[48-50] **PAn** can be also easily encapsulated into these fluorinated oligomeric aggregate cores to give the fluorinated oligomeric

nanocomposites-encapsulated **PAn** as a guest molecule possessing a good dispersibility and stability in water and traditional organic media such as methanol.[51, 52] This chapter shows that fluoroalkyl end-capped 2-(methacryloyloxy)ethanesulfonic acid oligomer [R_F-(MES)$_n$-R_F]/**PAn** nanocomposites can interact with a variety of basic compounds such as ammonia, sodium hydroxide, 2-hydroxyethylamine, tris(hydroxymethyl)aminomethane, and silica particles bearing 3-aminopropyl groups (***Amino***-SiO_2) to cause the smooth color change from green to wine-red (or purple) under room temperature, and the fluorinated composite film can be applicable to the ammonia sensor possessing a good reversible color-changing ability. In addition, it has been found that ***Amino***-SiO_2 particles can interact with R_F-(MES)*n*-R_F/**PAn** nanocomposites to cause the solvatochromic response. These results will be described in this chapter.

2.2. Experimental

2.2.1. Measurements

Molecular weight of R_F-$(MES)_n$-R_F oligomer (Mn = 13,700) was determined by using the gel permeation chromatography (Tokyo, Japan) calibrated pullulan (molecular weights 2000 ~ 50,000) standards by using 0.5 mol dm^{-3} Na_2HPO_4 aqueous solution as the eluent. Dynamic light-scattering (DLS) measurements were performed using Otsuka Electronics DLS-7000 HL (Tokyo, Japan). Ultraviolet-visible (UV-vis) spectra were recorded by using Shimadzu UV-1600 UV-vis spectrophotometer (Kyoto, Japan).

2.2.2. Materials

2-Methacrylolyoxyethanesulfonic acid was purchased from Polyscience, Inc. (PA, USA). Silica-nanoparticle methanol solution [30 % (wt): average particle size 11 nm (Methanol Silica-sol^{TR})] was received from Nissan Chemical Industrials (Tokyo, Japan). Aniline, 3-aminopropyltrimethoxysilane (APTMS), tetraethoxysilane (TEOS) and micrometer size-controlled 3-aminopropylsilica particles (average particle size 120 μm) were purchased

from Tokyo Chemical Industrial Co., Ltd. (Tokyo, Japan). Aqueous ammonia and ammonium persulfate were received from Wako Pure Chemical Industries (Osaka, Japan) and Kanto Chemical Co., Inc. (Tokyo, Japan), respectively. R_F-$(MES)_n$-R_F oligomer was prepared by reaction of fluoroalkanoyl peroxide with the corresponding monomer according to the previously reported method.[53)]

2.2.3. Preparation of fluoroalkyl end-capped 2-(methacryloyloxy) ethanesulfonic acid oligomer/polyaniline [R_F-$(MES)_n$-R_F/PAn] nanocomposites

R_F-$(MES)_n$-R_F/**PAn** nanocomposites were prepared according to the method described in chapter 1.[51)] Briefly, aniline (47 mg) was added to an aqueous solution (24 ml) of R_F-$(MES)_n$-R_F oligomer [R_F = $CF(CF_3)OC_3F_7$] (280 mg). The mixture was stirred with a magnetic stirring bar at room temperature for 30 min. An 11-ml ammonium persulfate (115 mg) aqueous solution was added dropwise to the solution containing aniline and fluorinated oligomer with continuous stirring at room temperature for 1 day. After the removal of solvent, the crude product was purified by the reprecipitation (H_2O/tetrahydrofuran) to give the expected R_F-$(MES)_n$-R_F/**PAn** nanocomposites. The nanocomposites thus obtained were dried in vacuo at 50 °C for 2 days to afford green-colored powders (262 mg).

2.2.4. Preparation of modified glass treated with fluoroalkyl end-capped 2-(methacryloyloxy)ethanesulfonic acid oligomer/polyaniline [R_F-(MES)$_n$-R_F/PAn] nanocomposites on the glass surface

The homogeneous aqueous solution (1 ml) of the R_F-(MES)$_n$-R_F/**PAn** nanocomposites (0.5 mg) was casted on the glass plate (18×18 mm^2 pieces) at room temperature. The cast plate thus obtained was dried at room temperature and then at 50 °C for 24 h under vacuum to afford the transparent green-colored film (film thickness 3 μm).

2.2.5. The ammonia sensing performance of the R_F-(MES)$_n$-R_F/PAn nanocomposite films

The sensing performance of the nanocomposites was tested by subjecting the nanocomposite cast film plate to ammonia vapor in a closed glass container containing aqueous 25 % ammonia (10 ml). The sample was characterized by measuring the UV-vis spectra at room temperature, and the interaction between ammonia vapor and the composite film leads to optical absorbance (wavelength) variation of **PAn**. The composite film plate was dried in vacuo at 50 °C after subjecting the composite film plate to ammonia vapor, and the dried composite film plate was similarly characterized by the UV-vis spectroscopy. The

sensitivity (S) was calculated as $(A-A_o)/A_o$ ratio, where A_o is the initial optical absorbance around at 600 nm at the sensor under dried conditions and A is the absorbance of the sensor when exposed to ammonia vapor.

2.2.6. Preparation of silica fine particles bearing amino groups

To a methanol solution (20 ml) of silica nanoparticles (1.0 g) were added 3-aminopropyltrimethoxysilane (APTMS 0.48 ml), tetraethoxysilane (TEOS 0.50 ml) and 25 % aqueous ammonia solution (0.50 ml). The mixture was stirred with a magnetic stirring bar at room temperature for 5 h. After the solvent was evaporated off, to the obtained crude products was added methanol (20 ml). The methanol solution was stirred with magnetic stirring bar at room temperature for 1 day, and then was centrifuged for 30 min. The expected silica fine particles bearing amino groups were easily separated from the methanol solution and then were washed with methanol and water in several times, respectively. Silica fine particles bearing amino group powders thus obtained were dried in vacuo at 50 °C for 2 days to afford purified particle powders (isolated yield 1.4 g; average particle size determined by dynamic light-scattering method: 36 nm). Silica fine particles bearing amino group powders (average

particle size: 102 nm) were also prepared by the similar method without the use of TEOS (isolated yield 1.2 g).

2.2.7. Preparation of R_F-(MES)$_n$-R_F/PAn/silica particles bearing amino groups blend hybrids

To an aqueous solution (5 ml) of R_F-(MES)$_n$-R_F/**PAn** nanocomposites (0.08 g/dm^3) was added silica fine particles bearing amino groups (average particle size: 40 nm, 75 mg). The mixture was stirred with a magnetic stirring bar at room temperature for 1 day and then was centrifuged for 30 min. The expected R_F-(MES)$_n$-R_F/**PAn**/silica fine particles bearing amino groups blend hybrids were easily separated from the aqueous solution. R_F-(MES)$_n$-R_F/**PAn**/silica fine particles bearing amino group blend hybrids thus obtained were dried in vacuo at 50 °C for 2 days to afford blue-colored powders (isolated yield 70 mg). Other R_F-(MES)$_n$-R_F/**PAn**/silica fine particles bearing amino groups blend hybrids were also similarly prepared by using 100-nm and 120-μm size-controlled silica particles bearing amino groups, and the isolated product yields were 68 and 69 mg, respectively.

2.3. Results and discussion

Fluoroalkyl end-capped 2-(methacryloyloxy)ethanesulfonic acid oligomer/polyaniline [R_F-$(MES)_n$-R_F/**PAn**] nanocomposites (average particle size determined by the dynamic light scattering measurements: 54 ± 5 nm) were prepared by the polymerization of aniline initiated by ammonium persulfate in the presence of the corresponding oligomer as shown in Scheme 2-1.[51)]

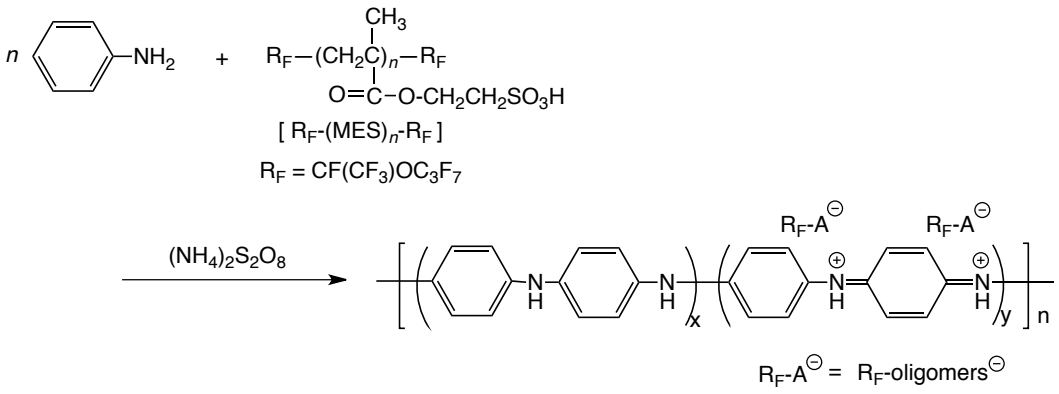

Scheme 2-1

The UV-vis spectra of the aqueous green-colored solution of R_F-$(MES)_n$-R_F/**PAn** nanocomposites have been measured, and the result is shown in Fig. 2-1.

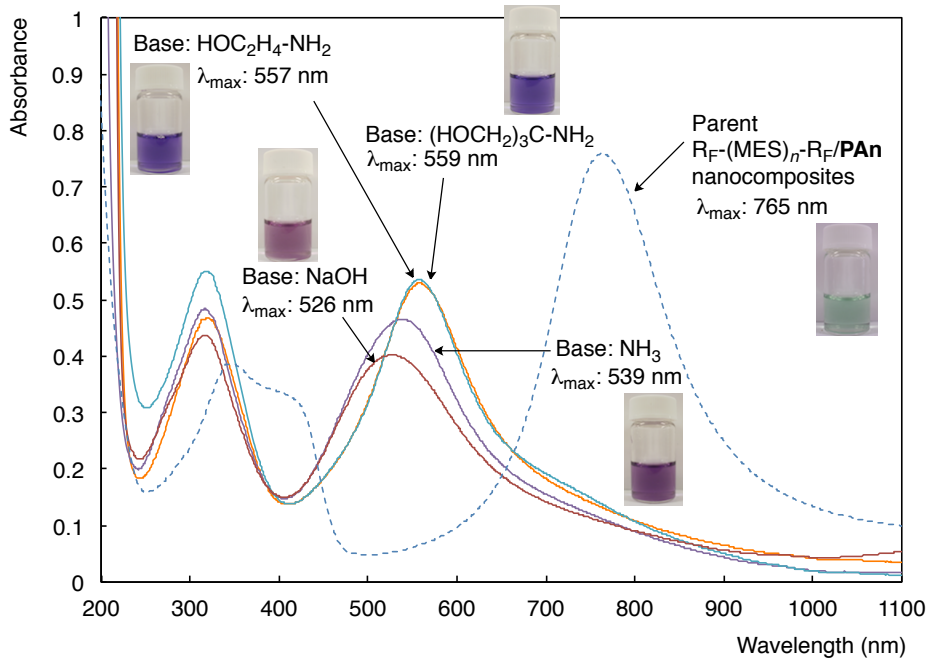

Fig. 2-1 UV-vis spectral change of aqueous solutions of R_F-$(MES)_n$-R_F/**PAn** nanocomposites [80 mg/dm^3] by the addition of aqueous solutions containing a variety of basic compounds [0.1 mol/dm^3]

Fig. 2-1 shows the clear absorption peak around at 765 nm, of whose peak is related to the π-polaron transition of the emeraldine salt type **PAn** in the nanocomposites.[51, 52] Interestingly, the smooth color change from green (λ_{max} 765 nm) to wine-red (λ_{max} 539 nm) have been observed by the addition of aqueous ammonia illustrated in Fig. 2-1. Not only ammonia but also other basic compounds such as tris(hydroxymethyl)aminomethane, 2-hydroxyethylamine and sodium hydroxide were effective for the color change from green to purple (or wine-red), and each clear blue-shifted absorption peak from 765 to 559 ~ 526 nm was observed after the addition of the corresponding basic compounds to the fluorinated **PAn** nanocomposites (see Fig. 2-1). However, basic compounds such 4-aminouracil and 9-aminoacridine were unable to

give the color change to cause the blue-shift behavior under similar conditions (data not shown). In this way, inorganic bases such as sodium hydroxide and ammonia were more effective for the blue-shift behavior of the nanocomposites, indicating that such basic compounds should interact smoothly with the emeraldine salt moieties in the composites to afford the effective formation of the emeraldine base as shown in Scheme 2-2.

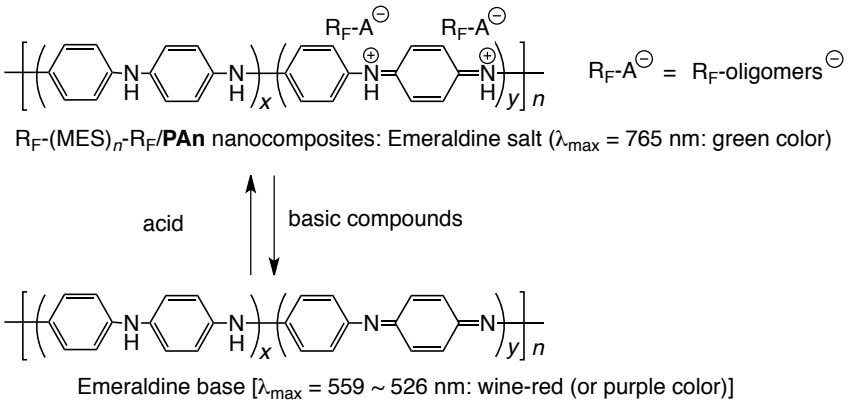

Scheme 2-2

Hitherto, it has been well known that **PAn** is sensitive to the pH change[54], and the smooth reversible reactions of **PAn** with bases (the doped state: emeraldine salts) and acids (undoped state: emeraldine base) are easily observed with the chemical color change from green to wine-red.

UV-vis spectra of the transparent green colored R_F-$(MES)_n$-R_F/**PAn** nanocomposite film were measured, and the result was shown in Fig. 2-2.

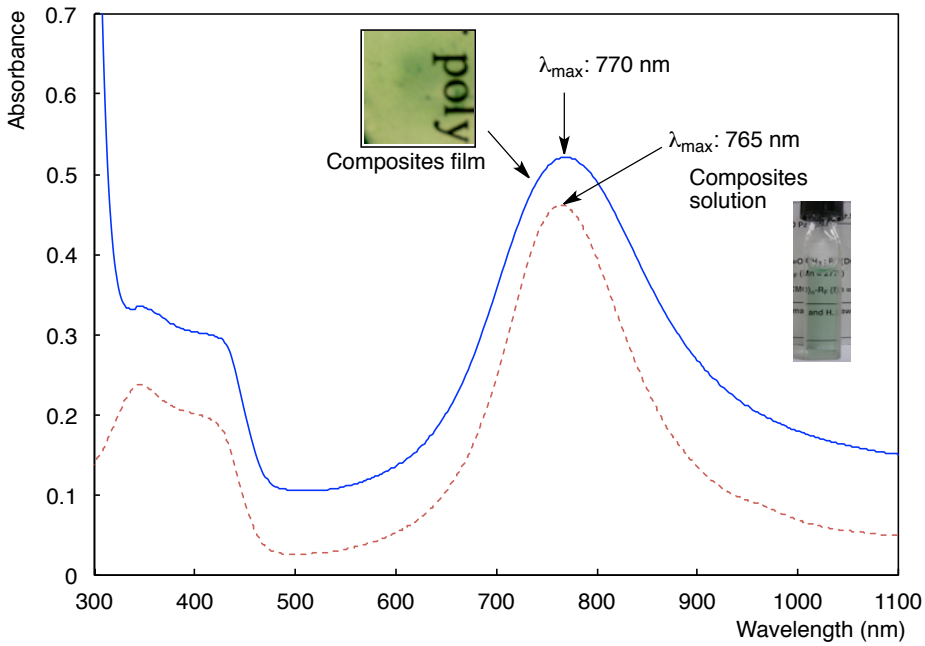

Fig. 2-2 UV-vis spectra of R_F-$(MES)_n$-R_F/**PAn** nanocomposite film and aqueous solution of R_F-$(MES)_n$-R_F/**PAn** nanocomposites (33 mg/dm^3)

As shown in Fig. 2-2, the composite film was found to give the similar π-polaron transition peak of the emeraldine salt type **PAn** around at 770 nm to that (765 nm) of the aqueous R_F-$(MES)_n$-R_F/**PAn** nanocomposites solution. Thus, the interaction of the R_F-$(MES)_n$-R_F/**PAn** nanocomposites with ammonia has been studied at room temperature.

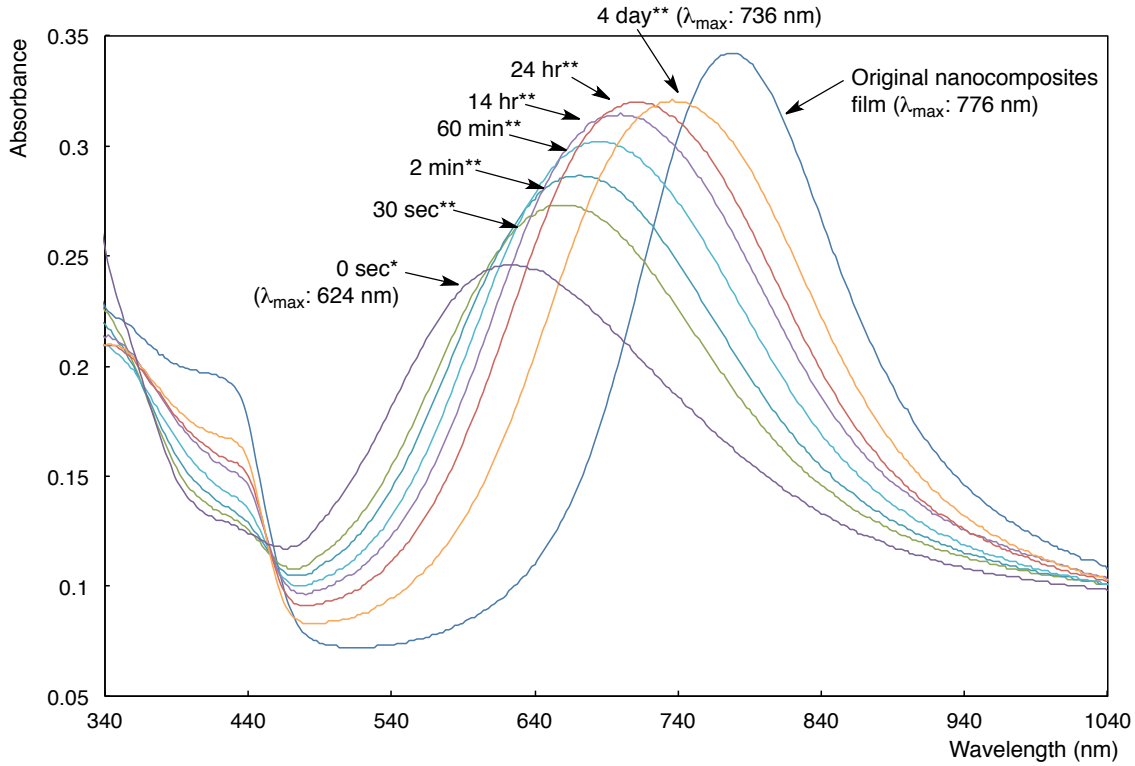

Fig. 2-3 Changes in the UV-vis spectra of the R_F-$(MES)_n$-R_F/**PAn** nanocomposite film after exposure to ammonia vapor and storage in the dark at room temperature.
*Just after exposure to ammonia vapor.
**Storage time in the dark.

Fig. 2-3 shows the characteristic absorption peak responses of the R_F-$(MES)_n$-R_F/**PAn** nanocomposites subjected to ammonia vapor and air alternation. It is noteworthy that the smooth blue-shift behavior of the polaron absorptions from 776 to 624 nm after exposure to ammonia vapor, indicating that the emeraldine salt moieties in the nanocomposites should react with ammonia to produce the emeraldine base moieties, giving the purple-colored film. After exposure to ammonia vapor, the nanocomposite film was placed in the dark. Interestingly, restoration to the original polaron wavelength and absorbance, which are accompanied through the interaction with the acidic substrate: R_F-$(MES)_n$-R_F oligomer in the

nanocomposites illustrated in Scheme 2-2, was realized for the nanocomposites by alternation of exposure to ammonia vapor and storage in the dark. Especially, not only the absorbances of the polaron absorption but also the polaron wavelengths were increased and red-shifted, respectively, with the increase of the storage time in the dark from 30 s to 4 day as shown in Fig. 2-3. This cycle was repeated several times, and a good repeatability for the color change of the nanocomposite film from green to purple was observed by alternation of exposure to ammonia vapor and storage in the dark under vacuum at 50 °C as shown in Fig. 2-4.

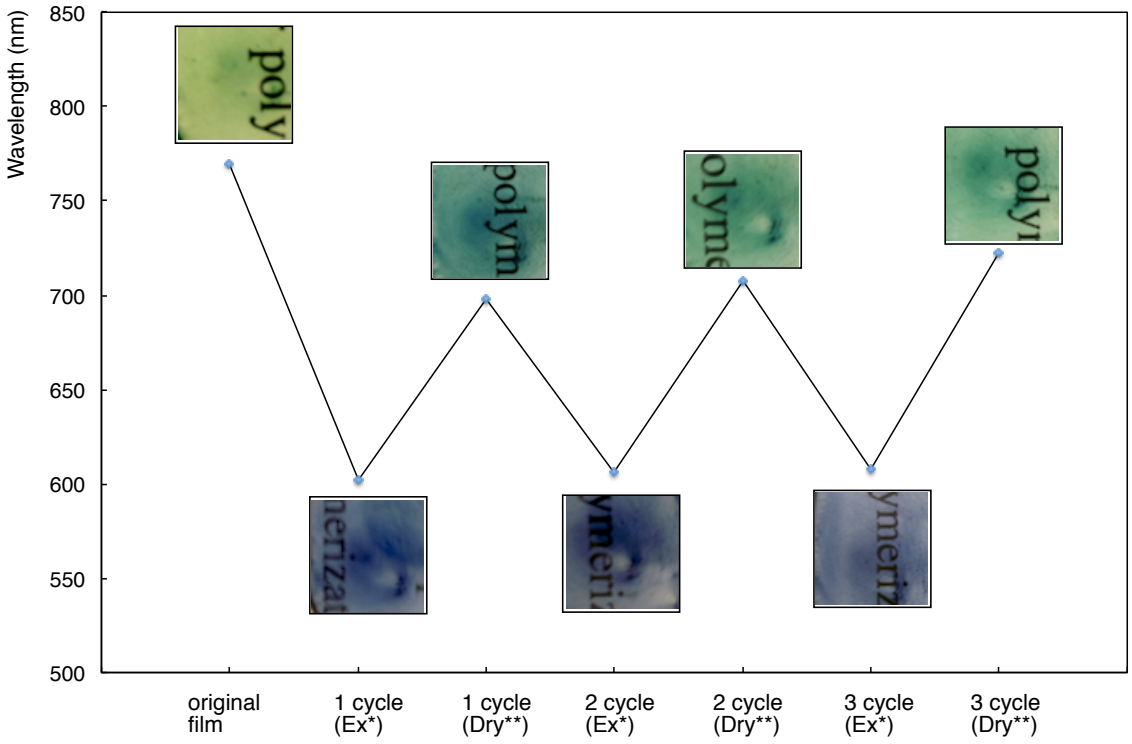

Fig. 2-4 Relationship between color change from green to purple and wavelength of the R_F-$(MES)_n$-R_F/**PAn** nanocomposites film for alternation of exposure to ammonia vapor and drying under vacuum at 50 °C. *Ex: exposure to ammonia vapor. **Dry: drying under vacuum at 50 °C.

The sensitivity (*S*) for the color change from green to purple illustrated in Fig. 2-3 was calculated to be 216 as $(A-A_o)/A_o$ ratio, where A_o is the initial optical absorbance around at 600 nm at the sensor under dried conditions and A is the absorbance of the sensor when exposed to ammonia vapor. This sensitivity value is superior to that (6) of the previously reported **PAn**/epoxy resin composite film or that (16) of the parent **PAn** film.[32] This finding would be due to the effective surface arrangements of **PAn** moieties in the fluorinated nancomposites because fluoralkyl end-capped oligomers can exhibit an excellent surface active characteristic on the modified film.[55]

The interaction of the R_F-$(MES)_n$-R_F/**PAn** nanocomposites with not only the basic compounds illustrated in Fig. 2-1 but also silica fine particles bearing amino groups have been studied, from the developmental view points of new fluorinated **PAn** nanocomposites imparted by silica moieties,. The results are shown in Scheme 2-3 and Fig. 2-5.

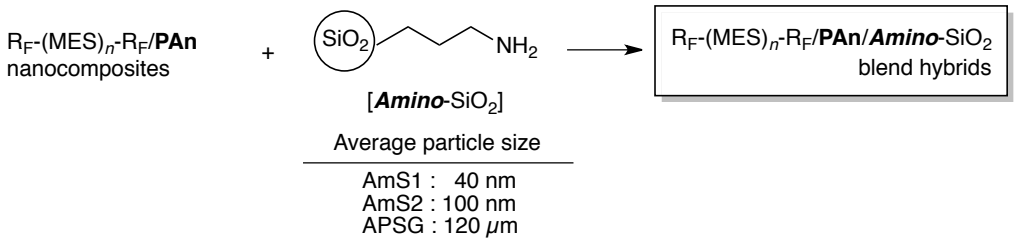

Scheme 2-3

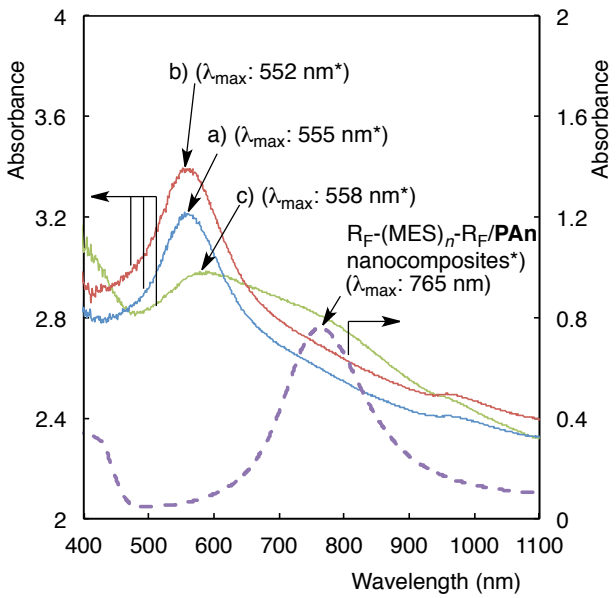

Fig. 2-5 UV-vis spectra of well-dispersed aqueous solutions of R_F-(MES)$_n$-R_F/**PAn**/***Amino***-SiO_2 blend hybrids. a) Particle size 40-nm ***Amino***-SiO_2 particles were used. b) Particle size 100-nm ***Amino***-SiO_2 particles were used. c) Particle size 120-μm ***Amino***-SiO_2 particles were used. *) Concentration of R_F-(MES)$_n$-R_F/**PAn** nanocomposites 0.08 g/dm^3; concentration of each ***Amino***-SiO_2 particles 15 g/dm^3

R_F-(MES)$_n$-R_F/**PAn** nanocomposites-silica particles bearing amino groups blend hybrids [R_F-(MES)$_n$-R_F/**PAn**/***Amino***-SiO_2] were isolated by the simple centrifugal separation of the well-dispersed aqueous solutions containing the corresponding green-colored nanocomposite powders and white-colored silica particles bearing amino group (***Amino***-SiO_2) particle powders as shown in Scheme 2-3. Each isolated color-changed (purple-colored) blend hybrid powder illustrated in Scheme 2-3 has a good dispersibility and stability toward not only water but also methanol, chloroform and fluorinated aliphatic solvent such as AK-225^{TR} (1 : 1 mixed solvents of $CF_3CF_2CHCl_2$ and $CFClHCF_2CF_2Cl$).

Thus, UV-vis spectra of well-dispersed aqueous solutions of R_F-(MES)$_n$-R_F/**PAn**/***Amino***-SiO_2 blend hybrids have been measured, and the results were shown in Fig. 2-5.

As shown in Fig. 2-5, ***Amino***-SiO_2 fine particles are also effective for the blue-shift of the polaron absorptions related to the **PAn** moieties in the nanocomposites from 765 to 552 ~ 555 nm, as well as ammonia, sodium hydroxide, tris(hydroxymethyl)aminomethane and hydroxyethylamine illustrated in Fig. 2-1. Especially, nanometer size-controlled ***Amino***-SiO_2 fine particles (36~102 nm) can afford a higher absorption peak than that of the micrometer size-controlled one (120 μm) under similar conditions (see Fig. 2-5).

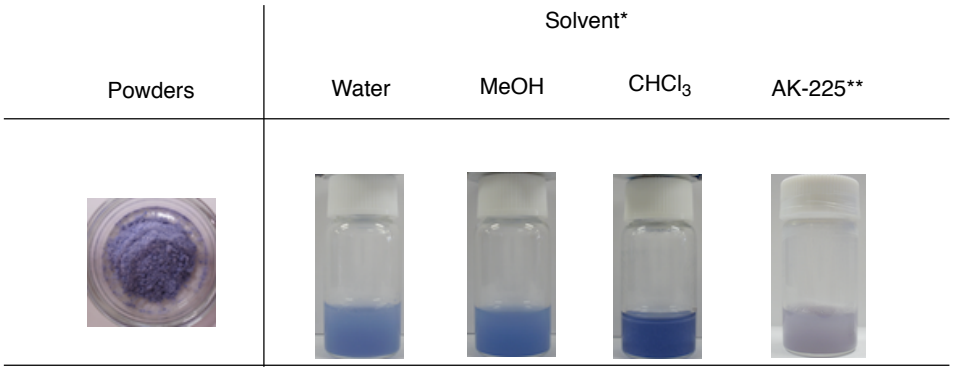

*) Concentration of R_F-$(MES)_n$-R_F/**PAn**/***Amino***-SiO_2 blend hybrid powders: 15 g/dm^3

**) 1:1 mixed solvents of $CF_3CF_2CHCl_2$ and $CFClHCF_2CF_2Cl$

Fig. 2-6 Photograph of R_F-$(MES)_n$-R_F/**PAn**/***Amino***-SiO_2 blend hybrid powders and their solutions

Purple-colored R_F-$(MES)_n$-R_F/**PAn**/***Amino***-SiO_2 blend hybrid powders, which were prepared by using the micrometer size-controlled ***Amino***-SiO_2 particles, were found to exhibit the solvatochromic behavior. This blend hybrid powders can afford the blue-colored well-dispersed solutions toward water, methanol and chloroform; however, unexpectedly, this hybrid can give the decolored (white-gray) solution toward fluorinated aliphatic solvent:

AK-225 as illustrated in Fig. 2-6. This unique solvatochromism behavior is well consistent with the absorption peaks, and the more blue-shifted polaron absorption peak was observed around at 526 nm in fluorinated solvent: AK-225, although the corresponding absorption peaks appeared around 588~599 nm in water, methanol and chloroform as shown in Fig. 2-7.

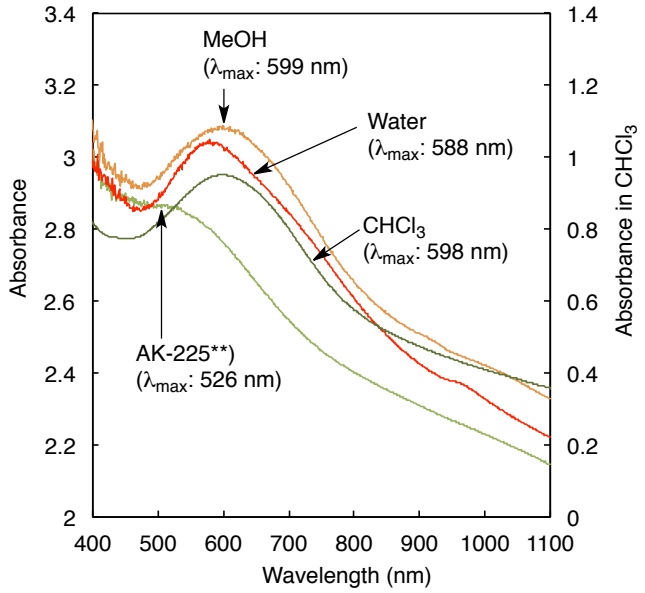

Fig. 2-7 UV-vis spectra of R_F-$(MES)_n$-R_F/**PAn**/***Amino***-SiO_2 blend hybrids, used blend hybrids refer to c) in Fig. 5 [concentration: 15 g/dm^3] in methanol, water, chloroform, and AK-225.
**) 1:1 mixed solvents of $CF_3CF_2CHCl_2$ and $CFClHCF_2CF_2Cl$

After the centrifugal separation of the decolored well-dispersed R_F-$(MES)_n$-R_F/**PAn**/***Amino***-SiO_2 blend hybrid AK-225 solution [see Fig. 2-8(**A**)], the decolored hybrid powders can be easily isolated as shown in Fig. 2-8(**B**). Of particular interest, it was found that these decolored powders was dispersed into methanol to give not a decolored solution but a blue-colored solution [see Fig. 2-8(**C**)], affording the same blue-colored solution to that of the

methanol in Fig. 2-6. This solvatochromic behavior is well consistent with those of the UV-vis absorption peaks in Figs. 2-8(**A**), (**C**).

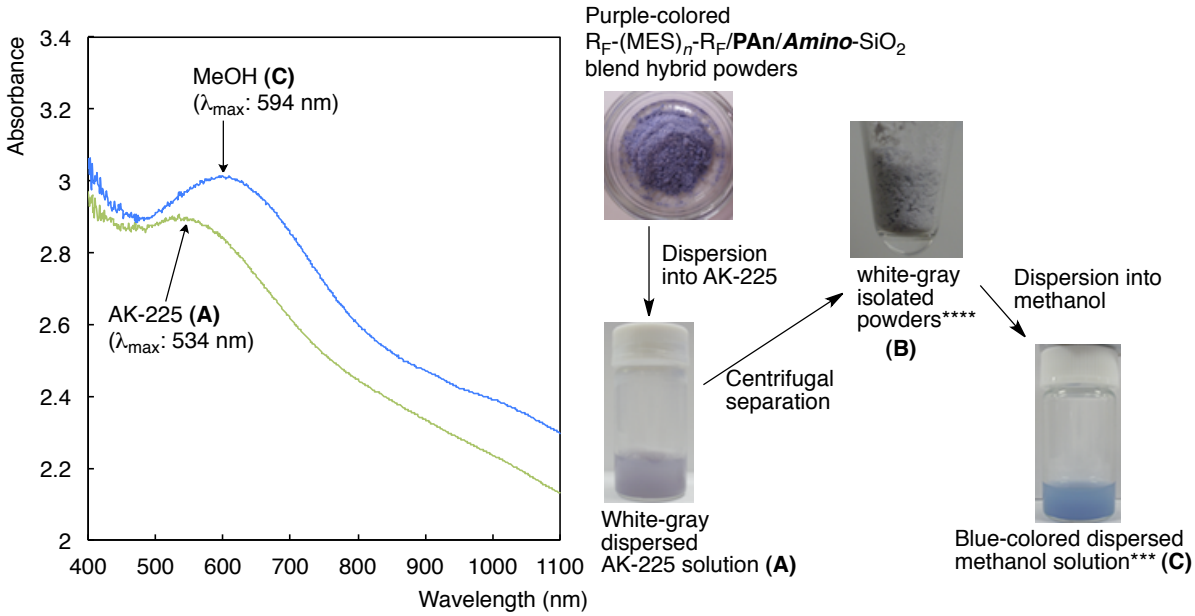

Fig. 2-8 UV-vis spectra of the R_F-$(MES)_n$-R_F/**PAn**/***Amino***-SiO_2 blend hybrids, used blend hybrids refer to *c)* in Fig. 5, [concentration: 15 g/dm^3] in AK-225 (1:1 mixed solvents of $CF_3CF_2CHCl_2$ and $CFClHCF_2CF_2Cl$) and ***methanol, and photograph of the R_F-$(MES)_n$-R_F/**PAn**/***Amino***-SiO_2 blend hybrids white-gray powders, which were isolated after the centrifugal separtion of the dispersed blend hybrids AK-225 solution. ***Blue-colored dispersed methanol solution was prepared by using the ****white-gray isolated powders

The isolation of the decolored hybrid powders [Fig. 2-8(**B**)] would be due to the effective interaction between the **PAn** moieties and ***Amino***-SiO_2 particles in the fluorinated nanocomposite cores. Because the nanocomposite cores would be more tightly constructed through not only the aggregations of end-capped fluoroalkyl segments in R_F-$(MES)_n$-R_F oligomers but also the incorporation of fluorinated solvent: AK-225, compared with those of water and hydrocarbon solvents such as methanol and chloroform. Such effective interaction

would afford the more blue-shifted absorption peak (λ_{max}: 526 ~ 534 nm) than those (λ_{max}: 588 ~ 599 nm) in water, methanol and chloroform to cause the decolored behavior.

2.4. Conclusion

R_F-$(MES)_n$-R_F/**PAn** nanocomposites, which were prepared by the polymerization of aniline initiated by ammonium persulfate in the presence of the corresponding oligomer, can interact with a variety of basic compounds such as ammonia, sodium hydroxide, tris(hydroxymethyl)aminomethane and hydroxyethylamine to cause the color change from green to wine-red (or purple) through the formation of the emeraldine base in the composites. The nanocomposite cast film can exhibit the color-switching behavior between green and purple, triggered by ammonia vapor as the basic compounds, and a good repeatability for this color change of the R_F-$(MES)_n$-R_F/**PAn** nanocomposite film surface by alternation of exposure to ammonia and storage in the dark. Interestingly, the sensitivity for the color change related to the **PAn** moieties was found to be extremely superior to that of previously reported **PAn**/epoxy resin composite film.[32] This finding would be due to the effective surface active characteristic of R_F-$(MES)_n$-R_F oligomer in the nanocomposites. Furthermore, R_F-$(MES)_n$-R_F/**PAn**/***Amino***-SiO_2 blend hybrids, which were prepared by the interaction of the corresponding R_F-$(MES)_n$-R_F/**PAn** nanocomposites with silica particles bearing amino groups, were found to give the solvatochromic behavior, and the hybrid powders can afford the blue-colored dispersion solutions toward water, methanol and chloroform; however, a

fluorinated solvent such as AK-225 enables this hybrid to afford the decolored (white-gray) dispersion solution. This selective color-changing behavior for the fluorinated solvent might be the first example. Thus, these present R_F-$(MES)_n$-R_F/**PAn**/basic compound composites will have high potential for new fluorinated functional hybrid materials toward the sensing fields.

References

1) A. A. Syed and M. K. Dinesan, *Talanta*, **38**, 815 (1991).

2) E. T. Kang, K. G. Neoh, and K. L. Tan, *Prog. Polym. Sci.*, **23**, 277 (1998).

3) J. C. Chiang and A. G. MacDiarmid, *Synth. Met.*, **1**, 193 (1986).

4) W. J. Feast, J. Tsibouklis, K. L. Pouwer, L. Groenendaal, and E. W. Meijer, *Polymer*, **37**, 5017 (1996).

5) L.-M. Hung, C.-H. Chen, and T.-C. Wen, *Electrochimica Acta*, **51**, 5858 (2006).

6) B. Wessling, *Polymer*, **2**, 786 (2010).

7) K. M. Molapo, P. M. Ndangili, R. F. Ajayi, G. Mbambisa, S. M. Mailu, N. Njomo, M. Masikini, P. Baker, and E. I. Iwuoha, *Int. J. Electrochem. Sci.*, **7**, 11859 (2012).

8) Y. Wang, *Int. J. Mater. Res.*, **105**, 3 (2014).

9) H. S Kolla, S. P. Surwade, X. Zhang, A. G. MacDiamid, and S. K. Manohar, *J. Am. Chem. Soc.*, **127**, 16770 (2005).

10) S. Virji, J. Huang, R. B. Kaner, and B. H. Weiller, *Nano Lett.*, **4**, 491 (2004).

11) J. Huang, S. Virji, B. H. Weiller, and R. B. Kaner, *J. Am. Chem. Soc.*, **125**, 314 (2003).

12) E. Song and J.-W. Choi, *Nanomaterials*, **3**, 498 (2013).

13) A. Drelinkiewicz, Z. Kalemba-Jaje, E. Lalik, and R. Kosydar, *Fuel*, **116**, 760 (2014).

14) I. Duboriz and A. Pud, *Sens. Actuators B: Chem.*, **190**, 398 (2014).

15) S. Palaniappan and C. Saravanan, *J. Appl. Polym. Sci.*, **118**, 518 (2010).

16) K. Chatterjee, P. Dhara, S. Ganguly, K. Kargupta, and D. Banerjee, *Sens. Actuators B: Chem.*, **181**, 544 (2013).

17) A. A. Athawale and V. V. Chabukswar, *J. Appl. Polym. Sci.*, **79**, 1994 (2001).

18) V. V. Chabukswar, S. Pethkar, and A. A. Athawale, *Sens. Actuators B*, **77**, 657 (2001).

19) S. Chen and G. Sun, *ACS Appl. Mater. Interfaces*, **5**, 6471 (2013).

20) A. Navarchian, Z. Hasanzadeh, and M. Joulazadeh, *Adv. Polym. Technol.,* **32**, 21356 (1–10) (2013).

21) Y. Zhu, J. Li, H. He, M. Wan, and L. Jiang, *Macromol. Rapid Commun.*, **28**, 2230 (2007).

22) A. L. Sharma, K. Kumar, and A. Deep, *Sens. Actuators A: Phys.*, **198**, 107 (2013).

23) A. L. Kukla, Y. M. Shirshov, and S. A. Piletsky, *Sens. Actuators B*, **37**, 135 (1996).

24) M. O. Ansari, M. M. Khan, S. A. Ansari, I. Amal, J. Lee, and M. H. Cho, *Mater. Lett.*, **114**, 159 (2014).

25) K. H. Hong, K. W. Oh, and T. J. Kang, *J. Appl. Polym. Sci.*, **92**, 37 (2004).

26) N. Menegazzo, B. Herbert, S. Banerji, and K. S. Booksh, *Talanta*, **85**, 1369 (2011).

27) Z. Jin, Y. Su, and Y. Duan, *Sens. Actuators B*, **72**, 75 (2001).

28) M. Wan, M. Li, J. Li, and Z. Liu, *Thin Solid Films*, **258**, 188 (1995).

29) M. Matsunaga, A. Okamoto, and Y. Sakai, *Sens. Actuators B*, **94**, 46 (2003).

30) M. E. Nicho, M. Trejo, A. Garcia-Valenzuela, J. M. Saniger, J. Palacios, and H. Hu, *Sens. Actuator B*, **76**, 18 (2001).

31) X. Yang, T. Zhaoa, Y. Yu, and Y Wei, *Synth. Met.*, **142**, 57 (2004).

32) A. Airoudj, D. Debarnot, B. Bêche, and F. Poncin-Epaillard, *Talanta*, **77**, 1590 (2009).

33) H. Sawada, *Chem. Rev.*, **96**, 1779 (1996).

34) H. Sawada, *J. Fluorine Chem.*, **105**, 219 (2000).

35) H. Sawada, *J. Fluorine Chem.*, **121**, 111 (2003).

36) H. Sawada, *Prog. Polym. Sci.*, **32**, 509 (2007).

37) H. Sawada, *Polym. Chem.* **3**, 46 (2012).

38) H. Sawada, J. Iidzuka, T. Maekawa, R. Takahashi, T. Kawase, K. Oharu, H. Nakagawa, and K. Ohira, *J. Colloid Interface Sci.*, **263**, 1 (2003).

39) H. Sawada, A. Sasaki, K. Sasazawa, T. Kawase, K. Ueno, and K. Hamazaki, *Colloid Polym. Sci.*, **283**, 583 (2005).

40) H. Sawada, A. Sasaki, K. Sasazawa, K. Toriba, H. Kakehi, M. Miura, and N. Isu, *Polym. Adv. Technol.*, **19**, 419 (2008).

41) H. Sawada, R. Furukuwa, K. Sasazawa, K. Toriba, K. Ueno, and K. Hamazaki, *J. Appl. Polym. Sci.*, **100**, 1328 (2006).

42) H. Sawada, R. Furukuwa, K. Sasazawa, M. Mugisawa, and K. Ohnishi, *Eur. Polym. J.*, **43**, 3258 (2007).

43) H. Sawada and K. Takahashi, *J. Colloid Interface Sci.*, **351**, 166 (2010).

44) K. Kijima, M. Nishida, F. Fukaya, M. Yoshida, and H. Sawada, *J. Polym. Sci. Part A: Polym. Chem.*, **51**, 2555 (2013).

45) H. Sawada, S. Izumi, K. Sasazawa, and M. Yoshida, *J. Colloid Interface Sci.*, **377**, 76 (2012).

46) H. Sawada, T. Tashima, Y. Nishiyama, M. Kikuchi, G. Kostov, Y. Goto, and B. Ameduri, *Macromolecules*, **44**, 1114 (2011).

47) S. Guo, H. Yosioka, Y. Kato, H. Kakehi, M. Miura, N. Isu, A. Manseri, H. Sawada, and B. Ameduri, *Eur. Polym. J.*, **58**, 79 (2014).

48) N. Durand, N. Graveau, P. Gaveau, G. Silly, B. Ameduri, and B. Boutevin, *Macromolecules*, **44**, 6249 (2011).

49) N. Durand, B. Boutevin, G. Silly, and B. Ameduri, *Macromolecules*, **44**, 8487 (2011).

50) N. Durand, D. Mariot, B. Ameduri, B. Boutevin, and F. Ganachaud, *Langmuir*, **27**, 4057 (2011).

51) H. Sawada, T. Tsuzuki-ishi, T. Kijima, M. Iizuka and M. Yoshida, *Colloid Polym. Sci.*, **289**, 1103 (2011).

52) H. Sawada, T. Tsuzuki-ishi, T. Kijima, J. Kawakami, M. Iizuka and M. Yoshida, *J. Colloid Interface Sci.*, **359**, 461 (2011).

53) H. Sawada, A. Ohashi, M. Baba, T. Kawase, and Y. Hayakawa, *J. Fluorine Chem.*, **79**, 149 (1996).

54) N. Kuramoto and E. M. Geniès, *Synth. Met.*, **68**, 191 (1995).

55) H. Sawada, K. Yanagida, Y. Inaba, M. Sugiya, T. Kawase, and T. Tomita, *Eur. Polym. J.*, **37**, 1433 (2001).

CHAPTER 3

Facile One-pot Preparation of Gold Nanoparticles in the Presence of Fluoroalkyl End-capped Oligomers, Fluoroalkyl End-capped Oligomers/Silica Nanocomposites and Fluoroalkyl End-capped Oligomers/Polyaniline Nanocomposites

3.1. Introduction

There have been hitherto numerous studies on the metal nanoparticles, especially, gold nanoparticles due to exhibiting unique optical and electronic properties together with a variety of applications in fields such as electronics, photonics, catalysts and biotechnology.[1–3] In general, a wide variety of chemical syntheses of gold nanoparticles with a narrow size distribution have been already reported by the use of photoreduction, radiolytic reduction, alcohol reduction and reduction using various reducing agents in association with protective polymers and surfactants to avoid the aggregation of gold nanoparticles resulting from Van der Waals interactions.[4–7] It has been already reported that partially fluoroalkylated polysoaps such as two fluoroalkyl end-capped oligomers can form the nanometer size-controlled self-assembled oligomeric aggregates with the aggregations of end-capped fluoroalkyl groups in aqueous and organic media.[8–13] These fluorinated oligomeric aggregates should interact with a variety of metal nanoparticles as guest molecules to give the colloidal stable fluorinated aggregates/metal nanoparticles composites.[14] In fact, the fluorinated oligomeric nanocomposite-encapsulated gold, silver and copper nanoparticles has been prepared through the reduction of these metal ions using sodium borohydride, poly(methylhydrosiloxane) and hydrazine.[15–21] In a variety of fluoroalkyl end-capped oligomers, unexpectedly, it has been

recently found that specified fluoroalkyl end-capped acryloylmorpholine–*N*-(1,1-dimethyl-3-oxobutyl)acrylamide cooligomer is applicable to the autoreduction of gold ions to give the corresponding cooligomer/gold nanocomposites.[22] From the developmental viewpoint of new fluorinated metal nanocomposite materials, it is of particular interest to develop new fluorinated oligomeric nanocomposite-encapsulated gold nanoparticles under numerous conditions. This chapter shows that not only fluoroalkyl end-capped acryloylmorpholine homooligomer and fluoroalkyl end-capped acrylic acid homooligomer but also the corresponding fluorinated homooligomers/silica nanocomposites can be applicable to the one-pot preparation of gold nanoparticles through the autoreduction of gold ions. Fluoroalkyl end-capped 2-methacryloyloxyethane sulfonic acid oligomer [R_F-(MES)$_n$-R_F] and fluoroalkyl end-capped 2-acrylamido-2-methylpropanesulfonic acid oligomer [R_F-(AMPS)$_n$-R_F] are not suitable for the autoreduction of gold ions; however, R_F-(MES)$_n$-R_F [or R_F-(AMPS)$_n$-R_F]/polyaniline (**PAn**) nanocomposites enabled the formation of gold nanoparticles through the reduction of **PAn** in the composites. The reversible conformational change of **PAn** was also observed during the gold nanoparticle formation. These results will be described in this chapter.

3.2. Experimental

3.2.1. Measurements

Molecular weights of R_F-$(ACA)_n$-R_F oligomer [Mn = 1,300], R_F-$(DMAA)_n$-R_F oligomer [Mn = 3,500] and R_F-$(ACMO)_n$-R_F oligomer [Mn = 7,600] were measured using a Shodex DS-4 (pump) and Shodex RI-71 (detector) gel permeation chromatography (Tokyo, Japan) calibrated with polystyrene standard using tetrahydrofuran (THF) as the eluent. Molecular weights of R_F-$(MES)_n$-R_F oligomer (Mn = 13,700) and R_F-$(AMPS)_n$-R_F oligomer [Mn = 20,500] were determined by using the same gel permeation chromatography calibrated pullulan (molecular weights 2,000 ~ 50,000) and poly(ethylene glycol) (molecular weight 1,000 ~ 40,000) standards, respectively, by using 0.5 mol dm^{-3} Na_2HPO_4 aqueous solution as the eluent. Dynamic light-scattering (DLS) measurements were performed using Otsuka Electronics DLS-7000 HL (Tokyo, Japan). Field-emission scanning electron microscopy (FE-SEM) images were measured by using a JEOL JSM-5300 (Tokyo, Japan). Transmission electron microscope (TEM) was measured by using JEOL JEM-1210 Electron microscopy (Tokyo, Japan). Ultraviolet-visible (UV-vis) spectra were recorded by using Shimadzu

UV-1600 UV-vis spectrophotometer (Kyoto, Japan). X-ray diffraction (XRD) measurements were performed by the use of Mac Science M18XHF-SRA (Tokyo, Japan).

3.2.2. Materials

N,N-dimethylacrylamide (DMAA) and acryloylmorpholine (ACMO) were obtained from Kohjin Co., Ltd., Tokyo, Japan. Acrylic acid was used as received from Toagosei Co., Ltd. (Tokyo, Japan). 3-Methacrylolyoxyethanesulfonic acid and 2-acrylamido-2-methylpropane-sulfonic acid were purchased from Polyscience, Inc. (PA, USA) and Wako Pure Chemical Industries, Ltd. (Osaka, Japan), respectively. R_F-$(ACA)_n$-R_F oligomer, R_F-$(DMAA)_n$-R_F oligomer, R_F-$(ACMO)_n$-R_F oligomer, R_F-$(MES)_n$-R_F oligomer and R_F-$(AMPS)_n$-R_F oligomer were prepared by reaction of fluoroalkanoyl peroxide with the corresponding monomers according to the previously reported methods.[23–26)]

3.2.3. Preparation of R_F-$(ACMO)_n$-R_F/Au nanocomposites

To an aqueous solution (5 ml) of R_F-$(ACMO)_n$-R_F oligomer [R_F = $CF(CF_3)OC_3F_7$ (60 mg)], an aqueous solution (1 ml) of $HAuCl_4$ (2 mmol/dm^3) was added. The mixture was

stirred with a magnetic bar at room temperature for 30 min to afford the wine red-colored solution. UV–vis spectrum of this solution afforded a plasmon absorption band around 546 nm related to the formation of gold nanoparticles. R_F-$(ACA)_n$-R_F/Au nanocomposites were also prepared under the similar conditions.

3.2.4. Preparation of R_F-$(ACMO)_n$-R_F/SiO_2/Au nanocomposites

To an aqueous solution (5 ml) of R_F-$(ACMO)_n$-R_F/SiO_2 nanocomposites (12 g/dm^3), which were prepared according to the previously reported method,[28, 29] an aqueous solution (1 ml) of $HAuCl_4$ (2 mmol/dm^3) was added. The mixture was stirred with a magnetic bar at room temperature for 2 days to afford the wine red-colored solution. UV–vis spectrum of this solution afforded a plasmon absorption band around 525 nm related to the formation of gold nanoparticles. After the solvent was evaporated off, methanol (25 ml) was added to the obtained products. The methanol solution was stirred with magnetic stirring bar at room temperature for 2 days and then was centrifuged for 30 min. The expected fluorinated nanocomposite was easily separated from the methanol solution. Fluorinated nanocomposite powders thus obtained were dried in vacuo at 50 °C for 2 days to afford purified particle

powders (40 mg). R_F-(ACA)$_n$-R_F/SiO_2/Au nanocomposites were also prepared under similar conditions (isolated yield 25 mg).

3.2.5. Preparation of R_F-(MES)$_n$-R_F/polyaniline (PAn)/Au nanocomposites

To an aqueous solution (5 ml) of R_F-(MES)$_n$-R_F/**PAn** nanocomposites (360 mg/dm^3), which were prepared according to the previously reported method,[28, 29] an aqueous solution (1 ml) of $HAuCl_4$ (2 mmol/dm^3) was added. The mixture was stirred with a magnetic bar at room temperature for 2 days to afford the wine red-colored solution. UV–vis spectrum of this solution afforded a plasmon absorption band around 535 nm related to the formation of gold nanoparticles. R_F-(AMPS)$_n$-R_F/**PAn**/Au nanocomposites were also prepared under the similar conditions.

3.2.6. Preparation of modified poly(vinyl alcohol) film treated with R_F-(ACMO)$_n$-R_F/Au nanocomposites

The modified poly(vinyl alcohol) (PVA) film was prepared by casting to aqueous solution (5 ml) of PVA (450 mg) and aqueous solution (5 ml) containing R_F-(ACMO)$_n$-R_F/Au

nanocomposites [R_F-$(ACMO)_n$-R_F oligomer, 10 g/dm^3; $HAuCl_4$, 333 μmol/dm^3] on the glass plates. The solvent was evaporated at room temperature, and the film formed peeled off and dried at 50 °C for 24 h under vacuum to afford the modified PVA film (film thickness 175 μm). The modified PVA film (film thickness 155 μm) treated with R_F-$(ACA)_n$-R_F/Au nanocomposites was also prepared under the similar conditions.

3.3. Results and discussion

A variety of fluoroalkyl end-capped oligomers, such as fluoroalkyl end-capped acrylic acid oligomer [R_F-$(ACA)_n$-R_F], acryloylmorpholine oligomer [R_F-$(ACMO)_n$-R_F], 2-acrylamido-2-methylpropanesulfonic acid oligomer [R_F-$(AMPS)_n$-R_F], 2-(methacryloyloxy)ethanesulfonic acid oligomer [R_F-$(MES)_n$-R_F] and *N,N*-dimethylacrylamide oligomer [R_F-$(DMAA)_n$-R_F] were studied on the preparation of gold nanoparticles through the autoreduction of gold ions in the presence of these oligomers. The results are shown in Scheme 3-1, Figs. 3-1 ~ 3-3.

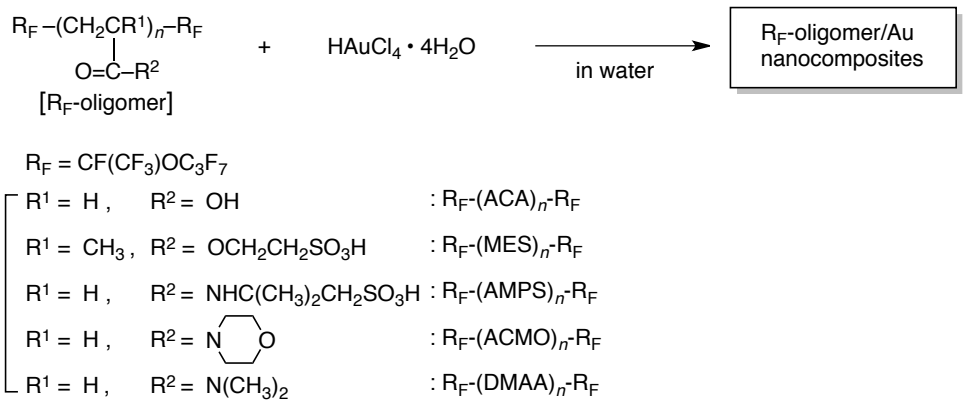

Scheme 3-1 Preperation of R_F-oligomer/Au nanocomposites by the autoreduction of gold ions in water

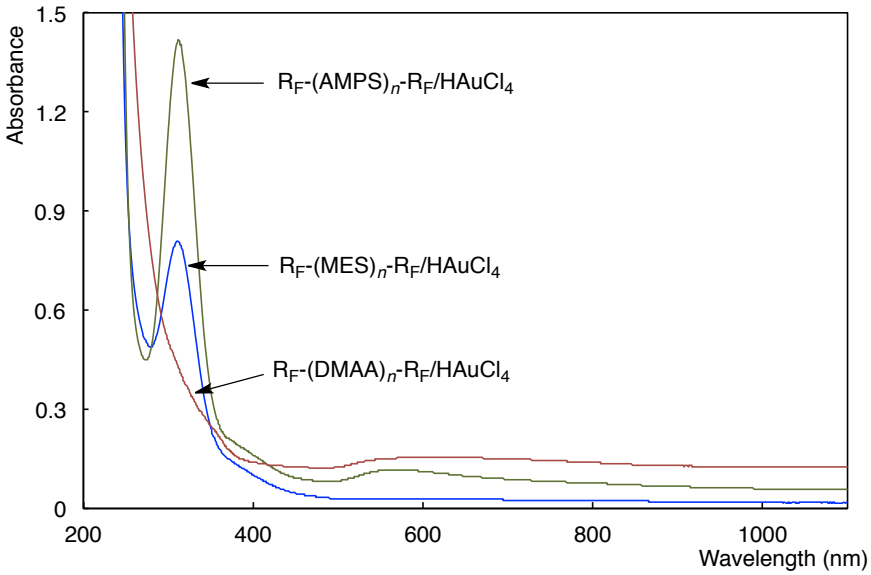

Fig. 3-1 UV-vis spectra of aqueous solutions of mixtures of R_F-oligomer [10 g/dm^3] and $HAuCl_4$ [333 μmol/dm^3]

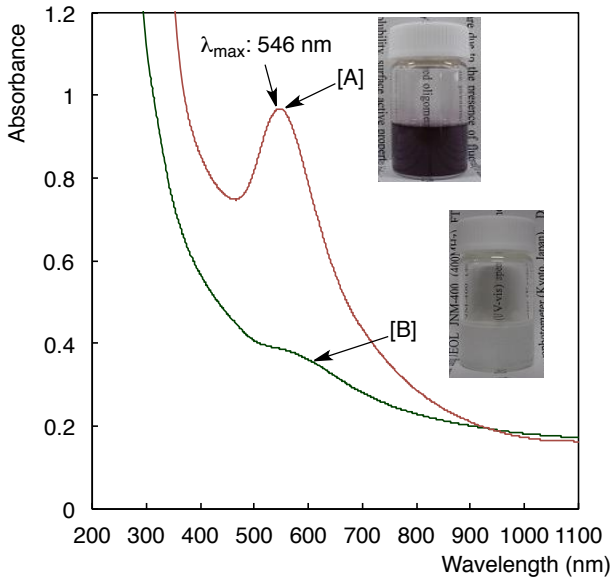

Fig. 3-2 UV-vis spectra of aqueous solutions of a mixture of R_F-(ACMO)$_n$-R_F oligomer [10 g/dm^3] and $HAuCl_4$ [333 μmol/dm^3] (A), and aqueous solution of a mixture of -(ACMO)$_n$- oligomer [10 g/dm^3] and $HAuCl_4$ [333 μmol/dm^3] (B)

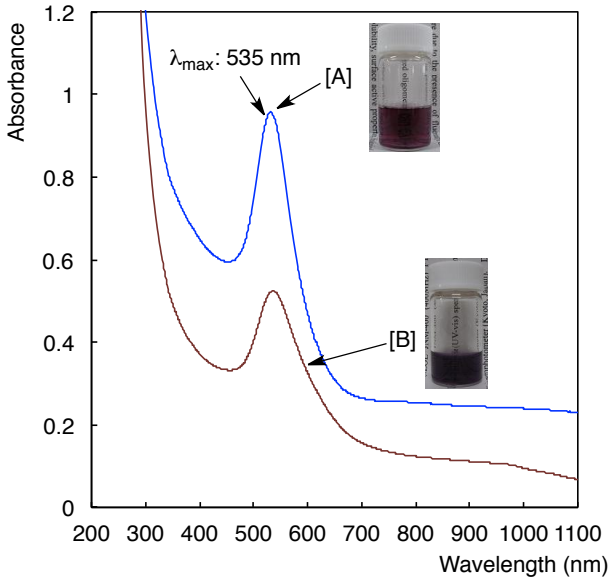

Fig. 3-3 UV-vis spectra of aqueous solution of a mixture of R_F-$(ACA)_n$-R_F oligomer [10 g/dm^3] and $HAuCl_4$ [333 μmol/dm^3] (A), and aqueous solution of a mixture of -$(ACA)_n$- oligomer [10 g/dm^3] and $HAuCl_4$ [333 μmol/dm^3] (B)

As shown in Scheme 3-1 and Fig. 3-1, R_F-$(AMPS)_n$-R_F, R_F-$(MES)_n$-R_F and R_F-$(DMAA)_n$-R_F oligomers were not effective for the preparation of gold nanoparticles under the autoreduction conditions. However, a sharp plasmon absorption band around 535 ~ 546 nm related to the formation of gold nanoparticles under the autoreduction of the gold ions in the presence of R_F-$(ACMO)_n$-R_F and R_F-$(ACA)_n$-R_F oligomers (see Figs. 3-2 and 3-3). The corresponding nonfluorinated -$(ACMO)_n$- oligomer was unable to give such plasmon absorption peak at all under the similar conditions (Fig. 3-2[**B**]). In contrast, a relatively weak plasmon peak was observed in the presence of the nonfluorinated -$(ACA)_n$- oligomer (Fig. 3-3[**B**]).

In order to clarify the formation of gold nanoparticles, the field-emission scanning electron micrograph (FE-SEM) and transmission electron microscopy (TEM) photograph of methanol solutions of R_F-$(ACA)_n$-R_F/Au nanocomposites and R_F-$(ACMO)_n$-R_F/Au nanocomposites in Scheme 3-1 have been measured, and the results were shown in Fig. 3-4 and Fig. 3-5.

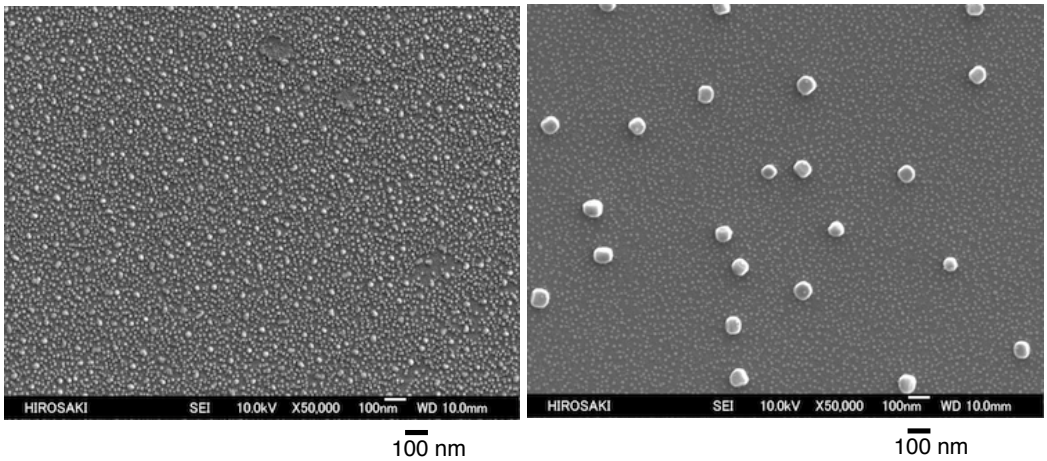

R_F-$(ACA)_n$-R_F/Au Nanocomposites R_F-$(ACMO)_n$-R_F/Au Nanocomposites

Fig. 3-4 Field emission scanning electron microscopy (FE-SEM) images of R_F-oligomer/Au nanocomposites methanol solutions

The FE-SEM pictures of R_F-$(ACA)_n$-R_F/Au nanocomposites and R_F-$(ACMO)_n$-R_F/Au nanocomposites showed the formation of very fine particles with mean diameters of 28.5 ± 3.2 and 82.1 ± 4.9 nm, respectively. Sizes of these composites in Scheme 3-1 were also measured in methanol by using DLS measurements. The sizes of these composites were nanometer size-controlled: 26.6 ± 6.4 and 106.8 ± 19.3 nm. As shown in Scheme 3-1 and Fig.

3-4, the similar particle sizes for these composites have been obtained in DLS and FE-SEM measurements, respectively. Especially, DLS measurements showed the increase of the size of R_F-$(ACA)_n$-R_F/Au nanocomposites and R_F-$(ACMO)_n$-R_F/Au nanocomposites, compared with those (10.9 ± 1.7 and 10.8 ± 1.1 nm) of the parent R_F-$(ACA)_n$-R_F and R_F-$(ACMO)_n$-R_F oligomeric aggregates, indicating that gold nanoparticles should be effectively encapsulated into the fluorinated oligomeric aggregate cores to give the corresponding fluorinated oligomer/gold nanocomposites. In fact, each TEM picture of these nanocomposites shows the effective encapsulation of gold nanoparticles into these fluorinated oligomeric aggregate cores (see Fig. 3-5).

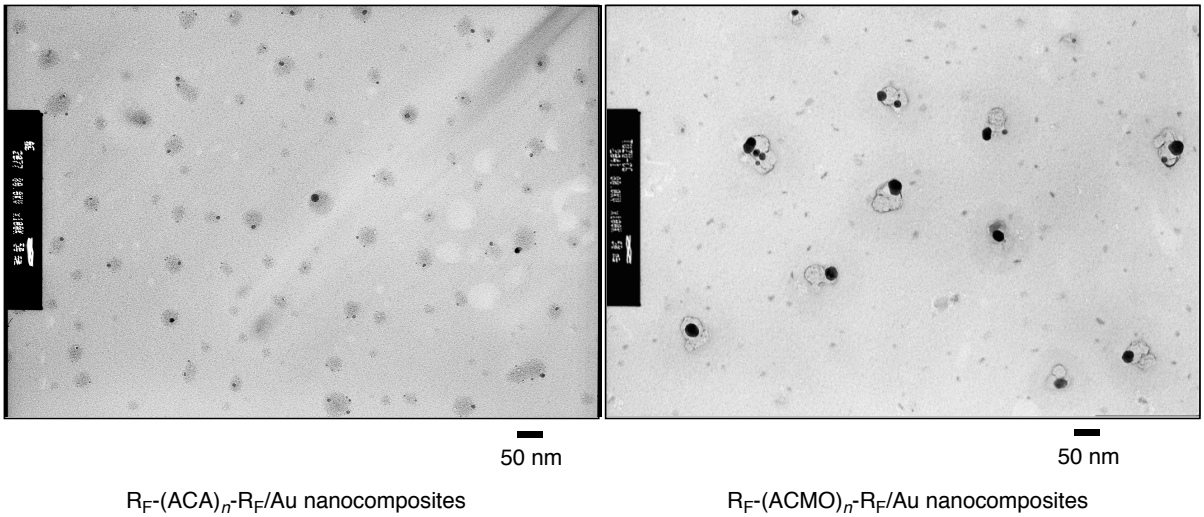

Fig. 3-5 Transmission electron microscopy (TEM) images of R_F-oligomer/Au nanocomposite methanol solutions

X-ray diffraction (XRD) patterns of R_F-$(ACA)_n$-R_F/Au nanocomposites and R_F-$(ACMO)_n$-R_F/Au nanocomposites also show the formation of gold nanoparticles, and each nanocomposite can give a clear XRD pattern related to the original gold nanoparticles (see Fig. 3-6).[30, 31)]

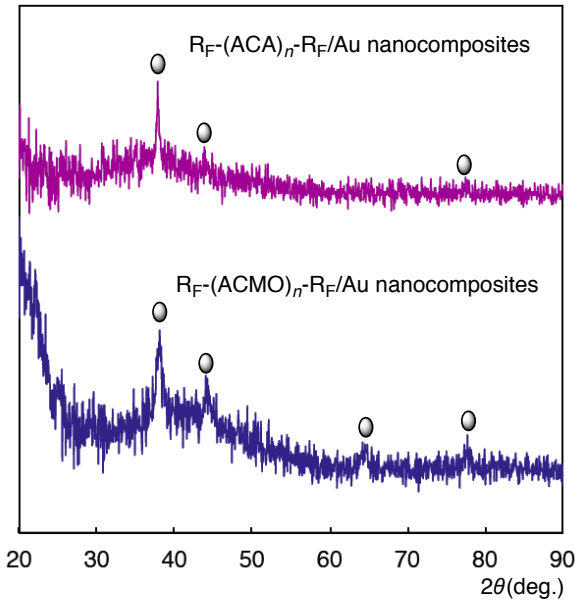

Fig. 3-6 X-ray diffraction (XRD) patterns of R_F-oligomer/Au nanocomposites

Hitherto, there have been numerous reports on the preparation of gold nanoparticles by the autoreduction of gold ions in the presence of water-soluble polymers. For example, gold nanoparticles can be easily prepared by the autoreduction of $HAuCl_4$ in the presence of poly(ethylene glycol)-*block*-poly[2-(*N,N*-dimethylamino)ethyl methacrylate] copolymer and polystyrene-*block*-poly[2-(*N,N*-dimethylamino)ethyl methacrylate] copolymer through an ion exchange process between H^+ $AuCl_4^-$ and protonated *N,N*-dimethylaminoethyl segments

(-N^+Me_2H Cl^-) in copolymer.[32, 33] Autoreduction of gold ions was also observed to give the gold nanoparticles in the presence of hyperbranched poly(ester amide)s,[34] poly(ε-caprolactone)/poly(*N*-vinyl-2-pyrrolydone) biodegradable triblock copolymer,[35] poly(vinyl)pyrrolidone,[36] poly[*tert*-butylstyrene-*block*-sodium (sulfamate-carboxylate-isoprene)],[37] poly(ethylene oxide)-poly(propylene oxide)-poly(ethylene oxide) block copolymers[38–42] and amphiphilic polyesters containing hydrophilic polyethylene oxide fragments, which acts as a reducing agent of gold ions[43] and poly(sodium acrylate)s[44]. In these polymers, it is well known that the tertiary amino groups in the hyperbranched poly(ester amide)s play a crucial role in the autoreduction of gold ions[34] and poly(sodium acrylate)s act as both reducing and stabilizing agent.[44] Thus, the autoreduction of gold ions through an ion exchange process between H^+ $AuCl_4^-$ and protonated ACMO segments in R_F-$(ACMO)_n$-R_F oligomer would occur smoothly in the fluorinated oligomeric aggregate cores. In contrast, the corresponding nonfluorinated -$(ACMO)_n$- oligomer cannot form such molecular aggregates to afford the gold nanoparticles through the autoreduction process under the similar conditions. R_F-$(ACA)_n$-R_F oligomer possesses carboxylate units as well as poly(sodium acrylate)s. Thus, gold ions should be effectively encapsulated into the R_F-$(ACA)_n$-R_F oligomeric aggregates cores to interact with the carboxylate units. Such interaction would enable the formation of gold nanoparticles in the fluorinated aggregate cores. On the other hand, the nonfluorinated

-(ACA)$_n$- oligomer cannot form the self-assembled molecular aggregates to give the effective interaction between the carboxylate units and the gold ions. This weak interaction would give the relatively reduced plasmon absorption peak illustrated in Fig. 3-3[**B**], quite similar to the use of poly(sodium acrylate)s.[44)]

Previously, it was reported that a variety of fluoroalkyl end-capped oligomers were applicable to the surface modification of traditional organic polymers such as poly(methyl methacrylate) (PMMA) to exhibit a good oleophobic characteristic imparted by fluorine.[45)] It has been also verified that these fluorinated oligomers could be arranged regularly on the modified PMMA film surface.[45)] Thus, these present fluorinated oligomers/Au nanocomposites have been applied to the modification of poly(vinyl alcohol) (PVA).

Fig. 3-7 shows the transparent wine red-colored modified PVA films, although the parent PVA film is transparent colorless. These modified PVA films were found to exhibit a sharp plasmon absorption peak around 541 ~ 545 nm related to the formation of Au nanoparticles, indicating that the gold nanoparticles should be well dispersed without the agglomeration between the metal particles in the cast films. In addition, the modified PVA films have been stored for more than 1 year under air atmosphere conditions at room temperature and found to be stable with keeping the same wine red color.

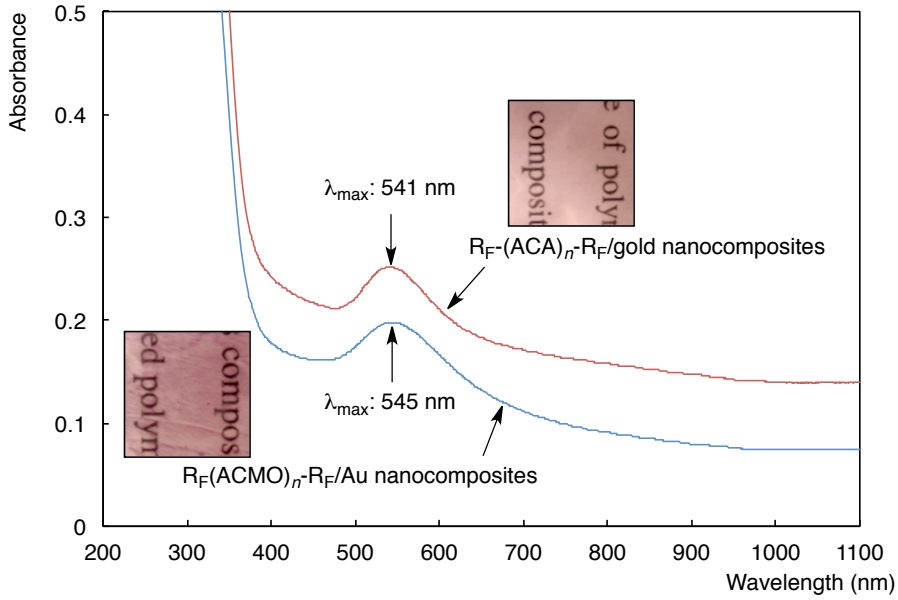

Fig. 3-7 UV-vis spectra of modified poly(vinyl alcohol) (PVA) films treated with R_F-oligomer/Au nanocomposites; Concentration of nanocomposites based on the used PVA: 11 wt%

Recently, much attention has been focused on the hybrid nanoparticles composed of metals and dielectric silica particle materials due to possessing potential applications in a variety of fields such as materials for catalysts and biomedical areas.[46–48] From the developmental viewpoint of new fluorinated functional hybrid materials, it is deeply desirable to explore new Au/SiO_2 hybrids imparted by fluorine. Thus, the preparation of R_F-$(ACA)_n$-R_F/SiO_2/Au nanocomposites and R_F-$(ACMO)_n$-R_F/SiO_2/Au nanocomposites had been studied, and the results are shown in Scheme 3-2 and Scheme 3-3.

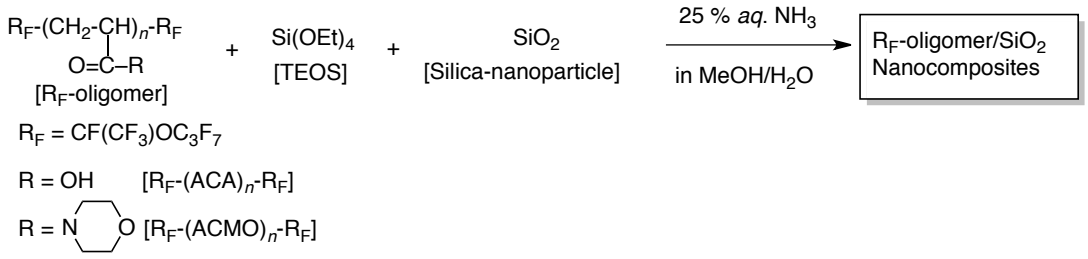

Used Oligomer (g)		Silica nanoparticles[a] [g]	TEOS [mL]	*aq.* NH_3 [mL]	MeOH [mL]	H_2O [mL]	Product Yeild[b] [%]	Size of the composites[c] [nm]
R_F-$(ACA)_n$-R_F	0.25	0.50	0.25	0.25	6	4	84	46.2 ± 9.5
R_F-$(ACMO)_n$-R_F	0.25	0.50	0.25	0.25	6	4	81	59.3 ± 7.4

a) Average particle size: 11 nm
b) Yields were based on R_F-oligomer, silica and TEOS
c) Determined by dynamic light scattering(DLS) measurements in methanol

Scheme 3-2

Firstly, R_F-$(ACA)_n$-R_F/SiO_2 nanocomposites and R_F-$(ACMO)_n$-R_F/SiO_2 nanocomposites have been prepared by using the sol–gel reactions of tetraethoxysilane (TEOS) in the presence of the corresponding oligomers and silica nanoparticles (average particle size 11 nm) according to the previously reported method.[27] The obtained nanocomposites are nanometer size-controlled fine particles (46 ~ 59 nm) (see Scheme 3-2).

Furthermore, the encapsulation of gold nanoparticles into these fluorinated oligomeric silica nanocomposite cores have been studied by the autoreduction of the gold ions in the presence of the fluorinated silica nanocomposites at room temperature as shown in Scheme 3-3.

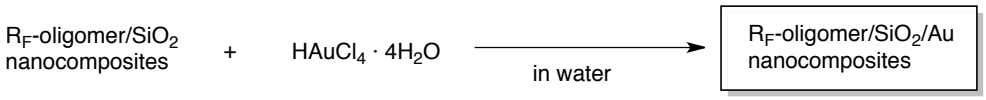

Used R_F-oligomer	R_F-oligomer/SiO_2 nanocomposites [mg]	$HAuCl_4$ [μmol]	Product yeild[a] [%]	Size of the composites[b] [nm]
R_F-$(ACA)_n$-R_F oligomer	60	2.0	41	96.6 ± 15.5 (46.2 ± 9.5)[c]
R_F-$(ACMO)_n$-R_F oligomer	60	2.0	67	96.6 ± 26.4 (59.3 ± 7.4)

a) Yields were based on R_F-oligomer/SiO_2 nanocomposites and $HAuCl_4$
b) Determined by dynamic light scattering(DLS) measurements
c) Size of the parent R_F-oligomer/SiO_2 nanocomposites

Scheme 3-3

The expected fluorinated oligomers/SiO_2 nanocomposite-encapsulated Au nanoparticles were obtained in 41 ~ 67 % isolated yields, and the obtained nanocomposites were found to exhibit a good dispersibility and stability in not only water but also traditional organic solvents such as methanol, *t*-butyl alcohol, tetrahydrofuran, ethyl acetate and chloroform. Thus, the size of these composites in methanol has been measured by dynamic light-scattering (DLS) measurements at 25 °C, and the results were also shown in Scheme 3-3.

Fluorinated silica nanocomposites in Scheme 3-3 were nanometer size controlled (a mean diameter 97 nm), and the increase of the size of the composites from 46 ~ 59 nm to 97 nm after the encapsulation of gold nanoparticles was observed, indicating that the gold nanoparticles can be effectively encapsulated into the fluorinated oligomers/SiO_2 nanocomposite cores to increase the size of the composites.

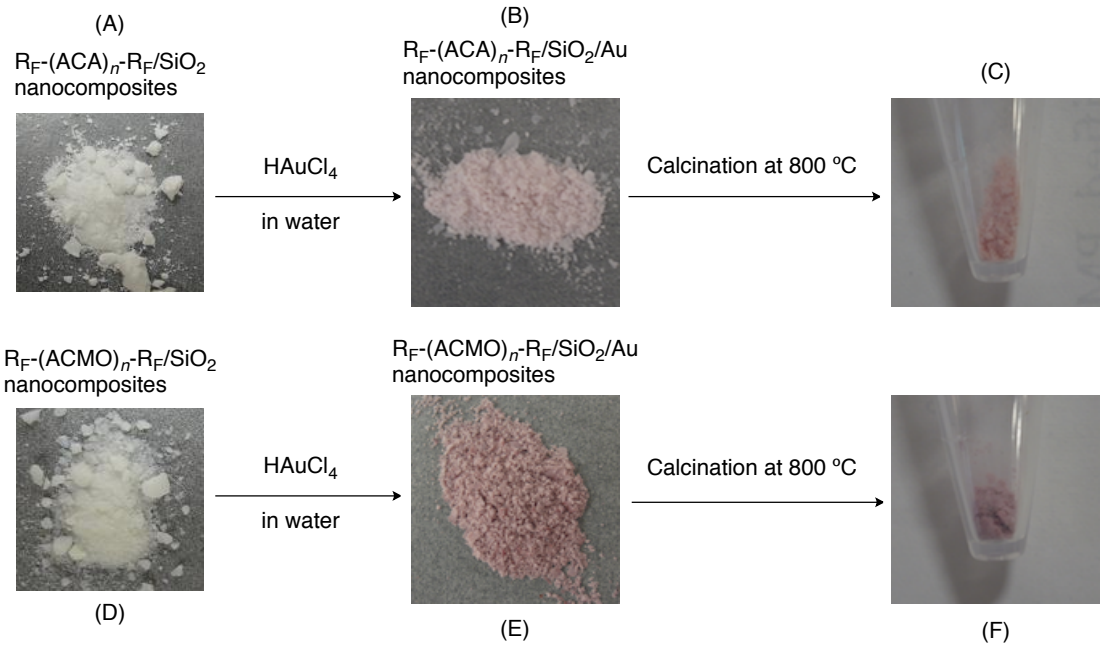

Fig. 3-8 Photograph of R_F-oligomer/SiO_2 nanocomposite powder and R_F-oligomer/SiO_2/Au nanocomposite powder before and after calcination at 800 °C

As shown in Fig. 3-8(**A**), (**B**), the obtained R_F-(ACA)$_n$-R_F/SiO_2 nanocomposites and R_F-(ACMO)$_n$-R_F/SiO_2 nanocomposites are white-colored powders; however, the corresponding nanocomposites as wine red-colored powders [Fig. 3-8(**B**), (**E**)] can be isolated after the encapsulation of gold nanoparticles into these composite cores. Interestingly, the similar-colored composite powders can be isolated even after calcination at 800 °C [Fig. 3-8(**C**), (**F**)]. These findings suggest that the encapsulation of gold nanoparticles into the nanocomposite cores should smoothly proceed to give the expected fluorinated silica nanocomposite-encapsulated gold nanoparticles by the autoreduction of gold ions in the presence of the composites at room temperature.

FE-SEM and TEM photographs of well-dispersed methanol solutions of R_F-$(ACA)_n$-R_F/SiO_2/Au nanocomposites and R_F-$(ACMO)_n$-R_F/SiO_2/Au nanocomposites have been recorded to clarify not only the formation of fluorinated oligomers/SiO_2/Au nanocomposite fine particles but also the presence of the gold nanoparticles in the composite cores,. In addition, UV–vis spectra of well-dispersed methanol solutions of these nanocomposites have been measured. These results are shown in Figs. 3-9 ~ 3-11.

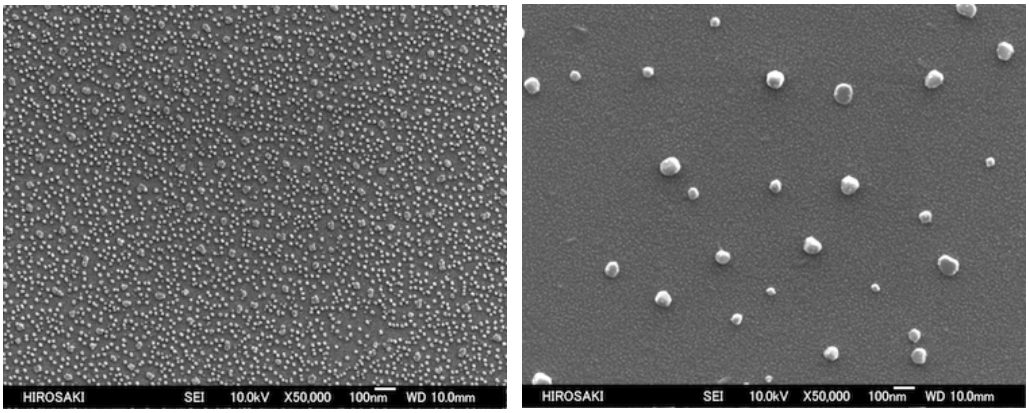

R_F-$(ACA)_n$-R_F/SiO_2/Au nanocomposites

R_F-$(ACMO)_n$-R_F/SiO_2/Au nanocomposites

Fig. 3-9 FE-SEM images of R_F-oligomer/SiO_2/Au nanocomposite methanol solutions

As shown in Fig. 3-9, FE-SEM pictures show that R_F-$(ACA)_n$-R_F/SiO_2/Au nanocomposites and R_F-$(ACMO)_n$-R_F/SiO_2/Au nanocomposites are very fine nanoparticles with a mean diameter 17.2 ± 5.2 and 66.6 ± 17.7 nm, respectively. Of particular interest, TEM photographs of R_F-$(ACA)_n$-R_F/SiO_2/Au nanocomposites and R_F-$(ACMO)_n$-R_F/SiO_2/Au

nanocomposites show that the gold nanoparticles can be encapsulated into these composite cores to give the corresponding fluorinated silica nanocomposite-encapsulated gold nanoparticles (see Fig. 3-10).

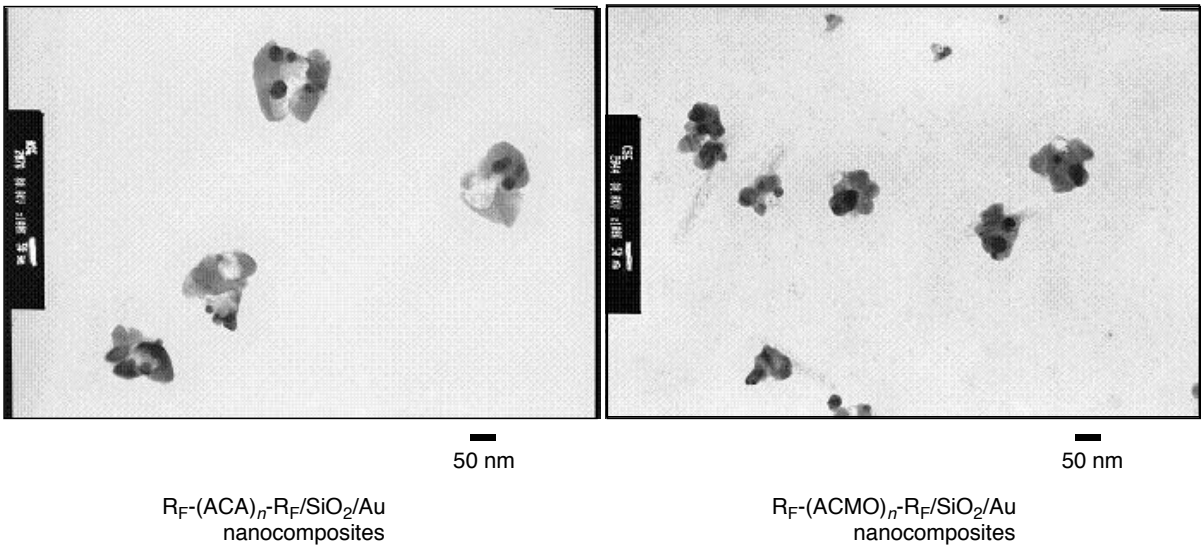

Fig. 3-10 TEM images of R_F-oligomer/SiO_2/Au nanocomposites

UV–vis spectra of well-dispersed methanol solutions (wine red-colored solutions) of R_F-(ACA)$_n$-R_F/SiO_2/Au nanocomposites and R_F-(ACMO)$_n$-R_F/SiO_2/Au nanocomposites have been measured, and the results were shown in Fig. 3-11.

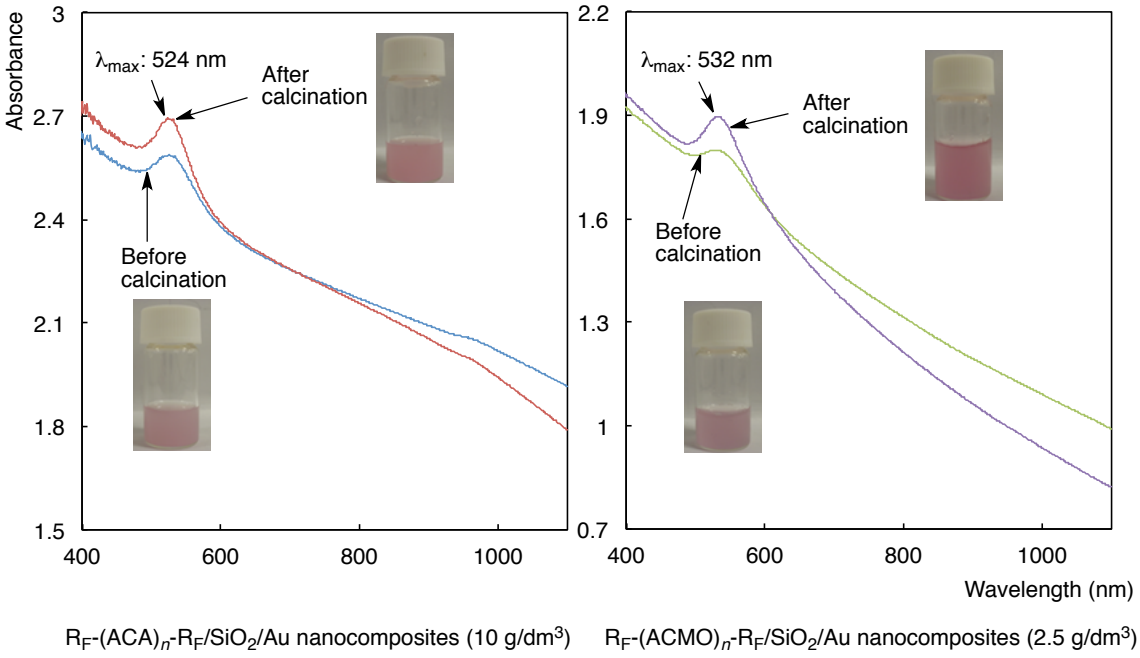

Fig. 3-11 UV-vis spectra of aqueous solutions of R_F-oligomer/SiO_2/Au nanocomposites before and after calcination at 800 ºC

The well-defined sharp plasmon absorption band around 524 ~ 532 nm can be observed, which was related to the formation of stable gold nanoparticles in the composites. Interestingly, the similar plasmon absorption peak was observed around 524 ~ 532 in these composites after calcination at 800 °C, indicating that almost the same size of the gold nanoparticles can be observed before and even after calcination. FE-SEM pictures of R_F-$(ACA)_n$-R_F/SiO_2/Au nanocomposites and R_F-$(ACMO)_n$-R_F/SiO_2/Au nanocomposites after calcination at 800 °C (see Fig. 3-9) also showed the similar particle sizes: 13.3 ± 2.6 and 84.7 ± 6.7 nm to those before calcination: 17.4 ± 5.2 and 66.6 ± 17.7 nm, respectively. Usually, it is well known that gold nanoparticles can more easily agglomerate each other, especially the

metal–support interaction is weak,[49] and the size of the gold nanoparticles supported on mesoporous silica hosts is likely to increase after calcination at 550 °C.[50] From this point of view, these present fluorinated oligomers/SiO_2 nanocomposite-encapsulated gold nanoparticles would have high potential in a variety of field such as materials for catalysts.

Among a variety of fluoroalkyl end-capped oligomers, R_F-$(ACA)_n$-R_F oligomer and R_F-$(ACMO)_n$-R_F oligomer have been shown to be useful for the preparation of gold nanoparticles by the autoreduction of the gold ions in the presence of these oligomers. R_F-$(ACA)_n$-R_F oligomer/ and R_F-$(ACMO)_n$-R_F oligomer/SiO_2 nanocomposites were also applied to the autoreduction of the gold ions. However, R_F-$(MES)_n$-R_F oligomer, R_F-$(AMPS)_n$-R_F oligomer and R_F-$(DMAA)_n$-R_F oligomer were unable to apply the autoreduction of the gold ions under the similar conditions. Polyaniline (**PAn**) is of particular interest, because of its environmental stability, controllable electrical conductivity and interesting redox properties associated with the nitrogen in the main chain.[51] Especially, **PAn**, in which benzene rings and amine groups coexist in polymer main chains, will be the ideal stabilizers for gold nanoparticles, and it has been reported that doped **PAn** can be also used as a reductant for the generation of gold nanoparticles.[51–53] R_F-$(MES)_n$-R_F oligomer and R_F-$(AMPS)_n$-R_F oligomer can be applicable for the preparation of the corresponding oligomers/**PAn** nanocomposites by the polymerization of aniline in the presence of these

oligomers catalyzed by ammonium persulfate as described in chapter 1. Thus, the gold nanoparticles were tried to encapsulate into these fluorinated **PAn** nanocomposite cores by the reduction of the gold ions with **PAn** in the fluorinated nanocomposites. These results are shown in Schemes 3-4, 3-5 and Fig. 3-12.

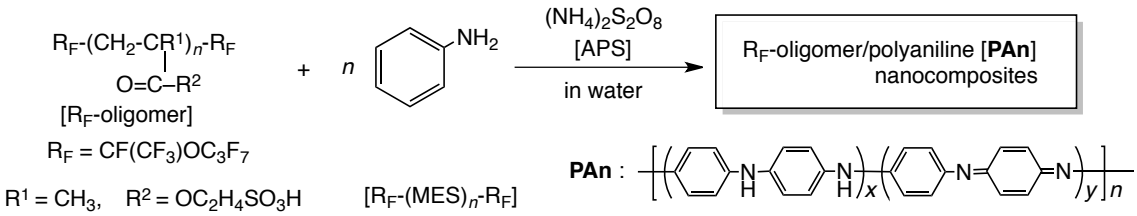

Used R_F-oligomer [mg]		Aniline [mg]	APS [mg]	Product yeild[a] [%]	Size of the composites[b] [nm]
R_F-$(MES)_n$-R_F	282	48	115	80	32.6 ± 4.5
R_F-$(AMPS)_n$-R_F	282	47	115	95	74.6 ± 7.1

a): Yields were based on R_F-oligomer and aniline
b): Determined by dynamic light scattering (DLS) measurements

Scheme 3-4

As shown in Scheme 3-4, R_F-$(MES)_n$-R_F oligomer/**PAn** nanocomposites and R_F-$(AMPS)_n$-R_F oligomer/**PAn** nanocomposites were obtained in 80 ~ 95 % isolated yields according to the previously reported method,[28, 29] and the size of these composites in methanol are nanometer size-controlled: 32.6 ± 4.5 and 74.6 ± 7.1 nm, respectively. In

addition, these fluorinated **PAn** nanocomposites were applied to the encapsulation of gold nanoparticles into these composite cores.

The encapsulation of gold nanoparticles was found to proceed smoothly at room temperature to give the expected fluorinated oligomers/**PAn** nanocomposites (see Scheme 3-5).

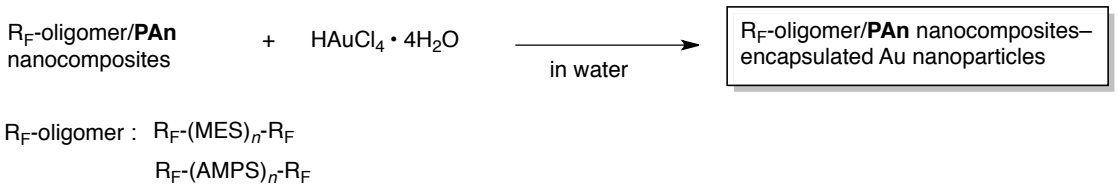

Scheme 3-5

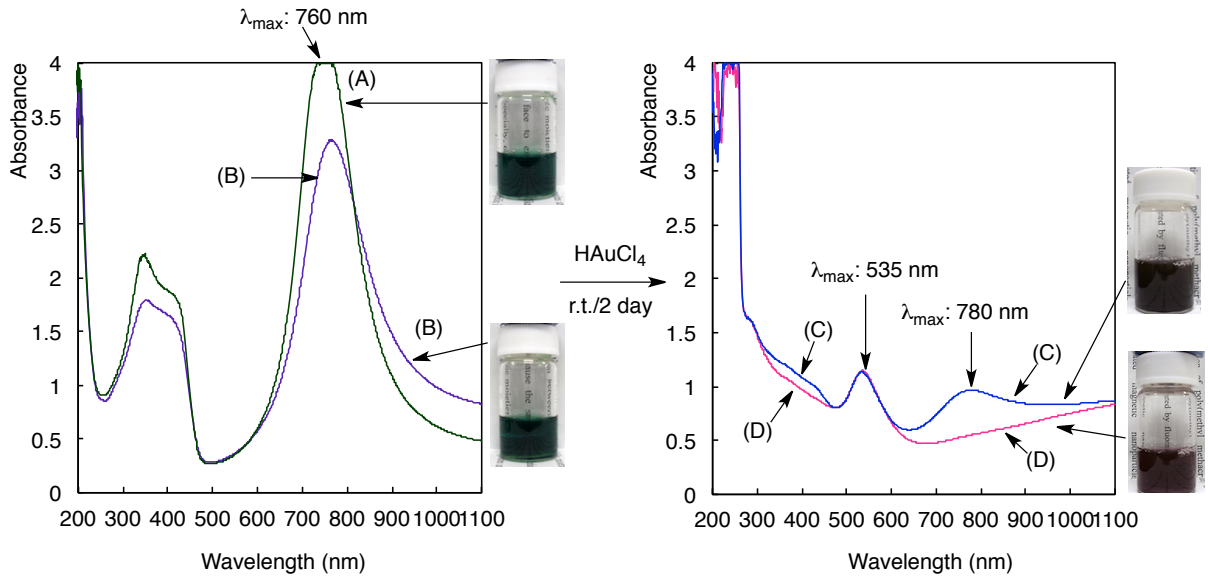

Fig. 3-12 UV-vis spectra of aqueous solutions of R_F-$(MES)_n$-R_F/**PAn** nanocomposites (A), R_F-$(AMPS)_n$-R_F/**PAn** nanocomposites (B), R_F-$(MES)_n$-R_F/**PAn**/Au nanocomposites (C), and R_F-$(AMPS)_n$-R_F/**PAn** nanocomposites (D). Concentration of R_F-oligomer/PAn nanocomposites, 300 mg dm^{-3}; $HAuCl_4$, 333 μmol dm^{-3}

The parent R_F-(MES)$_n$-R_F/**PAn** nanocomposites and R_F-(AMPS)$_n$-R_F/**PAn** nanocomposites afforded the transparent green-colored aqueous solutions, of whose color is related to π-polar transition around 760 nm [see Fig. 3-12(**A**), (**B**)]. However, interestingly, such π-polaron absorption has been dramatically disappeared to give newly a sharp plasmon absorption band around 535 nm related to the formation of gold nanoparticles, indicating that R_F-(MES)$_n$-R_F/**PAn** nanocomposites and R_F-(AMPS)$_n$-R_F/**PAn** nanocomposites can interact with the gold ions to afford the corresponding fluorinated oligomers/**PAn**/Au nanocomposites [see Fig. 3-12(**C**), (**D**)].

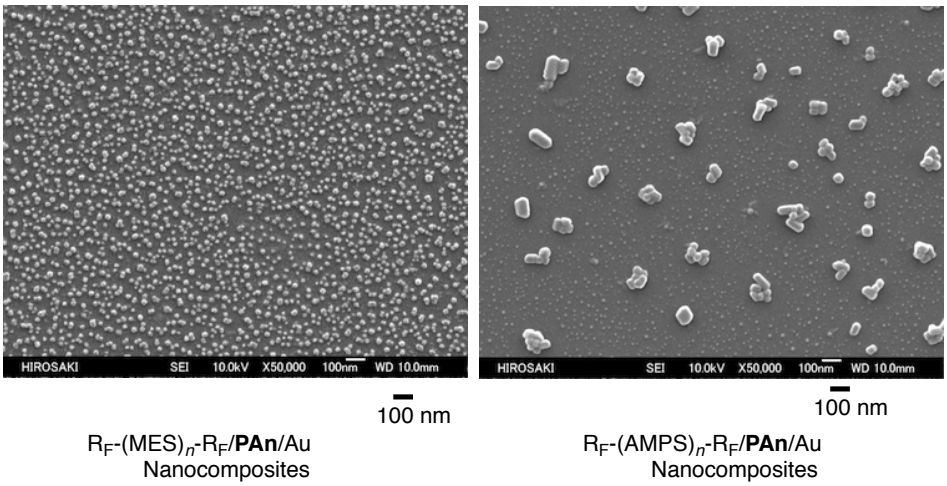

Fig. 3-13 FE-SEM images of R_F-oligomer/**PAn**/Au nanocomposites methanol solutions

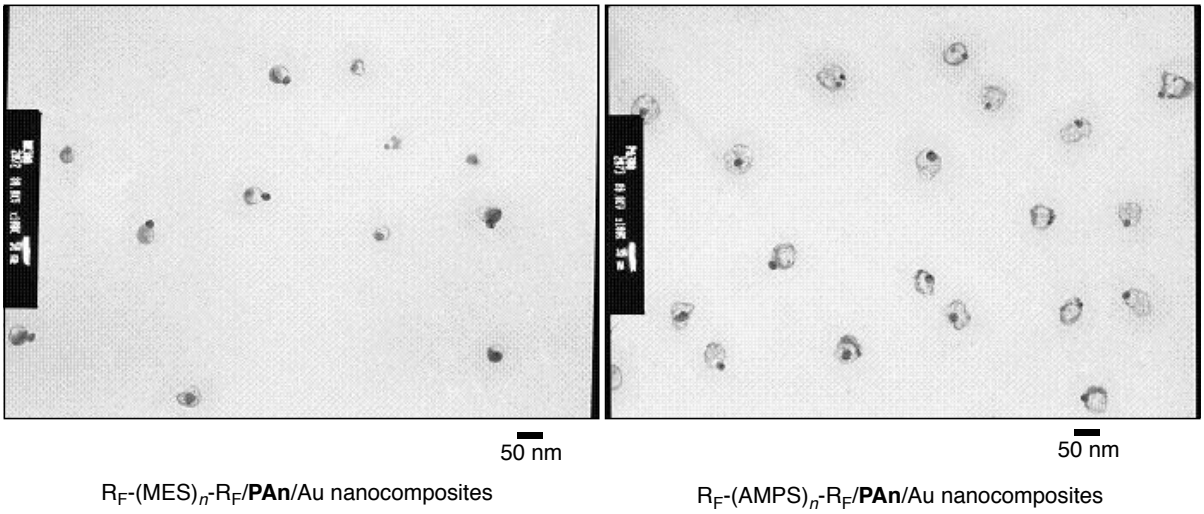

Fig. 3-14 TEM images of R_F-oligomer/**PAn**/Au nanocomposite methanol solutions

FE-SEM photographs of R_F-(MES)$_n$-R_F/**PAn**/Au nanocomposites and R_F-(AMPS)$_n$-R_F/**PAn**/Au nanocomposites show the formation of very fine nanoparticles with mean diameters: 20.3 ± 5.3 and 49.9 ± 10.8 nm, respectively (see Fig. 3-13). TEM pictures show that the gold nanoparticles were effectively encapsulated into these fluorinated oligomers/**PAn** nanocomposite cores (Fig. 3-14). XRD spectra of R_F-(MES)$_n$-R_F/**PAn**/Au nanocomposites also show the formation of gold nanoparticles in the nanocomposites, of whose spectra patterns are quite similar to those of the parent gold nanoparticles (see Fig. 3-15).[30, 31)]

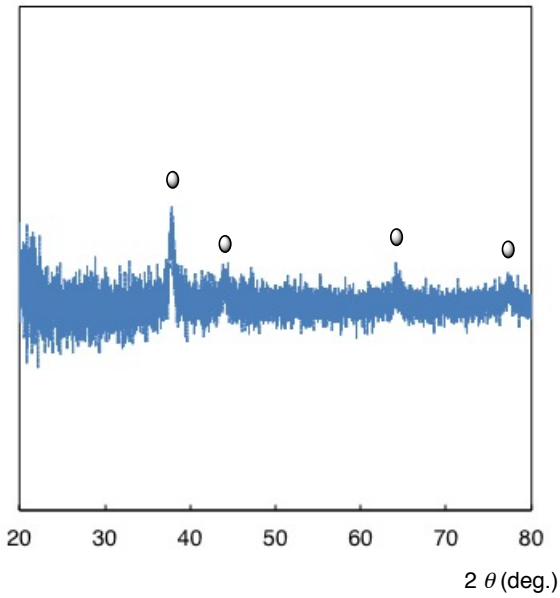

Fig. 3-15 XRD patterns of R_F-(MES)$_n$-R_F/**PAn**/Au nanocomposites

In this way, the smooth color change of the aqueous composite solutions from transparent green color to wine red color can be observed, which can be attributed from π-polaron transition (λ_{max}, 750 nm) of **PAn** to the plasmon absorption (λ_{max}, 550 nm) of gold nanoparticles. It was previously reported that fluoroalkyl end-capped oligomers [R_F-(M)$_n$-R_F: M = radical polymerizable monomers] can form the self-assembled fluorinated oligomeric aggregates through the aggregation of end-capped fluoroalkyl groups in aqueous and organic media.[9–15] Thus, **PAn** should be encapsulated into such fluorinated oligomeric aggregate cores as a guest molecule to give the fluorinated oligomers/**PAn** nanocomposites. These fluorinated **PAn** nanocomposites should enable the smooth interaction of the gold ions with the amine units in the **PAn** main chain to give the gold nanoparticles.

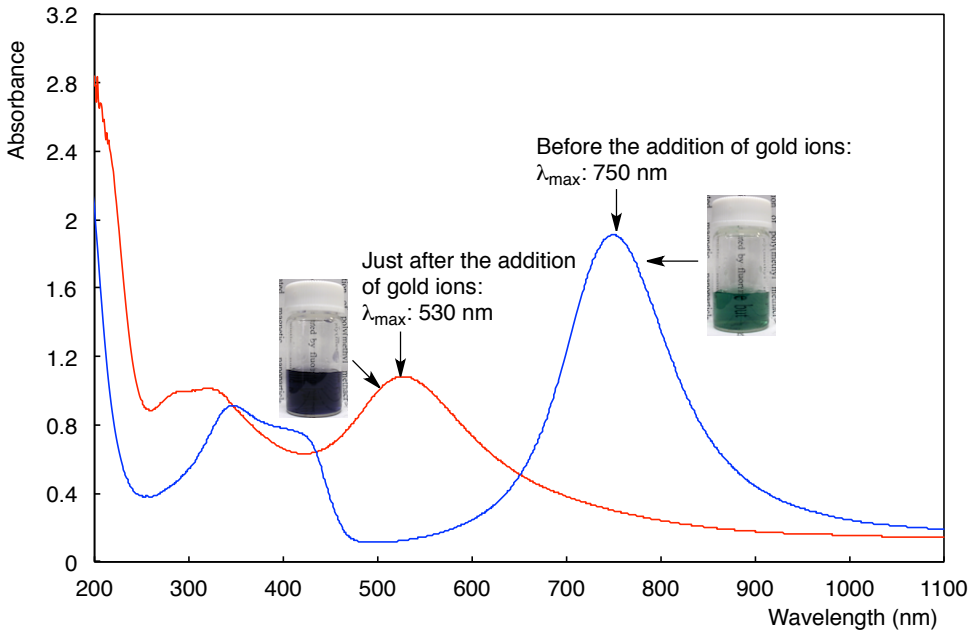

Fig. 3-16 UV-vis spectra change of aqueous solution of R_F-$(MES)_n$-R_F/**PAn** nanocomposites (100 mg dm^{-3}) before and after the addition of $HAuCl_4$ (111 μmol dm^{-3})

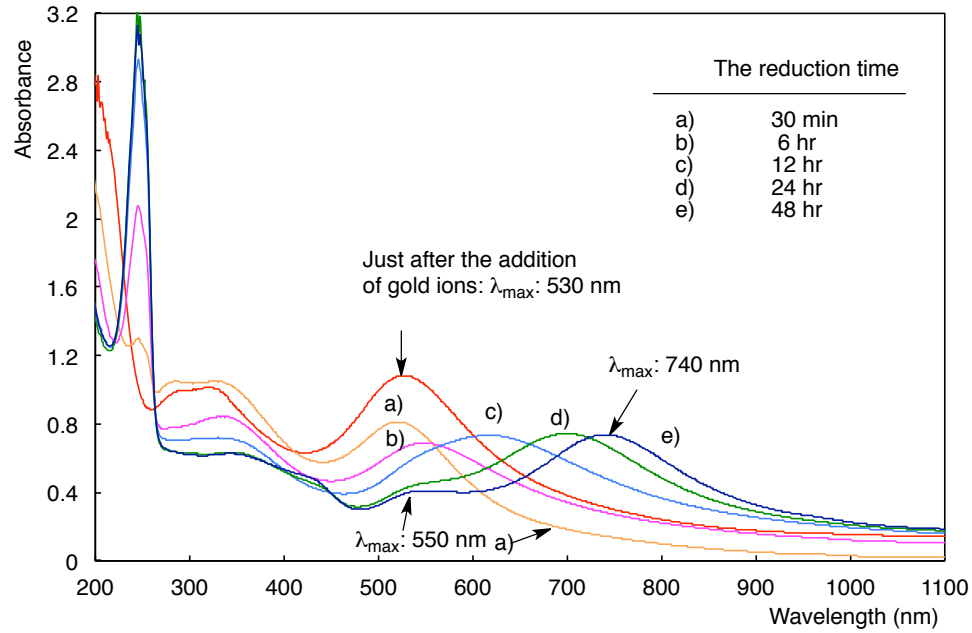

Fig. 3-17 Changes in the UV–vis spectra of the aqueous solutions of the R_F-$(MES)_n$-R_F/**PAn**/Au nanocomposites (concentration of the composites, 100 mg dm^{-3}; concentration of $HAuCl_4$, 111 μmol dm^{-3}) under the reduction by **PAn** in the nanocomposites

During such reduction process, a clear conformational change of **PAn** main chain was observed from the polyemeraldine salt (λ_{max}, around 750 nm) to the oxidized pernigraniline base (λ_{max}, around 530 nm) just after the addition of the gold ions as shown in Fig. 3-16.[54–58] The oxidized pernigraniline base would be formed through the reduction of the gold ions. The additional red-shifted behavior of the oxidized pernigraniline base absorption was observed from 530 to 740 nm with the increase of the reduction time from 30 min to 24 h (see Fig. 3-17), indicating the reversible conformational change from the oxidized pernigraniline base (λ_{max}, 530 ~ 575 nm) to the parent polyemeraldine salt (λ_{max}, 740 nm), with keeping the appearance of the plasmon absorption peak related to the formation of the gold nanoparticles around 550 nm during such process.

The outline of this process was illustrated in Fig. 3-18.

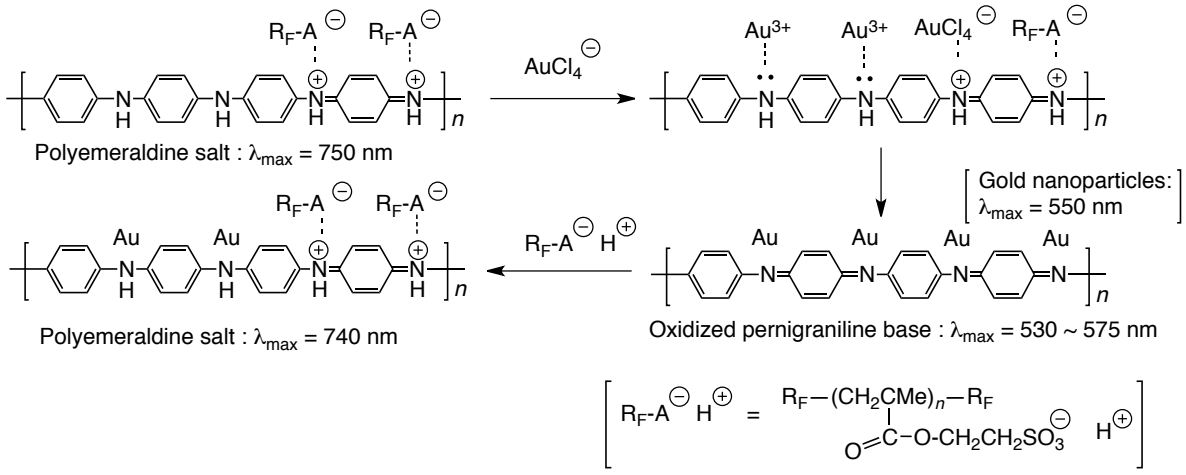

Fig. 3-18 Schematic illustration for the reversible conformational change of **PAn** main chain from the polyemeraldine base to the oxidized pernigraniline base under the reduction of the gold ions with the **PAn** in the nanocomposites

3.4. Conclusions

R_F-$(ACA)_n$-R_F oligomer and R_F-$(ACMO)_n$-R_F oligomer were applied to the autoreduction of the gold ions to give the corresponding oligomers/Au nanocomposites; although the other oligomers such as R_F-$(DMAA)_n$-R_F oligomer, R_F-$(MES)_n$-R_F oligomer and R_F-$(AMPS)_n$-R_F oligomer were not effective for the autoreduction of the gold ions under the similar conditions. The smooth autoreduction of the gold ions was not observed in the presence of the nonfluorinated -$(ACMO)_n$- oligomer, indicating that such autoreduction is likely to proceed through the interactions between the morpholino units in oligomers and the encapsulated gold ions in the fluorinated oligomeric aggregate cores to give the expected gold nanoparticles. R_F-$(ACA)_n$-R_F oligomer and R_F-$(ACMO)_n$-R_F oligomers were also applied to the autoreduction of the gold ions in the presence of the corresponding oligomers/SiO_2 nanocomposites. The obtained fluorinated silica nanocomposite-encapsulated Au nanoparticles were found to exhibit the similar plasmon absorption peaks related to the gold nanoparticles before and even after calcination at 800 °C, although the sizes of the usual gold nanoparticles in SiO_2 nanocomposites are sensitive to the temperature changes and the sizes of these composites are likely to increase through the agglomeration of gold particles. R_F-$(MES)_n$-R_F oligomer and R_F-$(AMPS)_n$-R_F oligomer are not applied to the autoreduction of

the gold ions; however, it was clarified that R_F-$(MES)_n$-R_F/**PAn** nanocomposites and R_F-$(AMPS)_n$-R_F/**PAn** nanocomposites are useful tools for the reduction of the gold ions. In this case, the reversible conformational changes of **PAn** main chain from the polyemeraldine salt to the oxidized pernigraniline base and then from the oxidized pernigraniline base to the parent polyemeraldine salt can be observed. Such reversible conformational change of **PAn** main chain might be a first example, because such smooth reversible conformational change with the gold ions of **PAn** main chain should occur in the fluorinated oligomeric aggregate cores.

References

1) R. B. Grubbs, *J. Polym. Sci. Part A Polym. Chem.*, **43**, 4323 (2005).

2) C. Lofton and W. Sigmund, *Adv. Funct. Mater.*, **15**, 1197 (2005).

3) P. M. Arnal, M. Comotti, and F. Schuth, *Angew. Chem. Int. Ed.*, **45**, 8224 (2006).

4) G. Wang, R. Guo, G. Kalyuzhny, G. P. Choi, and R. W. Murray, *J. Phys. Chem. B*, **110**, 20282 (2006).

5) S. K. Bhargava, J. M. Booth, S. Agrawal, P. Coloe, and G. Kar, *Langmuir*, **21**, 5949 (2005).

6) T. Tsuzuki-ishi and H. Sawada, *Oleo. Sci.*, **14**, 55 (2014).

7) S. K. Jewrajka and U. Chatterjee, *J. Polym. Sci. Part A Polym. Chem.*, **44**, 1841 (2006).

8) M. Meilikhov, K. Yusenko, D. Esken, S. Turner, G. V. Tendeloo, and R. A. Fischer, *Eur. J. Inorg. Chem.*, **2010**, 3701 (2010)

9) H. Sawada, *Chem. Rev.*, **96**, 1779 (1996).

10) H. Sawada and T. Kawase, *Kobunshi Ronbunshu*, **58**, 147 (2001).

11) H. Sawada and T. Kawase, *Kobunshi Ronbunshu*, **58**, 255 (2001).

12) H. Sawada, *J. Fluorine Chem.*, **105**, 219 (2000).

13) H. Sawada, *J. Fluorine Chem.*, **121**, 111 (2003).

14) H. Sawada, *Prog. Polym. Sci.*, **32**, 509 (2007).

15) H. Sawada, *Polym. Chem.* **3**, 46 (2012).

16) M. Mugisawa and H. Sawada, *Langmuir*, **24**, 9215. (2008).

17) H. Sawada, A. Sasaki, and K. Sasazawa, *Colloids Surf. A Physicochem. Eng. Aspects*, **337**, 57 (2009).

18) H. Sawada, A. Sasaki, K. Sasazawa, T. Kawase, K. Ueno, and K. Hamazaki, *Colloid Polym. Sci.*, **283**, 583 (2005).

19) H. Sawada, A. Sasaki, K. Sasazawa, T. Kawase, K. Toriba, H. Kakehi, M. Miura, and N. Isu, *Polym. Adv. Technol.*, **19**, 419 (2008).

20) H. Sawada, R. Furukuwa, K. Sasazawa, K. Toriba, K. Ueno, and K. Hamazaki, *J. Appl. Polym. Sci.*, **100**, 1328 (2006).

21) H. Sawada, R. Furukuwa, K. Sasazawa, M. Mugisawa, and K. Ohnishi, *Eur. Polym. J.*, **43**, 3258 (2007).

22) H. Sawada and K. Takahashi, *J. Colloid Interface Sci.*, **351**, 166 (2010).

23) H. Sawada, Y.-F. Gong, Y. Minoshima, T. Matsumoto, M. Nakayama, M. Kosugi, and T. Migita, *J. Chem. Soc., Chem. Commun*., 537 (1992).

24) H. Sawada, A. Ohashi, M. Baba, T. Kawase, and Y. Hayakawa, *J. Fluorine Chem.*, **79**, 149 (1996).

25) H. Sawada, S. Katayama, Y. Ariyoshi, T. Kawase, Y. Hayakawa, T. Tomita, and M. Baba, *J. Mater. Chem.*, **8**, 1517 (1998).

26) H. Sawada, Y. Yoshino, Y. Ikematsu, and T. Kawase, *Eur. Polym. J.*, **36**, 231 (2000).

27) H. Sawada, T. Narumi, A. Kajiwara, K. Ueno, and K. Hamazaki, *Colloid Polym. Sci.*, **284**, 551 (2006).

28) H. Sawada, T. Tsuzuki-ishi, T. Kijima, M. Iizuka and M. Yoshida, *Colloid Polym. Sci.*, **289**, 1103 (2011).

29) H. Sawada, T. Tsuzuki-ishi, T. Kijima, J. Kawakami, M. Iizuka and M. Yoshida, *J. Colloid Interface Sci.*, **359**, 461 (2011).

30) J. Han, Y. Liu, and R. Guo, *Adv. Funct. Mater.*, **19**, 1112 (2009).

31) S. A. Aromal, K. V. D. Babu, and D. Philip, *Spectrochim. Acta. Part A Mol. Biomol. Spectrosc.*, **96**, 1025 (2012).

32) M. Oishi, H. Hayashi, T. Uno, T. Ishii, M. Iijima, and Y. Nagasaki, *Macromol. Chem. Phys.*, **208**, 1176 (2007).

33) T. Ishii, H. Otuka, K. Kataoka, and Y. Nagasaki, *Langmuir*, **20**, 561 (2004).

34) Y. Bao, G. Shen, H. Liu, and Y. Li, *Polymer*, **54**, 652 (2013).

35) A. Leiva, C. Saldías, C. Quezada, A. Toro-Labbé, F. J. Espinoza-Beltrán, M. Urzúa, and L. Gargallo, *Eur. Polym. J.*, **45**, 3035 (2009).

36) S. Ayyappan, R. S Gopalan, G. N. Subbanna, and C. N. R. Rao, *J. Mater. Res.*, **12**, 398 (1997).

37) A. Meristoudi and S. Pispas, *Polymer*, **50**, 2743 (2009).

38) T. Sakai and P. Alexandridis, *Langmuir*, **20**, 8426 (2004).

39) T. Sakai and P. Alexandridis, *Macromol. Symp.*, **289**, 18 (2010).

40) D. Ray, V. K. Aswal, and J. Kohlbrecher, *Langmuir*, **27**, 4048 (2011).

41) T. Sakai and P. Alexandridis, *J. Phys. Chem. B*, **109**, 7766 (2005).

42) T. Sakai and P. Alexandridis, *Langmuir*, **21**, 8019 (2005).

43) A. Kohut, A. Voronov, V. Samaryk, and W. Peukert, *Macromol. Rapid Commun.*, **28**, 1410 (2007).

44) I. Hussain, M. Brust, A. J. Papworth, and A. I. Cooper, *Langmuir*, **19**, 4831, (2003).

45) H. Sawada, K. Yanagida, Y. Inaba, M. Sugiya, T. Kawase, and T. Tomita, *Eur. Polym. J.*, **37**, 1433 (2001).

46) M. A. Hossain, Y. Ikeda, T. Hara, and Y. Nagasaki, *Colloid Surf. B Biointerf.*, **102**, 778 (2013).

47) M.-Y. Park, S. Lim, S.-W. Lee, and S.-E. Park, *Macromol. Res.*, **17**, 307 (2009).

48) H. Zhu, Z. Pan, E. W. Hagaman, C. Liang, S. H. Overbury, and S. Dai, *J. Colloid Interf. Sci.*, **287**, 360 (2005).

49) H. Zhu, Z. Ma, J. C. Clark, Z. Pan, S. H. Overbury, and S. Dai, *Appl. Catal. A Gen.*, **326**, 89 (2007).

50) B. Lee, Z. Ma, Z. Zhang, C. Park, and S. Dai, *Microporous Mesoporous Mater.*, **122**, 160 (2009).

51) L. Li, G. Yan, J. Wu, X. Yu, and Q. Guo, *J. Colloid Interface Sci.*, **326**, 72 (2008).

52) J. Han, Y. Liu, and R. Guo, *Adv. Funct. Mater.*, **19**, 1112 (2009).

53) J. Wang, K. G. Neoh, and E. T. Kang, *J. Colloid Interface Sci.*, **239**, 78 (2001).

54) J. Kim, J. E. Lee, J. Lee, Y. Jang, S. Kim, S. Park, K. An, J. H. Yu, and T. Hyeon, *Angew. Chem. Int. Ed.*, **45**, 4789 (2006).

55) D. Nicolas-Debarnot and F. Poncin-Epaillard, *Anal. Chem. Acta*, **475**, 1 (2003).

56) B. C. Roy, M. D. Gupta, L. Bhoumik, and J. K. Ray, *Synth. Met.*, **130**, 27 (2002).

57) E. V. Strounina, R. Shepherd, L. A. P. Kane-Maguire, and G. G. Wallace, *Synth. Met.*, **135–136**, 289 (2003).

58) S. Bhadra, D. Khastgir, N. K. Singha, and J. H. Lee, *Prog. Polym. Sci.*, **34**, 783 (2009).

CHAPTER 4

Controlling Photochromism between Fluoroalkyl End-capped Oligomer/Polyaniline and /*N,N'*-Diphenyl-1,4-phenylenediamine Nanocomposites Induced by UV-light-responsive Titanium Oxide Nanoparticles

4.1. Introduction

Polyaniline (**PAn**)/inorganic composites have been considered as new class of materials due to their improved properties compared with those of pure conducting polymers and inorganic materials. For example, the combination of electrical conductivity of **PAn** and UV sensitivity of anatase TiO_2 are expected to find applications in electrochromic devices, nonlinear optical system and photochemical devises.[1)] It is in general difficult to prepare conducting polymers/inorganic nanoparticle composites by conventional blending or mixing in solutions or melt form, because such polymers are not in molten state and generally insoluble in common solvents. However, **PAn**/silica nanocomposites can be prepared by aqueous dispersion polymerization of the corresponding monomer in the presence of ultrafine silica particles.[2–5)] Similarly, there have been some reports on the preparation of **PAn**/TiO_2 nanocomposites through the chemical polymerization of aniline in the presence of TiO_2 nanoparticles under ultrasonic irradiation, in situ polymerization of aniline in the presence of TiO_2 nanoparticles and β-naphthalenesulfonic acid as both the dopant and template, and graft polymerization of aniline onto the TiO_2 nanoparticle surface modified with γ-aminopropyltriethoxysilane.[6–10)] Sulfonated polyaniline/TiO_2 nanocomposites can be also prepared by the copolymerization of aniline and orthoanilinic acid comonomer catalyzed by

ammonium persulfate in the presence of titania precursor under UV irradiation conditions.[11] Hitherto, there have been numerous studies on the development of fluoroalkyl end-capped oligomers/metal nanoparticle composites possessing not only a good surface active characteristic imparted by fluorine but also a good dispersibility and stability in a variety of solvents.[12, 13] In these fluorinated nanocomposites, especially, fluorinated oligomers/titanium oxide nanocomposites have been recently applied to the surface modification of glass to exhibit not only a completely superhydrophobic characteristic with a non-wetting property against water droplets but also a good oleophobicity imparted by fluoroalkyl segments in the composites on their surface.[14] Especially, the wettability for water on the modified surface can be switched between superhydrophobicity and superhydrophilicity by alternation of UV (ultraviolet) irradiation and dark storage with keeping a good oleophobicity on the modified surface treated with the fluorinated anatase-type titanium oxide nanocomposites.[14] Therefore, it is in particular interest to develop novel fluoroalkyl end-capped oligomers/**PAn**/titanium oxide nanoparticle composites, because these fluorinated composites have high potential applications imparted by not only fluorine but also **PAn** or titanium oxide toward a variety of areas such as conductive coating, charge storage, electrocatalyst, electrochromic devices, and photovoltaic cells.[15–18] This chapter shows that **PAn** and phenyl-capped aniline dimer (**An-dimer**: *N,N'*-diphenyl-1,4-phenylenediamine), which is considered to be an excellent

model of **PAn**, are applicable to the efficient preparation of fluorinated oligomer/**PAn**/TiO_2 nanocomposites and /**Andimer**/TiO_2 nanocomposites by the use of the corresponding oligomer/**PAn** and /**An-dimer** nanocomposites, with a particular emphasis on the evaluation of controlled photochromic behaviors between fluorinated **PAn**/TiO_2 and **An-dimer**/TiO_2 nanocomposites.

4.2. Experimental

4.2.1. Measurements

Molecular weight of R_F-$(MES)_n$-R_F oligomer (Mn = 13,700) was determined by using the gel permeation chromatography (Tokyo, Japan) calibrated pullulan (molecular weights 2000 ~ 50,000) standards by using 0.5 mol dm^{-3} Na_2HPO_4 aqueous solution as the eluent. Dynamic light-scattering (DLS) measurements were performed using Otsuka Electronics DLS-7000 HL (Tokyo, Japan). Field emission scanning electron microscopy (FE-SEM) images were measured by using a JEOL JSM-5300 (Tokyo, Japan). Ultraviolet-visible (UV-vis) spectra were recorded by using Shimadzu UV-1600 UV-vis spectrophotometer (Kyoto, Japan). UV light irradiation was carried out by using an AS ONE Handy UV Lamp SLUV-6 (Osaka, Japan).

4.2.2. Materials

2-Methacrylolyoxyethanesulfonic acid was purchased from Polyscience, Inc. (PA, USA). Aniline and **An-dimer** were purchased from Tokyo Kasei Kogyo Co., Ltd. Titanium oxide

nanoparticles (average size of anatase-type particles determined by DLS: 86 ± 10 nm) were received from Ishihara Sangyo Kaisha Ltd. (Osaka, Japan). R_F-$(MES)_n$-R_F oligomer was prepared by reaction of fluoroalkanoyl peroxide with the corresponding monomer according to the previously reported method.[24)]

4.2.3. Preparation of fluoroalkyl end-capped 2-(methacryloyloxy)ethanesulfonic acid oligomer/polyaniline [R_F-$(MES)_n$-R_F/PAn] nanocomposites

R_F-$(MES)_n$-R_F/**PAn** nanocomposites were prepared according to the method described in chapter 1.[19)] Briefly, aniline (47 mg) was added to an aqueous solution (24 ml) of R_F-$(MES)_n$-R_F oligomer [R_F = $CF(CF_3)OC_3F_7$] (280mg). The mixture was stirred with a magnetic stirring bar at room temperature for 30 min. An 11-ml ammonium persulfate (115 mg) aqueous solution was added dropwise to the solution containing aniline and fluorinated oligomer with continuous stirring at room temperature for 1 day. After the removal of solvent, the crude product was purified by the reprecipitation (H_2O/tetrahydrofuran) to give the expected R_F-$(MES)_n$-R_F/**PAn** nanocomposites. The nanocomposites thus obtained were dried in vacuo at 50 °C for 2 days to afford green-colored powders (262 mg).

4.2.4. Preparation of R_F-(MES)$_n$-R_F/An-dimer nanocomposites

R_F-(MES)$_n$-R_F/**An-dimer** nanocomposites were prepared according to the method described in chapter 1.[19] Briefly, R_F-(MES)$_n$-R_F oligomer [R_F = $CF(CF_3)OC_3F_7$: 60 mg] was added to a methanol solution (10 ml) of **An-dimer** (10 mg). The mixture was stirred with a magnetic stirring bar at room temperature for 1 day. After the removal of solvent, the nanocomposites thus obtained were dried in vacuo at 50 ºC for 2 days to afford light-blue colored powders.

4.2.5. Preparation of R_F-(MES)$_n$-R_F/PAn/TiO_2 nanocomposites

To an aqueous methanol solution [H_2O/MeOH = 1:1 (vol): 6 ml], were added R_F-(MES)$_n$-R_F/**PAn** nanocomposites (7 mg) and TiO_2 nanoparticles (6 mg). The mixture was stirred with a magnetic stirring bar at room temperature for 1 day to give well-dispersed R_F-(MES)$_n$-R_F/**PAn**/TiO_2 nanocomposites aqueous methanol solution. R_F-(MES)$_n$-R_F/ **An-dimer**/TiO_2 nanocomposites were also prepared under similar conditions.

4.3. Results and discussion

Fluoroalkyl end-capped 2-(methacryloyloxy)ethanesulfonic acid oligomer [R_F-$(MES)_n$-R_F]/polyaniline (**PAn**) nanocomposites were prepared by the polymerization of aniline catalyzed by ammonium persulfate [APS] in the presence of the corresponding oligomer as shown in Scheme 4-1.[19)]

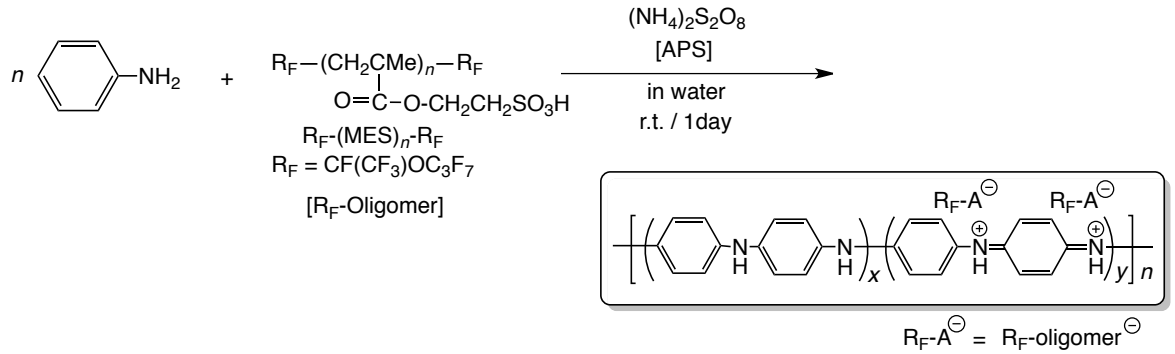

Scheme 4-1

R_F-$(MES)_n$-R_F/polyaniline (**PAn**)/TiO_2 nanocomposites by the interaction of R_F-$(MES)_n$-R_F/**PAn** nanocomposites with anatase-type titanium oxide nanoparticles (average particle size: 86 nm) have been tried to prepare in aqueous methanol solution [water/MeOH = 1/1 (vol)]. The R_F-$(MES)_n$-R_F/**An-dimer**/TiO_2 nanocomposites have been also prepared under similar conditions, for comparison. These results are shown in Scheme 4-2.

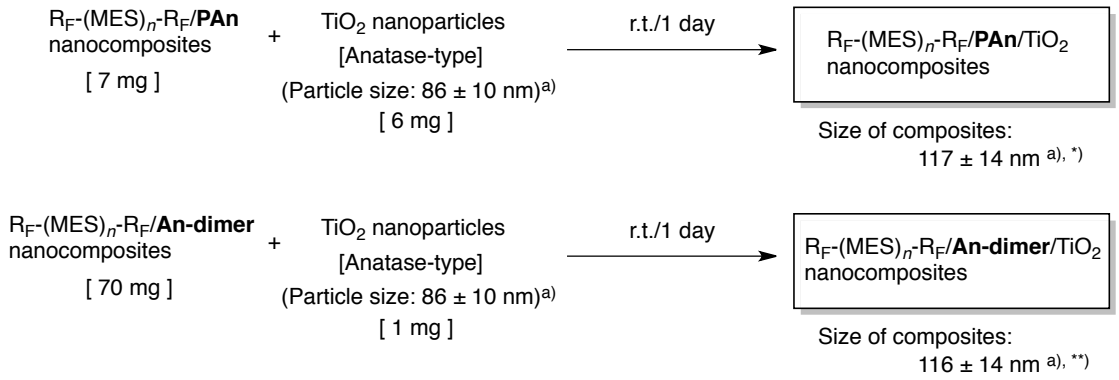

a) Determined by dynamic light scattering(DLS) measurements
*) Average particle size of parent of R_F-(MES)$_n$-R_F/**PAn** nanocomposites: 33 ± 5 nm
) Average particle size of parent of R_F-(MES)$_n$-R_F/An-dimer** nanocomposites: 11 ± 2 nm

Scheme 4-2

As shown in Scheme 4-2, R_F-(MES)$_n$-R_F/**PAn**/TiO_2 nanocomposites and R_F-(MES)$_n$-R_F/**An-dimer**/TiO_2 nanocomposites were prepared under mild conditions at room temperature by the interaction of the corresponding fluorinated **PAn** or **An-dimer** nanocomposites with TiO_2 nanoparticles. These obtained fluorinated nanocomposites were found to exhibit a good dispersibility and stability in aqueous methanol solutions. The size of these fluorinated nanocomposites have been measured in aqueous methanol solutions by using DLS measurements, and the size of green colored R_F-(MES)$_n$-R_F/**PAn**/TiO_2 nanocomposites or blue colored R_F-(MES)$_n$-R_F/**An-dimer**/TiO_2 nanocomposites was found to increase effectively from 33 or 11 nm to 117 or 116 nm by the interaction of the oligomer/**PAn** or **An-dimer** nanocomposites with TiO_2 nanoparticles.

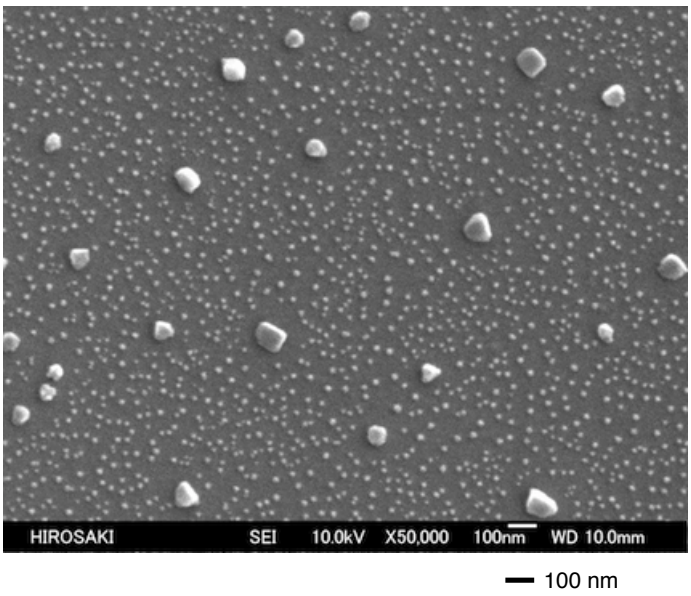

Fig. 4-1 Field emission scaning electron microscopy image of R_F-$(MES)_n$-R_F/**PAn**/ TiO_2 nanocomposites

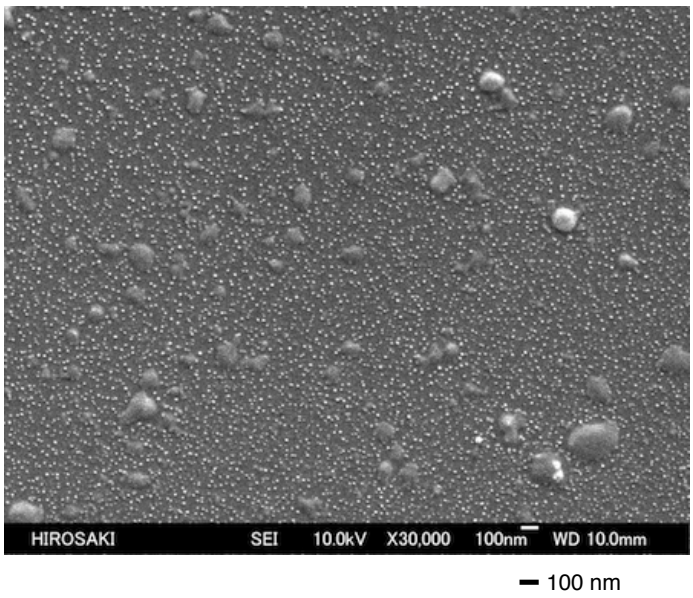

Fig. 4-2 Field emission scaning electron microscopy image of R_F-$(MES)_n$-R_F/**An-dimer**/ TiO_2 nanocomposites

Interestingly, FE-SEM images of these fluorinated nanocomposites show that TiO_2 nanoparticles in the composites are almost uniformly dispersed with no agglomeration, and

the average TiO_2 particle size in the nanocomposites is as follows: R_F-$(MES)_n$-R_F/**PAn**/TiO_2 nanocomposites: 83 nm; R_F-$(MES)_n$-R_F/**An-dimer**/TiO_2 nanocomposites: 114 nm (see Figs. 4-1 and 4-2). These values are well consistent with that (86 nm) of the used parent TiO_2 nanoparticles for the preparation of these nanocomposites. In addition, the color change of these nanocomposites was not observed in each case after the treatment with TiO_2 nanoparticles. TiO_2 has the advantages of high chemical stability and high photocatalytic activity.[20] Thus, the effect of UV light on the absorption spectra of the present fluorinated nanocomposites have been study, and the results were shown in Figs. 4-3 and 4-4.

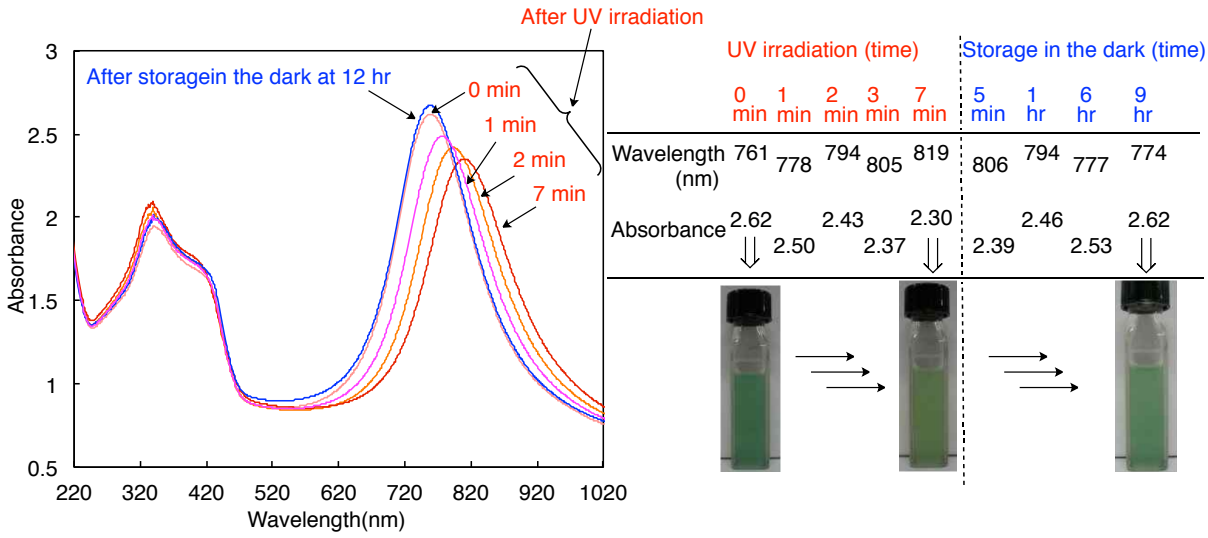

Fig. 4-3 UV-vis spectra and photographs of aqueous methanol soiutions of R_F-$(MES)_n$-R_F/**PAn**/TiO_2 nanocomposites after UV irradiation(λ_{max} = 365 nm) and storage in the dark at room temprature. Concentrations of R_F-$(MES)_n$-R_F/**PAn** nanocomposites 117 mg/dm^3; concentrations of TiO_2 nanoparticles 100 mg/dm^3.

As shown in Fig. 4-3, when R_F-$(MES)_n$-R_F/**PAn**/TiO_2 nanocomposites are illuminated under UV light (λ_{max}: 365 nm), not only the red-shift of the polaron absorptions from 761 to

819 nm but also the slight decrease of the absorbance have been observed with increasing the UV irradiation time. After the UV irradiated the nanocomposites solution was placed in the dark for 9 h. Interestingly, restoration to the original polaron wavelength and absorbance, which are accompanied by photochromism, was realized for the nanocomposites by alternation of UV irradiation and storage in the dark. This cycle was repeated several times, and a good repeatability for the polaron wavelength and the absorbance changes were observed (see Fig. 4-4).

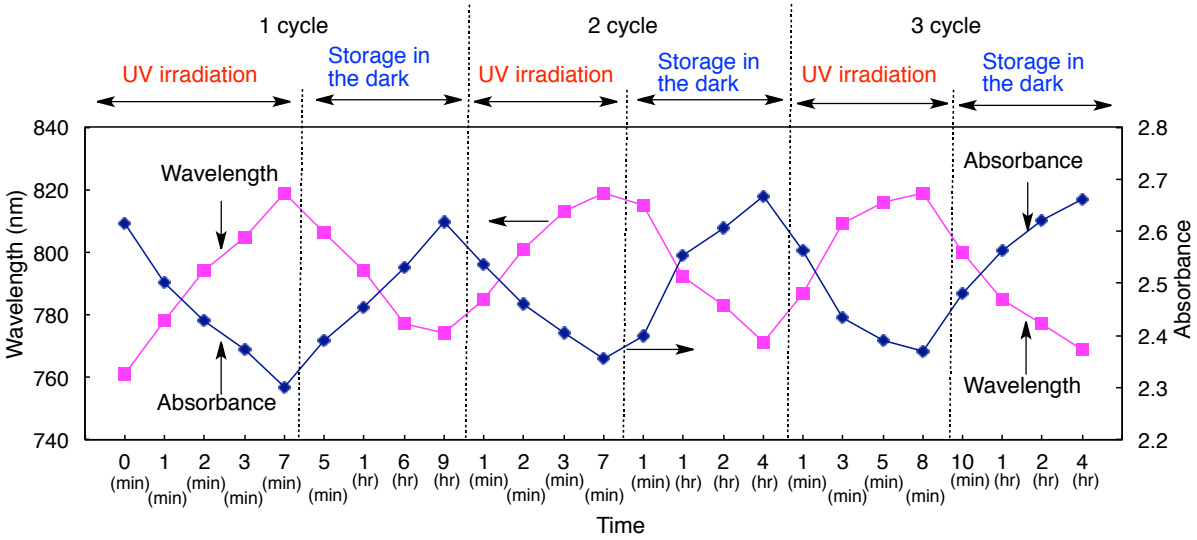

Fig. 4-4 Relationship between wavelength and absorbance of aqueous methanol solutions of R_F-$(MES)_n$-R_F/**PAn**/TiO_2 nanocomposites for alternation of UV irradiation and storage in the dark at room temperature.

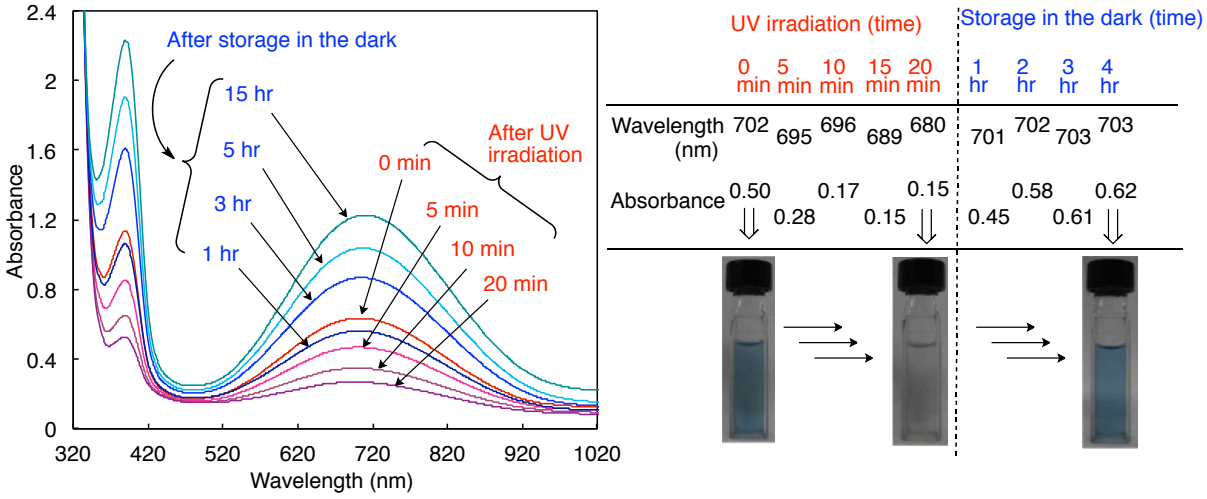

Fig. 4-5 UV-vis spectra and photographs of methanol soiutions of R_F-$(MES)_n$-R_F/**An-dimer**/TiO_2 nanocomposites after UV irradiation(λ_{max} = 365 nm) and storage in the dark at room temprature. Concentration of R_F-$(MES)_n$-R_F/**An-dimer** nanocomposites 1167 mg/dm^3; concentration of TiO_2 17 mg/dm^3.

On the other hand, unexpectedly, R_F-$(MES)_n$-R_F/**An-dimer**/TiO_2 nanocomposites were unable to afford the similar UV-driven reversible switching behavior between red-shift to blue-shift for the polaron absorptions shown in Fig. 4-5. Upon UV (λ_{max}: 365 nm) irradiation, the wavelength around 700 nm was not changed with the increase of UV irradiation time; however, the absorbance around 700 nm was found to decrease effectively under such conditions. The dramatic decrease of the absorbance caused the color change of the nanocomposites solution from the light blue to colorless. After the UV irradiated the dark storage of the nanocomposites solution caused the increase of the absorbance by the photochromism. This cycle was repeated several times, and the absorbance of alternate decrease and increase was observed with keeping no change of the wavelength (see Fig. 4-6).

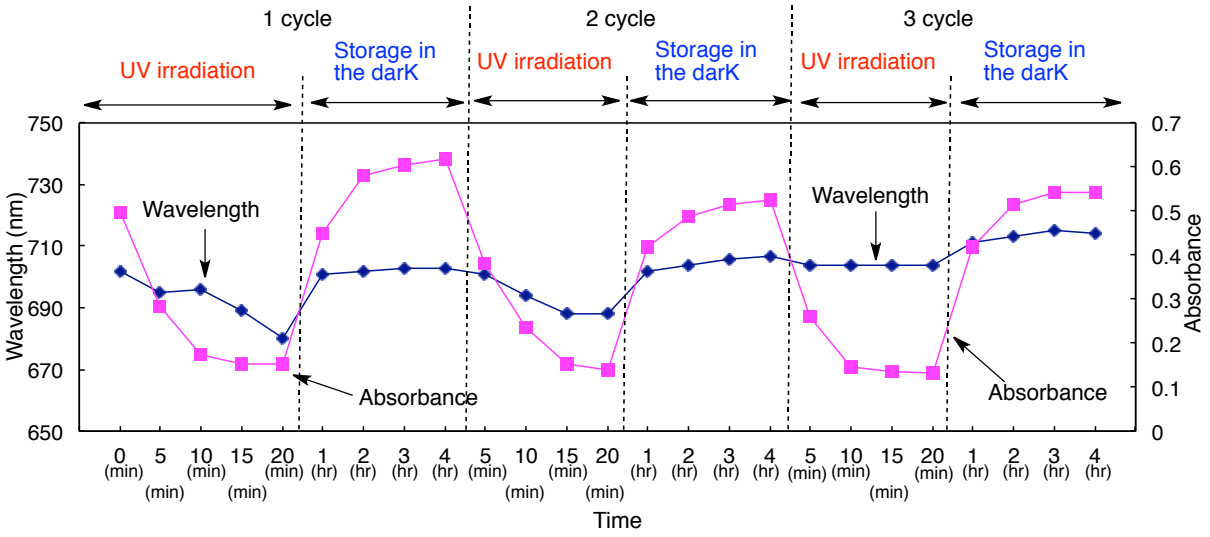

Fig. 4-6 Relationship between wavelength and absorbance of aqueous methanol solutions of R_F-(MES)$_n$-R_F/**An-dimer**/TiO_2 nanocomposites for alternation of UV irradiation and storage in the dark at room temperature.

It is well-known that the conduction band of TiO_2 and the LUMO level of the **PAn** are well compatible for the charge transfer, and the generated electrons by inducing **PAn** can be transferred to the conduction band of TiO_2, enhancing the charge separation.[9, 21, 22] In the present R_F-(MES)$_n$-R_F/**PAn**/TiO_2 nanocomposites, R_F-(MES)$_n$-R_F oligomer-doped **PAn** can absorb the visible light irradiation as semiconductive material and transfer the photogenerated electron (e^-) into the conduction band of the TiO_2 nanoparticles in the composites efficiently. Thus, the more delocalized polaron structures in the **PAn** thus obtained should afford the red-shifted absorptions. On the other hand, upon no UV irradiation the generated electrons, which were transferred to the conduction band of TiO_2, would be migrated to a positive charged hole (h^+) in **PAn** to regenerate the original polaron structures (see Fig. 4-7). In this way, it was suggested that reversible red-shifted and blue-shifted polar absorptions'

photochromic behavior is intelligently controlled by alternation of UV illumination and dark storage.

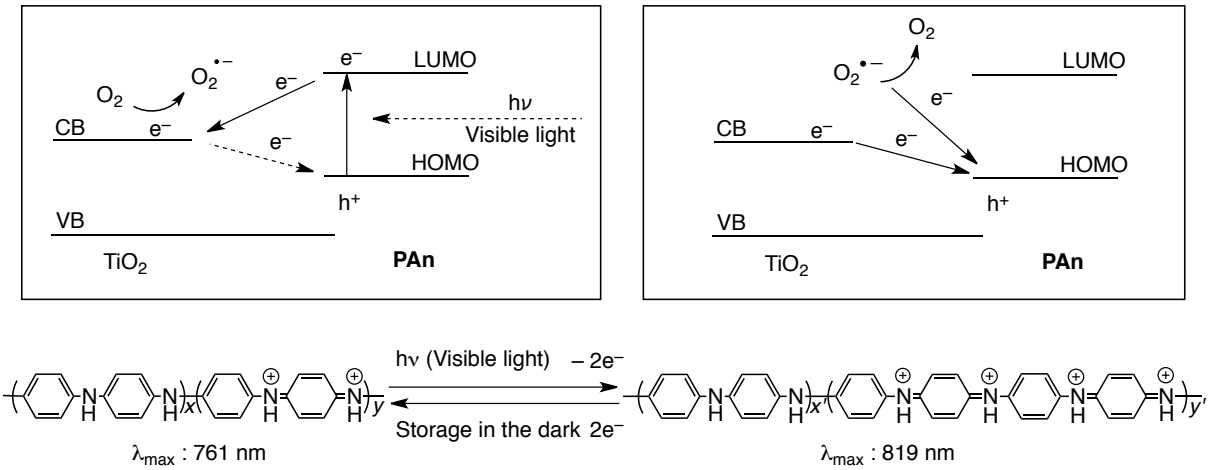

Fig. 4-7 Plausible mechanism for reversible red-shifted and blue-shifted polaron absorption's photochromic behavior in R_F-$(MES)_n$-R_F/**PAn**/TiO_2 nanocomposites controlled by alternation of UV irradiation and storage in the dark

In the case of R_F-$(MES)_n$-R_F/**An-dimer**/TiO_2 nanocomposites, the Spartan'04 AM1 semiempirical level molecular orbital theoretical studies[23] suggested that the HOMO energy level of the quinoid structure of **An-dimer** [C_6H_5–NH^+=C_6H_4=NH^+–C_6H_5] is lower (–15.42 eV) than that (–12.60 eV) of the partly quinoid cation-type phenyl-capped tetraaniline [C_6H_5–NH–C_6H_4–NH–C_6H_4–NH^+=C_6H_4=NH^+–C_6H_5], which is an excellent model for Brønsted acid doped-polyaniline. When R_F-$(MES)_n$-R_F/**An-dimer**/TiO_2 nanocomposites are illuminated under UV light, TiO_2 nanoparticles can absorb the visible light irradiation more effectively than that of **An-dimer** due to the lower HOMO energy level of **An-dimer**,

compared with that of partly acid-doped phenyl-capped tetraaniline (see Fig. 4-8). The generated electrons in the conduction band of the TiO_2 nanoparticles should be smoothly migrated to the LUMO of the quinoid-type **An-dimer**. Original **An-dimer** would be formed by the electron acceptance into the LUMO of quinoid-type **An-dimer** to afford the extreme decrease of the absorbance of the quinoid-type **An-dimer** around 700 nm. In contrast, the storage of the dark of this nanocomposite solution enables electron transfer from the LUMO of **An-dimer**, which was formed by the electron acceptance into the LUMO of quinoid-type **An-dimer**, to the positively charged TiO_2 balance band hole (h^+). Thus, electron-migrated **An-dimer** should afford the quinoid-type **An-dimer**, which can exhibit an absorption around 700 nm (see Fig. 4-8). In this way, a reversible color change from blue to colorless (a reverse absorbance change), which is accompanied by photochromism, can be realized for R_F-$(MES)_n$-R_F/**An-dimer**/TiO_2 nanocomposites by alternating UV irradiation and storage in the dark.

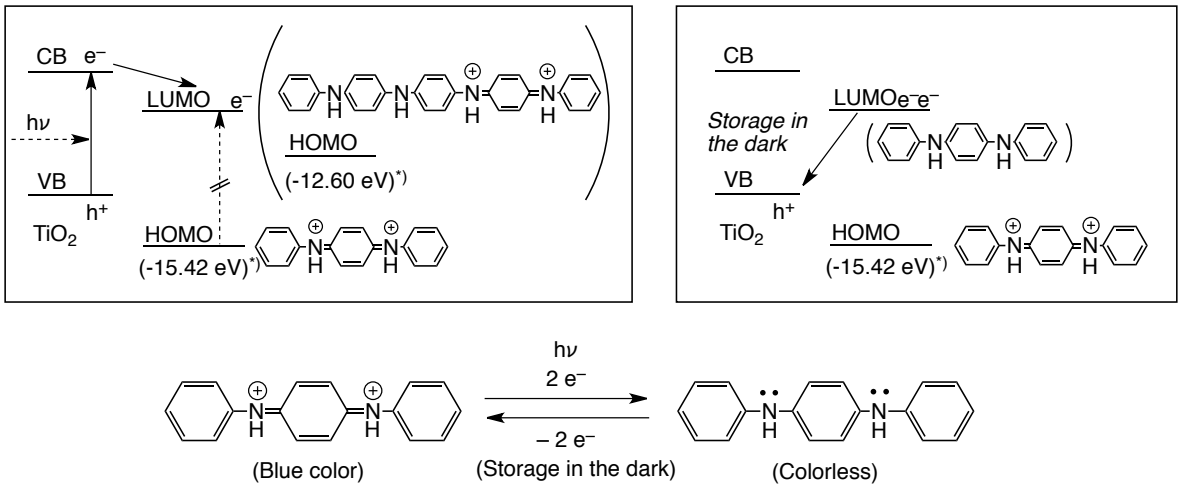

Fig. 4-8 Plausible mechanism for reversible color change from blue to colorless in R_F-$(MES)_n$-R_F/**An-dimer**/TiO_2 nanocomposites controlled by alternation of UV irradiation and storage in the dark

4.4. Conclusion

In conclusions, R_F-$(MES)_n$-R_F/**PAn** nanocomposites were found to afford the colloidal stable fluorinated oligomer/**PAn**/TiO_2 nanocomposites by the interaction of the corresponding oligomer/**PAn** nanocomposites with TiO_2 nanoparticles. Colloidal stable R_F-$(MES)_n$-R_F/ **An-dimer**/TiO_2 nanocomposites were also prepared under similar conditions. A reversible wavelength change from 760 to 820 nm corresponding to the polaron absorptions, which is accompanied by photochromism, was realized for R_F-$(MES)_n$-R_F/**PAn**/TiO_2 nanocomposites by alternating UV irradiation with storage in the dark. In contrast, interestingly, a reversible color change from blue to colorless (a reversible absorbance change), which is accompanied by photochromism, was realized for R_F-$(MES)_n$-R_F/**An-dimer**/TiO_2 nanocomposites by alternating UV irradiation with storage in the dark.

References

1) S.-J. Su and N. Kuramoto, *Synth. Met.*, **114**, 147 (2000).

2) H. Xia and Q. Wang, *J. Appl. Polym. Sci.*, **87**, 1811 (2003).

3) M. D. Butterworth, R. Corradi, J. Johal, S. F. Laschelles, S. Maeda, and S. P. Armes, *J. Colloid Interface Sci.*, **174**, 510 (1995).

4) M. Gill, J. Mykytiuk, and S. P. Armes, *Langmuir*, **8**, 2178 (1993).

5) N. J. Terrill, T. Crowley, M. Gill, and S. P. Armes, *Langmuir*, **9**, 2093 (1993).

6) M. Nagaraja, J. Pattar, N. Shashank, J. Manjanna, Y. Kamada, K. Rajanna, and H. M. Mahesh, *Synth. Met.*, **159**, 718 (2009).

7) L. Zhang, and M. Wan, *J. Phys. Chem. B*, **107**, 6748 (2003)

8) W. Feng, A. Fujii, H. Wu, K. Niihara, and K. Yoshino, *Bull. Chem. Soc. Jpn.*, **73**, 2627 (2000).

9) J. Li, L. Zhu, Y. Wu, Y. Harima, A. Zhang, and H. Tang, *Polymer*, **47**, 7361 (2006).

10) F.-Y. Chung and S.-M. Yang, *Synth. Met.*, **152**, 361 (2005).

11) M. R. Karim, K. T. Lim, M. S. Lee, K. Kim, and J. H. Yeum, *Synth. Met.*, **159**, 209 (2009).

12) H. Sawada, *Prog. Polym. Sci.*, **32**, 509 (2007).

13) H. Sawada, *Polym. J.*, **39**, 637 (2007).

14) E. Sawada, H. Kakehi, Y. Chounan, M. Miura, Y. Sato, N. Isu, and H. Sawada, *Composites Part B*, **41**, 498 (2010).

15) C. Bian, Y. Yu, and G. Xue, *J. Appl. Polym. Sci.*, **104**, 21 (2007).

16) H. Park and W. Choi, *Langmuir*, **22**, 2906 (2006).

17) M. R. Hoffmann, S. T. Martin, and D. W. Bahnemann, *Chem. Rev.*, **95**, 69 (1995).

18) D. Chowdhury, A. Paul, and A. Chattopadhyay, *Langmuir*, **21**, 4123 (2005).

19) H. Sawada, T. Tsuzuki-ishi, T. Kijima, M. Iizuka and M. Yoshida, *Colloid Polym. Sci.*, **289**, 1103 (2011).

20) A. Fujishima and K. Honda, *Nature*, **37**, 238 (1972).

21) G. K. R. Senadeera, T. Kitamura, Y. Wada, and S. Yanagida, *J. Photochem. Photobiol., A*, **164**, 61 (2004).

22) X. Li, D. Wang, G. Cheng, Q. Luo, J. An, and Y. Wang, *Appl. Catal., B*, **81**, 267 (2008).

23) Spartan'04, Wavefunction, Inc. 18401 Von Karman Avenue, Suite 370, Irvine, California 92612, USA.

24) H. Sawada, A. Ohashi, M. Baba, T. Kawase, and Y. Hayakawa, *J. Fluorine Chem.*, **79**, 149 (1996).

Conclusions

The results obtained from this study are summarized as follows:

1. Fluoroalkyl end-capped acrylic acid oligomer [R_F-(ACA)$_n$-R_F]/, 2-(methacryloyloxy)ethanesulfonic acid oligomer [R_F-(MES)$_n$-R_F]/, 2-acrylamido-2-methylpropanesulfonic acid oligomer [R_F-(AMPS)$_n$-R_F]/polyaniline [**PAn**] nanocomposites were prepared by the polymerization of aniline initiated by ammonium persulfate in the presence of the corresponding oligomers, respectively. These fluorinated oligomers were also applied to the preparation of the corresponding fluorinated oligomers/phenyl-capped aniline dimer (**An-dimer**: *N,N'*-diphenyl-1,4-phenylenediamine) nanocomposites by the interaction of the fluorinated oligomers with **An-dimer**. These fluorinated composites thus obtained were found to afford nanometer size-controlled fine particles possessing a good dispersibility and stability in water and traditional organic media such as methanol. UV–vis spectra of R_F-(MES)$_n$-R_F/**PAn** nanocomposites and R_F-(AMPS)$_n$-R_F/**PAn** nanocomposites showed the similar absorption peaks around 350, 430 and 780 nm to those of the usual Brønsted acid-doped **PAn**; however, interestingly,

R_F-(ACA)$_n$-R_F/**PAn** nanocomposites were found to exhibit only an absorption peak around 430 nm based on the polaron transition.

2. Fluoroalkyl end-capped 2-(methacryloyloxy)ethanesulfonic acid oligomer [R_F-(MES)$_n$-R_F]/polyaniline (**PAn**) nanocomposites, which were prepared by the polymerization of aniline initiated by ammonium persulfate in the presence of the corresponding oligomer, can cause the smooth color change from green to wine-red (or purple), triggered by a variety of basic compounds such as ammonia, sodium hydroxide, 2-hydroxyethylamine, tris(hydroxymethyl)aminomethane, and silica particles bearing 3-aminopropyl groups (***Amino***-SiO_2) under room temperature. It was found that the R_F-(MES)$_n$-R_F/**PAn** nanocomposites undergo a change in the color when they are exposed to ammonia vapor, and especially, a good reversible color change from green to wine-red color through the chemochromic behavior is observed when they are under air and exposure to ammonia vapor. Purple-colored R_F-(MES)$_n$-R_F/**PAn**/***Amino***-SiO_2 blend hybrids powders, which are prepared by the interaction of R_F-(MES)$_n$-R_F/**PAn** nanocomposites with ***Amino***-SiO_2 particles, can cause the solvatochromic response in water, methanol, chloroform and fluorinated aliphatic solvent to give the color change from blue to colorless (white-gray) in the fluorinated solvent.

3. A variety of fluoroalkyl end-capped oligomers, such as fluoroalkyl end-capped acrylic acid oligomer [R_F-(ACA)$_n$-R_F], acryloylmorpholine oligomer [R_F-(ACMO)$_n$-R_F], 2-acrylamido-2-methylpropanesulfonic acid oligomer [R_F-(AMPS)$_n$-R_F], 2-(methacryloyloxy)ethanesulfonic acid oligomer [R_F-(MES)$_n$-R_F] and *N,N*-dimethylacrylamide oligomer [R_F-(DMAA)$_n$-R_F], were applied to the autoreduction of gold ions to give the corresponding oligomers/gold nanocomposites, of whose sharp plasmon absorption bands are observed around 535 nm. In these fluorinated oligomers, R_F-(ACA)$_n$-R_F oligomer and R_F-(ACMO)$_n$-R_F were effective for the one-pot preparation of the gold nanoparticles under very mild conditions; although the other fluorinated oligomers and the corresponding non-fluorinated -(ACMO)$_n$- oligomer were unable to afford the gold nanoparticles. R_F-(ACA)$_n$-R_F/SiO_2 nanocomposites and R_F-(ACMO)$_n$-R_F/SiO_2 nanocomposites, which were prepared by the sol–gel reactions of tetraethoxysilane in the presence of silica nanoparticles and the corresponding oligomers under alkaline conditions, were also applied to the encapsulation of gold nanoparticles into these fluorinated nanocomposite cores through the autoreduction of gold ions at room temperature. Interestingly, these fluorinated oligomers/silica nanocomposite-encapsulated gold nanocomposites before and after calcination at 800 °C were found to exhibit the same plasmon absorption band around 525 nm. R_F-(MES)$_n$-R_F oligomer and R_F-(AMPS)$_n$-R_F oligomer are not suitable for the

autoreduction of gold ions; however, R_F-(MES)$_n$-R_F [or R_F-(AMPS)$_n$-R_F]/polyaniline [**PAn**] nanocomposites, which were prepared by the polymerization of aniline initiated by ammonium persulfate in the presence of the corresponding oligomer, enabled the formation of gold nanoparticles through the oxidation of **PAn** in the composites at room temperature. The reversible conformational change of **PAn** in the nanocomposites from the polyemeraldine salt to the oxidized pernigraniline base was observed during such oxidation process.

4. Colloidal stable fluoroalkyl end-capped 2-(methacryloyloxy)ethanesulfonic acid oligomer [R_F-(MES)$_n$-R_F]/polyaniline (**PAn**)/TiO_2 nanocomposites and R_F-(MES)$_n$-R_F/**An-dimer** (**An-dimer**: *N,N'*-diphenyl-1,4-phenylenediamine)/TiO_2 nanocomposites were prepared by the interactions of TiO_2 nanoparticles with R_F-(MES)$_n$-R_F/**PAn** nanocomposites or R_F-(MES)$_n$-R_F/**An-dimer** nanocomposites, which were prepared by the composite reaction of R_F-(MES)$_n$-R_F oligomer with **PAn** or **An-dimer**. These two types of fluorinated TiO_2 nanocomposites can exhibit quite different photochromic behaviors: R_F-(MES)$_n$-R_F/**PAn**/TiO_2 nanocomposites can exhibit a reversible wavelength change for polaron absorptions around 760 ~ 820 nm by alternation of UV irradiation and storage in the dark; in contrast, R_F-(MES)$_n$-R_F/**An-dimer**/TiO_2 nanocomposites can exhibit a reversible color change from blue to colorless (a reversible absorbance change) by the similar treatment.

Publications

1) H. Sawada, T. Tsuzuki-ishi, T. Kijima, M. Iizuka and M. Yoshida, "Preparation of novel fluoroalkyl end-capped oligomers/polyaniline and /*N,N'*-diphenyl-1,4-phenylenediamine nanocomposites", *Colloid Polym. Sci.*, **289**, 1103 (2011).

2) H. Sawada, T. Tsuzuki-ishi, T. Kijima, J. Kawakami, M. Iizuka and M. Yoshida, "Controlling photochromism between fluoroalkyl end-capped oligomer/polyaniline and *N,N'*-diphenyl-1,4-phenylenediamine nanocomposites induced by UV-light-responsive titanium oxide nanoparticles", *J. Colloid Interface Sci.*, **359**, 461 (2011).

3) T. Tsuzuki-ishi and H. Sawada, "Facile one-pot preparation of gold nanoparticles in the presence of fluoroalkyl end-capped oligomers, fluoroalkyl end-capped oligomers/silica nanocomposites, and fluoroalkyl end-capped oligomers/polyaniline nanocomposites", *Colloid Polym. Sci.*, **292**, 2959 (2014).

4) T. Tsuzuki-ishi and H. Sawada, “Color-changing behavior of fluoroalkyl end-capped 2-methacryloyloxyethanesulfonic acid oligomer/polyaniline nanocomposites, triggered by a variety of basic compounds”, *Colloid Polym. Sci.*, **293**, 1237 (2015).

(not described in this thesis)

5) T. Tsuzuki-ishi and H. Sawada, “Development of fluoroalkyl end-capped oligomeric nanocomposites-encapsulated metal nanoparticles”, *Oleo. Sci.*, **14**, 55 (2014).

Acknowledgements

The author sincerely thanks Prof. Hideo Sawada for his enormous support and insightful comments during the course of his study. Without Prof. Hideo Sawada's guidance and persistent help, this thesis would not have materialized.

Special thanks go to Prof. Isoshi Nukatsuka, Prof. Shunji Ito, Prof. Masaaki Okazaki, and Associate Prof. Jun Kawakami who provided valuable comments and discussions to this study, respectively. Special thanks also go to Prof. Masato Yoshida of Shimane University who gave helpful advice to this study. The author would like to thank to Mr. Yusei Tsushima, a technical staff at Hirosaki University who supported the electron microscopic observations such as FE-SEM and TEM. He would also like to thank present and past members of Sawada Laboratory for their generous cooperation and encouragements in everyday life.

Finally, the author would like to express his gratitude to his family and friends who gave moral support and warm encouragements.